STAR (#5)

DEPARTMENT OF MECHANICAL ENGINEERING AND MECHANICS
SCHOOL OF ENGINEERING
OLD DOMINION UNIVERSITY
NORFOLK, VIRGINIA 23508

DYNAMIC IDENTIFICATION FOR CONTROL OF LARGE SPACE STRUCTURES

By

Samir R. Ibrahim, Principal Investigator

Final Report
For the period ending May 1, 1983

Prepared for
National Aeronautics and Space Administration
Langley Research Center
Hampton, VA 23665

Under
Research Grant NSG-1649
Mr. Edwin J. Prior, Technical Monitor
Office of Director

November 1985

DEPARTMENT OF MECHANICAL ENGINEERING AND MECHANICS
SCHOOL OF ENGINEERING
OLD DOMINION UNIVERSITY
NORFOLK, VIRGINIA 23508

DYNAMIC IDENTIFICATION FOR CONTROL OF LARGE SPACE STRUCTURES

By

Samir R. Ibrahim, Principal Investigator

Final Report
For the period ending May 1, 1983

Prepared for
National Aeronautics and Space Administration
Langley Research Center
Hampton, VA 23665

Under
Research Grant NSG-1649
Mr. Edwin J. Prior, Technical Monitor
Office of Director

Submitted by the
Old Dominion University Research Foundation
P.O. Box 6369
Norfolk, VA 23508

November 1985

DYNAMIC IDENTIFICATION FOR CONTROL OF LARGE SPACE STRUCTURES

BY

Samir R. Ibrahim*

SUMMARY

The final report for NSG 1649, Dynamic Identification for control of Large Space Structures, consists of the following five journal articles:

(1) "A Parametric Study of the Ibrahim Time Domain Modal Identification Algorithm," The Shock and Vibration Bulletin, May 1981; 83N 10258

(2) "Large Modal Survey Testing Using the Ibrahim Time Domain Identification Technique," Journal of Spacecraft and Rockets, Vol. 19, No. 5, Sept. - Oct. 1982. 81A29449

(3) "Computation of Normal Modes from Identified Complex Modes," AIAA Journal, Vol. 21, No. 3, March 1983. 83A 22143

(4) "Dynamic Modeling of Structures from Measured Complex Modes," AIAA Journal Vol. 32, No. 6, June 1983. 83A32988

(5) "Time Domain Quasi-Linear Identification of Nonlinear Dynamic Systems," AIAA/ASME/ASCE/AHS 24th Structures, Structural Dynamics and Materials Conference, Lake Tahoe, Nevada, May 2-4, 1983. 84A36495

---

*Associate Professor, Department of Mechanical Engineering & Mechanics, School of Engineering, Old Dominion University, Norfolk, VA 23508.

Bulletin 51
(Part 3 of 3 Parts)

Reprinted From

THE SHOCK AND VIBRATION BULLETIN

Part 3
Analytical Methods, Dynamic Analysis, Vehicle Systems

MAY 1981

A Publication of
THE SHOCK AND VIBRATION INFORMATION CENTER
Naval Research Laboratory, Washington, D.C.

Office of
The Under Secretary of Defense
for Research and Engineering

A PARAMETRIC STUDY OF THE IBRAHIM TIME DOMAIN MODAL IDENTIFICATION ALGORITHM

Richard S. Pappa
Structural Dynamics Branch
NASA Langley Research Center
Hampton, Virginia

and

Samir R. Ibrahim
Department of Mechanical Engineering and Mechanics
Old Dominion University
Norfolk, Virginia

The accuracy of the Ibrahim Time Domain (ITD) identification algorithm in extracting structural modal parameters from free-response functions has been studied using computer-simulated data for 65 positions on an isotropic, uniform-thickness plate, with mode shapes obtained by NASTRAN analysis. Natural frequencies, damping factors, and response levels of the first 15 plate modes were arbitrarily assigned in forming the response functions, to study identification results over ranges of modal parameter values and user-selectable algorithm constants. Effects of superimposing various levels of noise onto the functions were investigated in detail. A particularly interesting result is that no detrimental effects were observed when the number of computational degrees-of-freedom allowed in the algorithm was made many times larger than the minimum necessary for adequate identification. This result suggests the use of a high number of degrees-of-freedom when analyzing experimental data, for the simultaneous identification of many modes in one computer run. Details of the procedure used for these identifications are included.

INTRODUCTION

A fundamental problem in experimental structural dynamics is the accurate determination of parameters characterizing the important vibration modes of a test structure. These parameters--natural frequencies, damping factors, and mode shapes--are used for a variety of purposes, including:

1. trouble-shooting excessive vibration or noise from mechanical equipment;
2. dynamic analysis of portions of a structure that are too difficult to model analytically;
3. refinement or verification of an analytical model; and
4. direct calculation of dynamic loads or response levels that a structure may experience during operation.

An additional future use of experimentally determined modal parameters, of current research interest to NASA, is in the active attitude control of large space structures.

Obviously, the applications and corresponding accuracies which are required of these data vary considerably. Results adequate for one use may be unacceptable for another. In addition, accuracy requirements for particular applications may be difficult to quantify and may be subject to error. Establishing the adequacy of experimental modal data still often includes a judgement of whether the most accurate set of data, within an allocated period of time, has been obtained.

Before the widespread use of minicomputers in the laboratory, modal testing and analysis were conducted almost exclusively with analog instrumentation. As the advantages of digital computation

because apparent, many data analysis techniques that had been developed on the analog systems were simply converted to their digital counterparts. These techniques are, in fact, still used today in successfully measuring the dominant modal patterns of "well-behaved" structures. Accompanying the conversion to digital-based laboratory equipment was an increased use of random force, as opposed to sinusoidal force, for exciting test structures. This trend was closely related to the revolutionary switch in the late 1960's to fast Fourier transform (FFT) methods for rapidly computing frequency-domain characteristics of random response signals. Although many structures are still tested with the classical multiple-shaker, sine-dwell approach, the majority of experimental dynamists now select the faster random-force methods for modal testing.

A standard step in the data-reduction phase of most modal test programs is the computation of frequency-domain characteristics of the measured structural responses. In controlled ground vibration tests where the input force(s) as well as the responses can be accurately measured, acceleration/force frequency response functions are usually formed; in cases where the input forces cannot be measured, the response information alone is used. Many single- and multi-degree-of-freedom algorithms have been developed to identify the structural modal parameters by curvefitting analytical expressions to these data [1]. Single-degree-of-freedom methods use a few data points near each resonant frequency for quickly estimating the modal parameters of one mode at a time. Because in these techniques it is assumed that the overall response near each resonance is dominated by the characteristics of a single mode, however, the degree of modal coupling in any frequency interval significantly affects identification results. On the other hand, multi-degree-of-freedom algorithms, developed to identify the parameters of several modes simultaneously, nearly always work well on data that can be reasonably analyzed with single-degree-of-freedom methods, but may differ appreciably in more difficult cases.

Various aspects of using time-domain response data rather than frequency-domain functions in the experimental modal identification of structures excited by random forces(s) have been discussed previously by Ibrahim [2-6]. An early multi-degree-of-freedom time-domain identification procedure [2] required numerical integration (assuming the measurement of acceleration responses) to obtain displacement and velocity time histories at each response measurement point, in addition to the measured acceleration time histories. This approach was later abandoned in favor of a more straightforward method [3] in which any one of displacement, velocity, or acceleration free-response functions are used in an eigenvalue solution scheme to obtain the desired modal parameters. This newer procedure is referred to in this paper as the ITD ("Ibrahim Time Domain") algorithm. The term "free-response" function is used throughout this paper to denote any of three time response forms which may be used in the identification algorithm: actual free-decays measured following random excitation of a structure; unit-impulse-response functions formed by inverse Fourier transformation of frequency response functions; or "random-decrement" functions [4] computed from random operating time histories.

The ITD algorithm has been used to analyze test data from several structures[7,eg]. As now implemented, the identification process is a "blind" technique, requiring a minimal amount of operator input to compute parameters for many modes from a set of free-response functions. A large number of structural modes, often 20 or more, are identified in a single computer run. In general, the parameters computed for the dominant modes of these structures agreed well with those obtained by other methods. Parameters for modes identified by the ITD analyses, but not determined with other analysis methods, however, lacked verification and their accuracy was rightfully questioned.

The work reported in this paper was initiated to help interpret these experimental results. For this study, computer-simulated free-response data, for linear, multi-mode models with known modal parameters, were processed with the ITD algorithm. The identified parameters were used to quantify the ability and accuracy of the identification process, to look for anomalous numerical behavior under severe identification conditions, and to compare results for ranges of the few user-selectable algorithm constants. The modeling approach consisted of constructing free-response functions for 65 positions on an isotropic, uniform-thickness rectangular plate by the linear summation of the free-responses of the first 15 analytical modes. The mode shapes were obtained from a finite-element analysis, and modal frequencies, damping factors, and response levels were arbitrarily assigned for each desired modal model. Various levels of noise, calculated on an rms-

percentage basis, were superimposed onto the free-response functions.

Techniques for obtaining distortion-free sets of free-response functions from experimental measurements, an important phase in the modal identification process when the ITD algorithm is used, are not addressed in this paper.

Somewhat new terminology is used in describing the algorithm. To avoid confusion in correlating the identification results with the usage of the free-response data in the procedure, complete details of the technique are included. The methods used in constructing the free-response functions and in quantifying the accuracy of identified mode shapes are described in the following report sections. The remainder of the report contains a summary of the identification results. These data illustrate typical identification accuracies over a wide range of simulated modal models and user-selectable algorithm constants.

LIST OF SYMBOLS

$a_k + ib_k$	k'th complex eigenvalue of [A]
$[A]$	the "system" matrix
$[A]^T$	Transpose of [A]
C	a damping coefficient
$(C/C_c)_k$	damping factor (fraction of critical damping) of k'th mode
f_k	frequency corresponding to k'th eigenvalue of [A]
f_x	multiples of the frequency $1/(2(\Delta t)_3)$
f_π	"folding frequency" based on $(\Delta t)_1$
i	measurement station index
j	time index
k	mode index
K	a spring constant
m	number of assumed modes (= NDOF)
M	a mass
N_1, N_2, N_3	number of time samples corresponding to $(\Delta t)_1$, $(\Delta t)_2$, and $(\Delta t)_3$
p_o	number of response measurements available
s	number of time samples in each free-response function (= NCOL)
t_j	time instant j
T	total time length of response functions
x_{ij}	free-response of station i at time instant j
$(\Delta t)_1$	time increment between the two response matrices, $[\Phi]$ and $[\hat{\Phi}]$
$(\Delta t)_2$	time increment in forming "transformed stations"
$(\Delta t)_3$	time increment between data in upper and lower halves of the response matrices
$\Delta\tau$	an arbitrary time increment
ϵ	a small uncertainty in an eigenvalue determination
θ_k	angular position of k'th eigenvalue in the a-b plane
λ_k	characteristic value of mode k
$[\Lambda]$	a matrix of complex exponentials
σ_k	damping value of k'th mode (= real part of characteristic value)
σ_{k2}	damping value of k'th mode using alternate method
$[\Phi]$	response matrix whose rows contain the free-response functions
$[\hat{\Phi}]$	The $[\Phi]$ matrix delayed $(\Delta t)_1$
$\{\psi\}_k$	complex eigenvector of mode k
$[\Psi]$	matrix whose columns are the system's eigenvectors
$[\hat{\Psi}]$	the $[\Psi]$ matrix with responses delayed $(\Delta t)_1$
$(\omega_d)_k$	damped natural frequency of k'th mode (= imaginary part of characteristic value)
$(\omega_n)_k$	undamped natural frequency of k'th mode

Abbreviations

ITD	Ibrahim Time Domain (technique)
MAR	Modal Amplitude Ratio
MCF	Modal Confidence Factor
MSCC	Mode Shape Correlation Constant
NCOL	Number of Columns in $[\Phi]$ and $[\hat{\Phi}]$
NST	Number of (measurement) Stations used in calculation of OAMCF
OAMCF	Overall Modal Confidence Factor
RMS	Root-Mean-Square (value)
SF	data Sampling Frequency (= reciprocal of time interval between data samples)

THEORY OF THE IDENTIFICATION TECHNIQUE

The Eigenvalue Solution Approach

The characteristic equation for a classical single-degree-of-freedom structural system, governed during its free response by

$$M\ddot{x} + C\dot{x} + Kx = 0 \qquad (1)$$

is $\lambda^2 M + \lambda C + K = 0$, and the general solution form is $x(t) = \psi e^{\lambda t}$. For an overdamped system, ψ and λ are both real-valued; for an underdamped system, they are complex, occurring in conjugate pairs.

In the more common underdamped case, the roots of the characteristic equation

are $\lambda = \sigma \pm i\,\omega_d$, where ω_d is the damped natural frequency in radians/second, $\omega_n = \sqrt{\sigma^2 + \omega_d^2}$ the undamped natural frequency, and $\zeta = \sigma/\omega_n$ the damping factor or fraction of critical damping, C/C_c.

For a linear multi-degree-of-freedom system with m excited modes, the free response of the structure at any (measurement) station i and instant of time t_j can be expressed by the summation of the individual response of each mode as:

$$x_i(t_j) = x_{ij} = \sum_{k=1}^{2m} \psi_{ik}\, e^{\lambda_k t_j} \qquad (2)$$

where ψ_{ik} and λ_k are both complex numbers, in general. Note that the summation extends to $2m$ since there are $2m$ roots of the characteristic equation.

Free-response values for $2m$ stations and s instants of time, calculated using Eq. (2), can be arranged into matrix form as:

$$\begin{bmatrix} x_{11} & x_{12} & \cdots & x_{1s} \\ x_{21} & x_{22} & \cdots & x_{2s} \\ \cdot & & & \cdot \\ \cdot & & & \cdot \\ \cdot & & & \cdot \\ x_{2m,1} & & \cdots & x_{2m,s} \end{bmatrix}$$

$$= \begin{bmatrix} \psi_{11} & \psi_{12} & \cdots & \psi_{1,2m} \\ \psi_{21} & \psi_{22} & \cdots & \psi_{2,2m} \\ \cdot & & & \cdot \\ \cdot & & & \cdot \\ \cdot & & & \cdot \\ \psi_{2m,1} & & \cdots & \psi_{2m,2m} \end{bmatrix} \times$$

$$\begin{bmatrix} e^{\lambda_1 t_1} & e^{\lambda_1 t_2} & \cdots & e^{\lambda_1 t_s} \\ e^{\lambda_2 t_1} & e^{\lambda_2 t_2} & \cdots & e^{\lambda_2 t_s} \\ \cdot & & & \cdot \\ \cdot & & & \cdot \\ \cdot & & & \cdot \\ e^{\lambda_{2m} t_1} & & \cdots & e^{\lambda_{2m} t_s} \end{bmatrix} \qquad (3)$$

or simply

$$[\Phi] = [\Psi]\,[\Lambda] \qquad (4)$$

$$(2m \times s) = (2m \times 2m)(2m \times s)$$

Similarly, free-response values $(\Delta t)_1$ later in time than those in Eq. (2), measured at the same stations, can be expressed as:

$$x_i\left[t_j + (\Delta t)_1\right] = \sum_{k=1}^{2m} \psi_{ik}\, e^{\lambda_k\left[t_j + (\Delta t)_1\right]}$$

$$= \sum \left[\psi_{ik}\, e^{\lambda_k (\Delta t)_1}\right] e^{\lambda_k t_j}$$

$$= \sum_{k=1}^{2m} \hat{\psi}_{ik}\, e^{\lambda_k t_j} \qquad (5)$$

or, in matrix form, for $2m$ stations and s instants of time:

$$[\hat{\Phi}] = [\hat{\Psi}]\,[\Lambda] \qquad (6)$$

$$(2m \times s) = (2m \times 2m)(2m \times s)$$

For $s >= 2m$, $[\Psi]$ and $[\hat{\Psi}]$ are related through Eqs. (4) and (6), eliminating $[\Lambda]$, by:

$$[A]\,[\Psi] = [\hat{\Psi}] \qquad (7)$$

$$(2m \times 2m)(2m \times 2m) = (2m \times 2m)$$

where

$$[\Phi]^T\,[A]^T = [\hat{\Phi}]^T \qquad (8)$$

$$(s \times 2m)(2m \times 2m) = (s \times 2m)$$

Since the columns of $[\Psi]$ and $[\hat{\Psi}]$ are related from Eq. (5) by $\{\hat{\Psi}\}_k = e^{\lambda_k (\Delta t)_1} \{\Psi\}_k$, the complete system can now be placed in the form of a single eigenvalue problem as:

$$[A]\{\psi\}_k = e^{\lambda_k (\Delta t)_1} \{\psi\}_k \qquad (9)$$

The matrix $[A]$ is referred to in this paper as the "system matrix," and contains information characterizing the complete set of modal parameters of the system.

The desired structural (damped) natural frequencies and damping factors are determined from the eigenvalues of $[A]$, $e^{\lambda_k(\Delta t)_1} = a_k + ib_k$, by:

$$(\omega_d)_k = 2\pi f_k = \frac{1}{(\Delta t)_1} \tan^{-1}(b_k/a_k)$$

$$\sigma_k = \frac{1}{2(\Delta t)_1} \ln(a_k^2 + b_k^2) \qquad (10)$$

$$(C/C_c)_k = \frac{\sigma_k}{\sqrt{\sigma_k^2 + (\omega_d)_k^2}}$$

The eigenvectors of $[A]$ are the desired (complex) structural mode shapes, $\{\psi\}_k$.

Equations (8) and (9) form the basics of the solution approach: free-response functions are placed into the rows of Φ and $\hat{\Phi}$; $[A]^T$ is obtained by a least-squares solution of Eq. (8); and the complex eigenvalues and eigenvectors of $[A]$ are then found, to which the system's modal parameters are directly related.

The dimension 'm' is referred to throughout this paper as the "number of allowed (computational) degrees-of-freedom," NDOF. This term should not be confused with the more widely used meaning of "degrees-of-freedom" as the number of independent spatial coordinates necessary to define the motion of a system. The "number of assumed modes" or the "order of the math model" are other descriptors that have been used to denote this fundamental analysis constant. The matrix dimension 's,' the number of columns in $[\Phi]$ amd $[\hat{\Phi}]$ (i.e., the number of time samples used from each free-response function), is referred to throughout as NCOL. The matrices $[\Phi]$ and $[\hat{\Phi}]$ are referred to as the two "response matrices."

Three distinct, user-selectable, time shifts are used in positioning overlapping segments of the measured free-response functions into the rows of the response matrices. The fundamental time increment between all data placed into $[\Phi]$ and $[\hat{\Phi}]$ is $(\Delta t)_1$. Two other time shifts, denoted by $(\Delta t)_2$ and $(\Delta t)_3$, will be discussed in the report section entitled "Transformed Stations and Modal Confidence Factors." The number of consecutive time samples corresponding to each of the shifts will be denoted hereafter by simply N_1, N_2, and N_3, respectively.

Figure 1 provides an example of the placement of free-response data into the two response matrices, assuming that three response functions are available. In this example, NDOF and NCOL are selected equal to 7 and 30, and the three data shifts, N_1, N_2, and N_3, are 3, 8, and 4. This figure should be used as a reference in clarifying the definition of each of these five primary user-selectable analysis constants.

Solution Considerations

Equations (8) and (9) are forms whose computer solution have been studied in depth by numerical analysts. Eq. (8) is an over-determined system of simultaneous linear equations, and Eq. (9) is an algebraic eigenvalue problem, where the (2m) eigenvalues of $[A]$ are $e^{\lambda_k(\Delta t)_1}$ and the corresponding eigenvectors are $\{\psi\}_k$.

The "conventional transpose approach" of solving Eq. (8) consists of pre-multiplying both sides by $[\Phi]$ and then solving for $[A]^T$ by any of several methods for the solution of 2m simultaneous linear equations in 2m unknowns. This is the approach used for the results shown in this paper. In particular, pre-multiplying Eq. (8) by $[\Phi]$ results in:

$$([\Phi]\,[\Phi]^T)\,[A]^T = ([\Phi]\,[\hat{\Phi}]^T) \qquad (11)$$

Equation (11) was then solved by a standard Gaussian elimination subroutine using an LU decomposition of the $([\Phi]\,[\Phi]^T)$ matrix of coefficients.

Other methods are available for solving Eq. (8) which do not require the pre-multiplication of each side by $[\Phi]$, [8,9]. These methods have been developed for the express purpose of increasing the solution accuracy when the matrix of coefficients, in this case $[\Phi]^T$, is ill-conditioned; the pre-multiplication will increase any ill-conditioning of the coefficient matrix. A limited number of comparison identifications have been run using two other computer subroutines available for the solution of Eq. (8), namely:

1. by singular value decomposition of the coefficient matrix using Householder transformations, obtaining the isometric matrix $[U]$ and orthogonal matrix $[V]$,

such that $[\Phi]^T=[U][Q][V]^T$, where the singular values comprise the diagonal matrix [Q]. The least-squares solution is then formed by $[A]^T=[V][Q\dagger][U]^T[\Phi]^T$, where $[Q\dagger]$ contains the reciprocals of the non-zero values of [Q].

2. by using Householder transformations to perform the QR decomposition of the coefficient matrix, where [Q] is an orthogonal matrix and [R] is an upper triangular matrix. The least-squares solution is then formed as $[A]^T=[R]^{-1}[Q_1]^T[\Phi]^T$, where [Q] is partitioned in the form $[Q]=(Q_1,Q_2)$ with $[\Phi]^T=[Q_1][R]$.

In all cases run using these other methods, no changes in the computed modal parameters were observed to the precision used in printing the results shown in this paper. On the other hand, each of the two methods described above required considerably more computer memory to implement using available FORTRAN subroutines than the conventional transpose approach. In both cases, the $[\Phi]^T$ and $[\hat{\Phi}]^T$ matrices--each of size $(s \times 2m)$--needed to reside in core, whereas the transpose method was implemented with two matrices of order 2m each. For a typical s/2m ratio of 3 used in many of the identifications, selection of either optional solution method required a factor of 6 times more core storage.

The details of available techniques for the solution of Eq. (8) are compiled in several numerical analysis textbooks [8,9]. A subroutine pack containing a standardized set of computer code for implementing these methods is available [10].

The numerical techniques for solving Eq. (9) are not as plentiful; the QR method advocated by Wilkinson [8,11], is the accepted approach for determining the complete set of real and complex eigenvalues and eigenvectors of [A], a fully-populated general matrix with real elements. This is the method used to obtain all results presented in this paper. A subroutine pack [12] containing standardized code for the computer solution of eigenvalue problems is also available.

"Transformed Stations" and "Modal Confidence Factors"

Two aspects of the practical implementation of the method described thus far, which have been discussed in previous papers [2,3,5], are: (1) processing data when the number of available free-response measurements is less than the number of rows in $[\Phi]$ (equal to twice the number of degrees-of-freedom desired in the identification process), and (2) distinguishing those eigenvalues of [A] corresponding to the desired structural modes from those eigenvalues corresponding to "noise modes," computed whenever NDOF is larger than the number of structural modes contributing to the responses.

When the number of response measurements that are available, say p_o, is less than the number of computational degrees-of-freedom which are desired, fewer than half the rows of $[\Phi]$ are filled by the original, unshifted, response functions. Under these circumstances, "assumed" or "transformed" stations [2] are created for the additional rows of both response matrices by simply shifting the original functions placed in the first p_o rows by multiples of a second user-selectable time shift, $(\Delta t)_2$: $(\Delta t)_2$, $2(\Delta t)_2$, $3(\Delta t)_2$, etc., until the upper halves of both matrices are filled. This process of adding transformed stations does not mathematically affect the eigenvalues of the system matrix, [A], assuming perfect identification. (If NDOF is selected smaller than p_o, only NDOF of the available response functions are used in the analysis.)

The bottom halves of the two response matrices are formed by duplicating the upper rows, but delaying an additional user-selectable time shift, $(\Delta t)_3$. The rationale for filling only the upper halves of the matrices with the available response functions (and transformed stations) and filling the bottom halves with a time-shifted form of the upper halves is based on the calculation of "Modal Confidence Factors," to be discussed next.

If two segments of a free-response function obtained from the same measurement station, but separated by an arbitrary time interval $\Delta\tau$, are placed into different rows of the response matrices, the elements in each computed eigenvector of [A] corresponding to these two rows, ψ_{ik} and $\psi^{\dagger}_{ik}$, will be related (again assuming perfect identification) by:

$$\psi^{\dagger}_{ik} = \psi_{ik}\, e^{\lambda_k \Delta\tau} \qquad (12)$$

for each linear structural mode k.

This fundamental property, Eq. (12), and the time-shift relationship between the data in the upper and lower halves of the response matrices, $(\Delta t)_3$, are used in the calculation of "Modal Confidence Factors," MCF [5], devised to distinguish "noise modes" from the desired structural modes. The (complex-valued) MCF's for accurately identified linear structural modes--one MCF calculated for each of the first p_o elements in each computed (complex) eigenvector of [A]--will cluster near unity in amplitude and near 0° in phase; those calculated for "noise modes" will be randomly distributed in value. To form the MCF's, the first p_o elements in the lower halves of the computed eigenvectors are compared with "expected" values for these elements, calculated using Eq. (12) by the product of the corresponding p_o upper-half eigenvector elements and the complex exponentials, $e^{\lambda_k (\Delta t)_3}$, where λ_k are the computed characteristic values. The MCF is defined as the amplitude ratio and phase difference between each of these "expected" values and the corresponding values computed by the eigenvalue analysis. If the amplitude ratio is greater than 1.0, the reciprocal is taken. The phase angle is normalized to range between -180° and 180°. Obtaining MCF values near 100% in amplitude and 0° in phase is certainly a necessary (but not sufficient) condition to indicate that an accurate identification of a linear structural mode of the system has been made.

This process can be thought of as the comparison of two sets of eigenvectors, corresponding to the same set of eigenvalues, computed simultaneously for the system using two different segments of the available free-response functions. An important user advantage in obtaining both sets of eigenvectors in one eigensolution is that no effort is needed to "pair up" corresponding eigenvectors if somewhat different eigenvalues are computed for each set of segments. A single eigenvalue set is obtained using information derived from both sets of data, and the two eigenvector sets are correctly compared in the computer analysis with no user decisions required.

An MCF is calculated in this manner for each of the p_o stations, for each identified complex eigenvalue. To compact this information to a more manageable level, an "Overall MCF," OAMCF, is calculated for each computed complex eigenvalue) as the percentage of p_o stations whose MCF values are at least 95% in amplitude and within 10° of 0.0 in phase. The OAMCF parameter, introduced for this study, has been found very effective in distinguishing the desired structural modes from the "noise modes," and is a fundamental part of the identification results presented in this paper. Its value has been found to provide a good characterization of the p_o MCF's calculated for each mode and, in general, a closer examination of the individual station-by-station MCF data was unnecessary.

The time shift $(\Delta t)_3$ should not be selected equal to either $(\Delta t)_1$ or $(\Delta t)_2$. If equal to $(\Delta t)_1$, all MCF's will be computed as 100% in amplitude and 0° in phase, and be of no use. If equal to $(\Delta t)_2$, and at least one transformed station has been used, $[\phi]$ and $[\hat{\phi}]$ will each have two identical rows and Eq. (8) cannot be solved. Setting $(\Delta t)_3$ equal to one-half the value of $(\Delta t)_2$ has been found satisfactory in most cases. To clarify the relationship between these time shifts, refer again to Fig. 1, which shows a typical placement of data into the response matrices when three free-response functions are used.

CONSTRUCTION OF THE SIMULATED FREE-RESPONSE FUNCTIONS

Mode shapes used in constructing the simulated free-response functions were obtained from a NASTRAN finite-element analysis of an isotropic, uniform-thickness plate with 8 × 24 square elements. Data for 65 stations were obtained by using the analytical mode shape data (for motion normal to the plate only) from every other grid point in both directions, including the outside border. The first 15 modes of this analysis were used in forming the responses. For each desired modal model, a damped natural frequency, damping factor, and response amplitude were arbitrarily selected for each mode. The effects of randomizing the initial phase angle for all stations of each mode and of selecting other than 0° or 180° between the stations in a mode (i.e., complex modes) were studied for several cases, and no changes in the identification accuracy were noted. Thus, unless otherwise stated, the contribution of each mode in the responses was represented as a damped cosine function multiplied by an appropriate (positive or negative) mode shape amplitude constant.

That is, each free-response function was formed as

$$x_i(t_j) = \sum_{k=1}^{15} \psi_{ik} \, e^{-\sigma_k t_j} \cos\left[(\omega_d)_k t_j\right] \tag{13}$$

For this study, each simulated free-response function consisted of 1000 data points calculated using Eq. (13), at a sampling rate of 400 samples per second. Uniformly distributed noise was added to these functions on a function-by-function, rms-percentage basis, with the rms value of each noise-free function calculated using all 1000 available data points. The mode shapes used in forming each modal model were assigned to the 15 mode indices in the order determined by the finite-element analysis.

For ease in interpreting identification results, the modal frequencies were arbitrarily selected for all models in this study (i.e., the natural frequencies of the plate obtained from the NASTRAN normal-mode analysis were not used). Many of the simulated models were formed by spacing the 15 modal frequencies every 2 Hz from 10.0 to 38.0 Hz, and setting the modal damping factors and response amplitudes equal for each of the modes. Each of these basic modal models are characterized by a single modal damping factor and noise percentage, and are referred to throughout this paper for simplicity as "baseline models."

EVALUATION OF IDENTIFICATION ACCURACY

The accuracy of all mode shape identifications for this study has been quantified by computing a "Mode Shape Correlation Constant," MSCC, between the identified mode shapes and each of the 15 input mode shapes. The constant is calculated in a manner analogous to that of coherence, often computed in time-series analysis work. The functional form is that of the square of the correlation coefficient defined in basic statistics, computed between two sequences of complex numbers.

Mathematically, if $\{\psi_1\}$ is a known input (complex) mode shape, and $\{\psi_2\}$ is an identified (complex) mode shape:

$$\text{MSCC} = \frac{|\{\psi_1\}^T \{\psi_2\}^*|^2}{[\{\psi_1\}^T \{\psi_1\}^*][\{\psi_2\}^T \{\psi_2\}^*]} \times 100 \tag{14}$$

where ^{T} denotes the transpose and * the complex conjugate.

The MSCC between two mode shapes will always range from zero--for no resemblence of the two shapes--to 100%--for perfect resemblence. Values intermediate between 0.0 and 100.0 can be interpreted as the amount of coherent information in the two compared mode shapes.

The accuracy of identified frequency and damping parameters was assessed by direct observation only.

RESULTS AND DISCUSSION

In processing a set of free-response functions with the identification algorithm, five primary user-selectable constants must be chosen. They are NDOF, NCOL, $(\Delta t)_1$, $(\Delta t)_2$, and $(\Delta t)_3$. Secondary considerations include the selections of data sampling rate and analog or digital filtering ranges, the particular stations to be analyzed in one computer run, and the absolute starting times of the free-response data (i.e., whether any data points are skipped at the beginning of the functions). An optimum selection of the analysis options is a function of the characteristics of the data being analyzed, and "cookbook" instructions are difficult to develop. The results to be shown in this section, however, provide guidelines for their selection and for judging the sensitivity of the choices, and illustrate identification accuracies which may be expected.

All results shown in this paper were obtained using a vectorized version of the code on Langley's CDC Cyber 203 (formerly Star-100) computer. Typical CPU times for identification were 15 seconds for NDOF = 65 and NCOL = 390, and 340 seconds for NDOF = 200 and NCOL = 968. The required computer time varied approximately as the number of columns used in $[\phi]$ and $[\hat{\phi}]$, NCOL, and as the square of the number of allowed computational degrees-of-freedom, NDOF.

Some Baseline Model Results

Figure 2 shows the time- and frequency-domain responses at measurement Station No. 1 (a corner of the plate) for three of the baseline models analyzed in the study. In Figs. 2(a) and 2(b), the damping factor, C/C_c, of all 15 modes was set to 2%. The rms noise levels in these two cases were 2% and 20%, respectively. Similarly, Fig. 2(c) shows the response of Station No. 1 with

all 15 modes assigned 5% damping and 10% noise. The dashed lines on the time history plots designate the range of points used from each function in ITD analyses whose results will be presented in Table I and Figs. 3 through 5. The center and right-hand plots in Fig. 2 show the quadrature (imaginary) component and modulus, respectively, of the Fourier transform of the corresponding free-response function.

Table I contains MSCC values for these three identifications calculated between each of the 15 input mode shapes and each identified mode (whose OAMCF was 2% or larger), rounded to the nearest whole number. Also included are the identified frequencies in Hertz, the identified damping factors in percent, and the OAMCF for each mode. The column to the right of the OAMCF data contains the number of stations of 65, NST, that were used in calculating the corresponding OAMCF value; only those stations with non-negligible modal response (at least 3% of the maximum value of the mode) are included in the calculation. This 3% criterion was imposed on the calculation of OAMCF because many of the selected 65 measurement stations were located exactly on mode shape node lines; the variance in the calculated MCF data for these stations was generally high, as to be expected, because very small modal amplitudes identified for these stations were used in the calculations. Each of these identifications were run using NDOF of 65 and NCOL of 390. The other 50 "modes" obtained in each identification were "noise modes," differentiated by low (<2%) OAMCF values.

For these identifications, the user-selectable time-shift constants, $(\Delta t)_1$, $(\Delta t)_2$, and $(\Delta t)_3$, were set to 3/SF, 8/SF, and 4/SF, respectively, where SF is the data sampling rate. The values $N_1 = 3$, $N_2 = 8$, $N_3 = 4$ were used in obtaining all identification results shown in this paper, unless otherwise noted. (These are the values selected for Fig. 1 in illustrating a typical placement of free-response data into the two response matrices.)

Figure 3 shows the 15 identified (complex) mode shapes for the 2%-damping, 2%-noise baseline model, corresponding to the data contained in Table I. These identified mode shapes are indistinguishable from those used in constructing the model. Note that the ITD algorithm identifies complex mode shapes, consisting of a magnitude and phase at each selected measurement station: the identified mode-shape phase angles are included adjacent to each mode shape, assigned by consecutive station number from the center of the circle to the outer ring, as depicted in the lower-right corner of Fig. 3; the data for the accompanying mode shape plots were obtained by the product of the identified mode-shape amplitudes and the cosine of the corresponding phase angle.

Figures 4 and 5 show the mode shapes identified for the two other baseline models whose results were presented in Table I, also using NDOF of 65 and NCOL of 390 in the analyses. As before, only those "modes" with an OAMCF of at least 2% are shown. In Fig. 4, for the 2%-damping, 20%-noise model, the identified shapes are also indistinguishable from the exact, input mode shapes, and the phase-angle scatter averages only a few degrees. Identification results for the 5%-damping, 10%-noise model, provided in Fig. 5, show mode shapes that are slightly distorted for modes 11 through 14, with significant phase angle scatter in several of the modes. In interpreting these results, however, the reader is cautioned that more accurate identifications are obtainable for these models; as shown later, allowing higher degrees-of-freedom in the identification will increase the accuracy to some degree. These identifications all used NDOF of 65 and NCOL of 390, and the results typify the effects of changing modal damping and noise level while holding all of the algorithm constants fixed.

Note in Table I that an MSCC of 100% was calculated for each of the accurately identified mode shapes of the 2%-damping, 2%-noise baseline model, shown in Fig. 3. Also of interest in these MSCC results is the slight "blending" of the higher-numbered mode shapes for the 5%-damping, 10%-noise model, corresponding to the small distortions seen in the plots in Fig. 5.

The Number of Allowed Degrees-of-Freedom

The number of computational degrees-of-freedom allowed in the identification, NDOF, should be selected equal to the number of modes excited in the responses if the free-response functions are noise-free. For any deviation of the response data from the exact analytical form--that is, some level of superimposed noise--more degrees-of-freedom than this must be allowed for accurate identification. It is somewhat intuitive that better identification of the underlying deterministic modal data may result when one allows for the calculation of extra "noise modes," in addition to the number of actual structural modes contributing to the responses, to provide

an outlet in the assumed model for the noise contribution.

To illustrate the effect of increasing the allowed degrees-of-freedom, identified modal frequencies for the 2%-damping baseline model, using values of NDOF from 1 to 75, are plotted in Figs. 6 and 7 for each of eight increasing levels of superimposed noise. At each value of NDOF, the identified frequencies are denoted by vertical line segments at the corresponding frequencies, whose heights are proportional to the OAMCF value computed for each mode. As before, only those identified "modes" with negligible OAMCF (less than 2%) are not shown. When the individual segments align to form a solid, vertical line, the OAMCF's are all 100% and the identified modal frequency is invariant with increasing NDOF. On examining these eight plots, a consistent trend in the requirement for increased degrees-of-freedom to accurately identify all 15 frequencies, with increased noise level, is noted. Another interesting trend is that after an NDOF level is attained for each noise level where all 15 frequencies are accurate, increasing NDOF above this value did not degrade the frequency identification accuracy. These plots will be referred to as "NDOF-frequency maps," and have been found very useful in interpreting experimental identification results. The identifications at each NDOF level in Figs. 6 and 7 were run using NCOL of 300.

The lowest value of NDOF for accurate identification has been found in this study to be related to the signal-to-noise ratios of the modal responses. The considerable shifting of the frequency "lines" in these NDOF-frequency maps at low values of NDOF results largely from setting all 15 modal response levels equal. When experimental data are processed, the lowest NDOF values for identification of each made vary considerably more between modes than the data shown in Figs. 6 and 7, due to different response levels, and almost no line shifting occurs.

Typical accuracy at much higher allowed degrees-of-freedom are included in Table II for the 2%-damping, 20%-noise baseline model with analyses at NDOF of 65, 200, 250, and 300. These identifications used all 1000 data points in each of the 65 response functions; that is, NCOL was made as large as possible in each case. Although the parameters for all 15 modes are of acceptable accuracy for most applications at NDOF of 200, it is interesting that the accuracy (of the damping factors) continued to increase as NDOF was raised beyond this point. Only those "modes" with an OAMCF of less than 2% are excluded from these results; at NDOF of 300, for example, 285 additional "noise modes" were computed, all of which are differentiated by the OAMCF parameter. Also very important is that no anomalous identification problems or numerical instabilities were observed in this or any other identification conducted in this study using such high values of NDOF. These results suggest that the ITD algorithm, used with a high number of degrees-of-freedom, may accurately identify all of the excited structural modes, for large modal surveys, in one computer run.

Note that the results shown in Table II for NDOF of 65 were not as accurate as those shown earlier in Table I for analysis of the same 2%-damping, 20%-noise baseline model; the results in Table I were obtained using NCOL of 390 and those in Table II with NCOL of 993. The effects of the selection of NCOL on identification accuracy will be addressed in a later report section.

The Selection of $(\Delta t)_1$

To help understand the effects of the user-selectable algorithm constant $(\Delta t)_1$ (the time increment between corresponding data in the two response matrices), note from Eq. (9) that the computed eigenvalues of $[A]$, $a_k + ib_k$, are exponential functions of the product of the system's characteristic values, λ_k, and $(\Delta t)_1$. The desired structural modal frequencies and damping factors are then calculated directly from these eigenvalues by Eqs. (10). Using these relationships, loci of constant damping factor are plotted in Fig. 8 in the complex a-b plane, for $f_d = \omega_d/(2\pi)$ ranging from 0 to $1/(2(\Delta t)_1)$. A typical eigenvalue of $[A]$ is denoted by point 'k,' whose corresponding natural frequency in radians/sec is simply the angle θ_k divided by $(\Delta t)_1$. Since equal damping values, σ_k, lie on equal radii in the a-b plane, by Eq. (10), the contours of constant damping factor (equal to the damping value divided by the undamped natural frequency) will converge to the point (1,0) for $f_d = 0$ and separate from one another as f_d increases. As C/C_c increases, the contours lie inside one another, until, at 100%, the locus is simply the positive x-axis.

The frequency in Hertz corresponding to $\theta_k = \pi$, denoted as f_π, is the

point at which the identified frequencies will "fold" because of the circular nature of the exponential function--analogous to the well-known "Nyquist folding-frequency" which results from the circular nature of the discrete Fourier Transform. That is, all identified frequencies will fall in the range 0 to f_π, regardless of their actual value; only those modal frequencies no larger than f_π will be correctly calculated. The value of f_π is simply $1/(2(\Delta t)_1)$. Of course, this "eigenvalue aliasing" will lead to erroneous frequency and damping factor results for modes with frequencies greater than f_π contributing to the response functions used in the identification; as with the well-understood Nyquist-frequency aliasing, however, the phenomenon can also be used beneficially, with the results accordingly adjusted, if the data are pre-filtered to contain information only in a certain, known frequency interval.

Obviously, for two eigenvalues of [A] separated by ε, any inaccuracy in their calculation may translate to a considerable inaccuracy in their corresponding modal frequencies and damping factors, depending on the location in the a-b plane. To quantify this characteristic, Fig. 9 provides contours of minimum and maximum percent deviation in the identified modal frequencies and damping factors for three magnitudes of uncertainty in the eigenvalue determination. Note, in Fig. 9(a), that percent frequency deviations are nearly independent of damping level, and are large only for values less than $0.1\ f_\pi$ (because the data are shown on a percent-deviation basis, and f is small in this range). For all three uncertainty levels, the percent frequency deviations are no greater than 2% at all frequencies at least $0.2\ f_\pi$, for $C/C_c \leq 10\%$. The envelopes of maximum percent deviation in the damping factor identification, on the other hand, are considerably larger, as shown in Fig. 9(b). These data suggest that damping factors derived from eigenvalues of [A] subtending small angles in the a-b plane may be subject to appreciable error.

As $(\Delta t)_1$ increases, the frequency interval corresponding to eigenvalues located at $\theta_k = 0$ and $\theta_k = \pi$ decreases, and the eigenvalues for any two modal frequencies separate in the a-b plane. When this occurs, a more accurate analysis generally can be made of a smaller total frequency interval. Figure 10 shows typical results of this effect in the identification of the 2%-damping, 20%-noise baseline model for two selections of N_1 (the number of data samples corresponding to the time-shift interval $(\Delta t)_1$). The results in Fig. 10(a) were obtained with $N_1 = 1$ and those in Fig. 10(b) with $N_1 = 3$, holding all other algorithm constants unchanged. In the polar plots of Fig. 10, the symbols denote the locations of all identified eigenvalues of [A] in the a-b plane; the eigenvalues corresponding to the 15 structural modes, distinguishable from the "noise modes" whose OAMCF's were all less than 2%, lie approximately equally spaced along the 2%-damping (dashed) line in each figure. As shown in the tabulated results, the identification accuracies of both damping factors and mode shapes were improved when N_1 was increased from 1 to 3.

An Alternate Method for Calculating Modal Damping

In addition to the straightforward calculation method for the desired modal damping factors using the eigenvalues of [A], shown in Eq. (10), limited study has been done of an alternate method using the first p_o elements in the upper and lower halves of the computed eigenvectors--data used previously in computing the MCF values. Based on experience, the identified damping factors often show the greatest variance of all the computed modal parameters. By assuming that the eigenvector data are more accurate than the identified damping data, a method similar to the reverse process used in computing the MCF data can be used to obtain a second estimate of the modal damping factors.

Mathematically, a form analogous to that for obtaining the amplitude of a frequency response function using the Fourier components of input and response signals can be used to compute an average modal amplitude ratio between the 'upper' and 'lower,' p_o-element, mode shape vectors. In particular, if $\{\psi_U\}$ is an upper identified (complex) mode shape, and $\{\psi_L\}$ is a lower identified (complex) mode shape, a Modal Amplitude Ratio (MAR) can be calculated as:

$$MAR = \frac{|\{\psi_U\}^T \{\psi_L\}^*|}{\{\psi_U\}^T \{\psi_U\}^*} \qquad (15)$$

from which an alternate modal damping factor can be calculated, using the corresponding damped natural frequency, ω_d, obtained directly from the eigenvalue of [A], by:

$$(C/C_c)_k = \frac{\sigma_{k2}}{\sqrt{\sigma_{k2}^2 + (\omega_d)_k^2}} \qquad (16)$$

where $\sigma_{k2} = \ln(MAR)/(\Delta t)_3$.

This estimate of modal damping was found more accurate in many cases--but not all--particularly for modes with poor signal-to-noise ratios. Figure 11 shows modal damping factors identified by each of the two methods for the 2%-damping, 50%-noise baseline model for NDOF in steps of 20 from 60 to 200. Only data for the first 10 modes are included. Although the data for modes 1 and 2 (circle and square symbols) are significantly over-estimated by either method, overall, the data in Fig. 11(b), obtained indirectly using the eigenvector and identified frequency data, cluster appreciably closer to the true value of 2% than the data in Fig. 11(a), calculated directly from the eigenvalues of [A].

When the modal damping is calculated using this alternate method, an MSCC between the upper and lower p_o-element vectors used in the calculation should also be formed to be used as an indication of the consistency of the eigenvector data, which may itself be inaccurate. A conservative approach would certainly be to calculate the damping factors by both methods, and use any discrepancy in their values as a indicator of inaccurate identification. Unless otherwise noted, the damping identification results shown in this paper were obtained using the direct calculation method from the eigenvalues of [A].

Modal Response Level

In all identification results presented thus far, the response levels of all 15 modes in the simulated models were set equal; for actual experimental data this would not be the case. To examine identification accuracy of modes with significantly different response level, Figs. 12(a) and 12(b) show NDOF-frequency maps for the 2%-damping, 2%-noise baseline model when the response level of mode 8 (at 24 Hz) was reduced to 1% and 5%, respectively, of the level selected for each of the other 14 modes. The 1%-response case represents the approximate lower limit at which this mode was identifiable for NDOF up to 75. Compared with a similar plot shown earlier in Fig. 6(c) for all modes of equal response level, note that these plots have several randomly scattered dots, corresponding to "modes" with OAMCF less than 2%, the cutoff used for plotting the data shown in Figs. 6 and 7. This cutoff criterion was removed for these plots to allow the 24-Hz mode data in Fig. 12(a) to be discernible.

Although Figs. 12(a) and 12(b) show that the 24-Hz modal frequency was identified in both cases, these data do not indicate the accuracy of either the identified mode shapes or modal damping factors; this information is included in Figs. 12(c) and 12(d), respectively. In Fig. 12(c), MSCC's calculated between the identified mode shapes and the known input shape are plotted for each case as a function of NDOF. For the 5%-response case, denoted by the square symbols, the MSCC is essentially 100% for all NDOF above 46; for the 1%-response case, on the other hand, the MSCC value does not rise above the 83% level. In fact, when the 1%-response model was analyzed using NDOF of 250, the MSCC of the 24-Hz mode remained at approximately 83%.

Identified modal damping factors for these cases, calculated both using Eq. (10) and by the alternate method discussed in the previous report section, are shown in Fig. 12(d). In all cases, the data appear to be approaching the correct value of 2% with increasing NDOF; the results for the 5%-response case being closer to the true value than those for the 1%-response case. Additionally, the damping factors calculated by the alternate method using the computed eigenvector data are more accurate at each value of NDOF than the damping factors calculated directly from the identified eigenvalues of [A].

The Selection of NCOL

In establishing the two response matrices, both the number of rows (equal to twice NDOF) and the number of columns, NCOL, must be selected for each identification. As shown in NDOF-frequency maps in Figs. 6, 7, 12(a), and 12(b), the minimum required NDOF is related to the signal-to-noise ratio of the modes. The value for NCOL, denoted by 's' in the THEORY section of this report, is restricted to be at least twice NDOF, so that Eq. (8) contains no fewer equations than unknowns. An intuitive upper limit in selecting NCOL corresponds to the time at which the free-response signal for the mode to be identified becomes smaller than the noise level; beyond this point each additional data point used from the response functions would provide more noise than additional information to the identification algorithm.

The effects of the selection of NCOL on identification results for the 2%-damping, 20%-noise baseline model are shown in Fig. 13. To estimate the time at which the superimposed noise exceeds the signal information in the free-responses, a 20-point, running mean-square value, averaged over all 65 functions used for the model, is plotted in Fig. 13(a). These data have been normalized so that the asymptotically approached noise level corresponds to 0 dB. Since all 15 modes have the same response level in this model, the mean-square value of the free-response signal for each mode equals the mean-square noise level when the function of Fig. 13(a) equals 10 log(16) or 12 dB. This corresponds to NCOL of approximately 225.

Using NDOF of 65, all 15 modal frequencies for this model were accurately identified for NCOL ranging from 200 to 950, and their values are not shown. Of interest, though, are the corresponding MSCC values and identified modal damping factors for these cases. These results are shown in Figs. 13(b) and 13(c), respectively. To maintain clarity, data for only the first five modes (which typify the results obtained for all 15 identified structural modes) are included. Of particular interest in these figures is the rapid deterioration of the identification results when NCOL is less than 200. Above NCOL of 200, the MSCC data are affected only slightly as NCOL increases to 950, although a slight downward trend is noted for NCOL greater than 300. Optimum mode shape identification was obtained for NCOL ranging from 200 to 300. The identified modal damping factors, on the other hand, diverge from the selected value of 2% considerably faster than the MSCC data from 100%, as shown in Fig. 13(c). Selecting NCOL near 200 would also provide the best damping identification over the range of NCOL from 170 to 950. It is of interest to note that the identified damping factors in Fig. 13(c) all tend to approach the correct value of 2% as NCOL decreases. This effect is similar to that shown in Fig. 11(a) for an increase in NDOF with NCOL held constant.

Close Natural Frequencies

A classic problem using any modal identification technique is the accurate determination of the modal parameters for two or more structural modes of approximately the same natural frequency. Assuming no attempt was made to apportion the force used in exciting the structure, the response levels of two modes close in frequency may well be approximately equal in a set of response measurements obtained during wide-band force excitation. If T seconds of data are available for analysis, the corresponding frequency-domain functions will be determined to a resolution of 1/T Hz by Fourier methods. For the models constructed in this study, T = 2.5 seconds, which corresponds to a frequency resolution of 0.4 Hz. To obtain accurate modal parameters with methods that rely on visual determination of response peaks in frequency spectra or frequency response functions is unreasonable when the modal frequency separation approaches the frequency resolution value.

To study the frequency resolution ability of the ITD algorithm, several modal models were constructed by moving the frequency of mode 8, originally at 24.0 Hz in the baseline model, to a lower value, close to mode 7 at 22.0 Hz. All 14 other modes were maintained at their original spacing of 2 Hz from 10.0 to 38.0 Hz. Table III shows the identification results using the 2%-damping, 2%-noise baseline model, for 0.10, 0.05, and 0.01 Hz frequency separation between modes 7 and 8. Sixty-five degrees-of-freedom, with NCOL of 390, were used in the identifications. At each frequency separation value, the damping in mode 8 was successively changed from 2% (the same value assigned to mode 7), to 3%, to 10%. For all three frequency separations, near-perfect identification of the parameters for all 15 modes was obtained for the cases when the mode 8 damping was either 3% or 10%. Identification accuracy of modes 7 and 8 in the cases where both modes were assigned 2% damping successively deteriorated as the frequency separation was decreased. These trends are consistent with the fact that two modes, although of equal natural frequency, will correspond to different eigenvalues of [A] if their damping factors are different—the larger the difference in damping, the larger the corresponding eigenvalue separation.

To extend the study of eigenvalue resolution one step further, modal models were constructed with five of the 15 modal frequencies set to 22.0 Hz. Figure 14 provides identification results for two of these models: Fig. 14(a) with the five modes assigned damping factors of 1, 2, 3, 4 and 5%; and Fig. 14(b) with damping factor assignments of 2, 4, 6, 8 and 10%. Of course, as shown in the frequency spectrum plots, only one response peak is discernible at 22 Hz in both cases. The parameters of all 15 modes were accurately identified in each model, as shown, when the

percentage of added noise was held to a very low level: 0.01% in the $\Delta C/C_c$ = 1% case and 0.1% in the $\Delta C/C_c$ = 2% case. Although these noise levels are extremely low--often unattainable with experimental data--these results do illustrate the potential accuracy of the method and the relationship between noise level and the attainable eigenvalue resolution. These two identifications were run with NDOF of 65; the same models could be identified with somewhat higher noise levels at the (computational) expense of allowing more degrees-of-freedom.

A Condition on the Selection of $(\Delta t)_3$

The selection of the time shift between the upper and lower halves of the two response matrices, $(\Delta t)_3$, can significantly affect the identification accuracy of modes at or near certain frequencies; in particular, if all of the data in the lower halves are obtained by delaying the data in the upper halves by $(\Delta t)_3$, frequencies $f_x = n/(2(\Delta t)_3)$, for integer values of n, will not be identified. Using a different time shift on one or more of the stations will help alleviate this problem, which may occur whenever $f_x < f_\pi$. Of course, selecting $(\Delta t)_3 < (\Delta t)_1$ will always eliminate the condition by forcing the lowest value of f_x to be larger than f_π, the upper limit of the analysis range.

CONCLUDING REMARKS

Using simulated free-response functions, the Ibrahim Time Domain (ITD) algorithm has been found capable of accurately identifying known, structural modal parameters over a wide range of frequency separations, damping factors, mode response levels, signal-to-noise ratios, and user-selectable algorithm constants. It has been found that the modal parameters can often be identified in cases of poor signal-to-noise ratio if sufficient computational degrees-of-freedom are allowed in the identification process. A significant finding is that no detrimental effects were observed when many times more degrees-of-freedom were allowed than the minimum necessary for reasonable identification; this result suggests the use of a high number of degrees-of-freedom for the "blind" use of the algorithm in analyzing experimental data.

For many of the models analyzed, the identified modal frequencies and mode shapes were more accurate than the corresponding modal damping factors. When the identified damping factors were plotted as a function of either the number of allowed degrees-of-freedom, NDOF, or the number of time samples used from each response function, NCOL, however, the correct values were often asymptotically approached. An alternate method for calculating modal damping, using the identified eigenvectors and modal frequencies, was found more accurate in some instances than using the identified eigenvalues directly.

For each set of user-selectable algorithm constants, direct correlation was found between the variance in the identification results and the signal-to-noise level of the responses. In analyzing noisy data, when sufficient degrees-of-freedom were allowed in the analyses, all natural frequencies and mode shapes were identified with good accuracy in nearly every instance. Low values of Overall Modal Confidence Factor, OAMCF, for modes with reasonably identified mode shapes, were usually indicative of inaccuracy in the estimated damping factors. For noise-free input data, the identification accuracy of all parameters approached the computational accuracy of the computer.

The required computer time varied approximately as the number of columns in the response matrices, NCOL, and as the square of the number of allowed degrees-of-freedom, NDOF. Typical CPU times for identification on the CDC Cyber 203 computer were 15 seconds using NDOF of 65 and NCOL of 390, and 340 seconds using NDOF of 200 and NCOL of 968.

Related areas of work which need further attention include the study of:

1. techniques to minimize noise and distortion on free-response functions from experimental measurements;
2. effects of structural nonlinearities on ITD identification results; and
3. resolution and roundoff errors which may occur in using the technique on smaller-wordlength computers.

REFERENCES

[1] Brown, D. L., Allemang, R. J., Zimmerman, R., and Mergeay, M.: Parameter Estimation Techniques for Modal Analysis. SAE Paper 790221. Feb. 1979.

[2] Ibrahim, S. R., and Mikulcik, E. C.: The Experimental Determination of Vibration Parameters from Time Responses. Shock and Vibration Bulletin. No. 46, Part 5, Aug. 1976, pp. 187-196.

[3] Ibrahim, S. R., and Mikulcik, E. C.: A Method for the Direct Identification of Vibration Parameters from the Free Response. Shock and Vibration Bulletin. No. 47, Part 4, Sept. 1977, pp. 183-198.

[4] Ibrahim, S. R.: Random Decrement Technique for Modal Identification of Structures. J. Spacecraft and Rockets. Vol. 14, No. 11, Nov. 1977, pp. 696-700.

[5] Ibrahim, S. R.: Modal Confidence Factor in Vibration Testing. J. Spacecraft and Rockets. Vol. 15, No. 5, Sept. 1978, pp. 313-316.

[6] Ibrahim, S. R.: Application of Random Time Domain Analysis to Dynamic Flight Measurements. Shock and Vibration Bulletin. No. 49, Part 2, Sept. 1979, pp. 165-170.

[7] Hanks, B. R., Miserentino, R., Ibrahim, S. R., Lee, S. H., and Wada, B. K.: Comparison of Modal Test Methods on the Voyager Payload. SAE Paper 781044. Nov. 1978.

[8] Wilkinson, J. H., and Reinsch, C.: Handbook for Automatic Computation, Vol. II, Linear Algebra. Springer-Verlag, Heidelberg. 1971.

[9] Forsythe, G. E., and Moler, C. B.: Computer Solution of Linear Algebraic Systems. Prentice-Hall, Englewood Cliffs, N.J. 1967.

[10] Dongarra, J. J., Bunch, J. R., Moler, C. B., and Stewart, G. W.: LINPACK User's Guide. SIAM Press. 1979.

[11] Wilkinson, J. H.: The Algebraic Eigenvalue Problem. Oxford University Press, London. 1965.

[12] Garbow, B. S., and Dongarra, J. J.: Path Chart and Documentation for the EISPACK Package of Matrix Eigensystem Routines. Argonne National Laboratory, Applied Mathematics Division, TM-250, 1975.

TABLE I.- IDENTIFICATION RESULTS FOR THREE BASELINE MODELS.

NDOF = 65; NCOL = 390 in each identification. (All "Noise Modes" had OAMCF < 2%)

C/C_c = 2% in all modes. 2% noise. (See Figure 3 for mode shapes)

MODE NO.	FREQUENCY, HZ	C/C_c, %	OAMCF	NST	MSCC WITH INPUT MODE NO. -														
					1	2	3	4	5	6	7	8	9	10	11	12	13	14	15
1	10.000	2.042	100	65	100	0	0	0	6	0	0	0	0	0	8	0	11	0	0
2	11.999	2.047	100	48	0	100	0	0	0	3	0	0	0	0	0	4	0	0	0
3	14.002	2.020	100	60	0	0	100	0	0	0	4	0	0	1	0	0	0	9	0
4	15.998	1.990	100	48	0	0	0	100	0	0	0	0	4	0	0	0	0	0	4
5	17.998	2.004	100	65	6	0	0	0	100	0	0	0	0	0	0	0	5	0	0
6	20.001	1.999	100	48	0	3	0	0	0	100	0	0	0	0	0	6	0	0	0
7	21.998	1.993	100	60	0	0	4	0	0	0	100	0	0	2	0	0	0	2	0
8	24.000	2.005	100	63	0	0	0	0	0	0	0	100	0	0	1	0	1	0	0
9	26.001	2.012	100	52	0	0	0	4	0	0	0	0	100	0	0	0	0	0	6
10	28.001	2.016	100	60	0	0	1	0	0	0	2	0	0	100	0	0	0	2	0
11	30.002	2.016	100	57	8	0	0	0	0	0	0	1	0	0	100	0	1	0	0
12	31.996	2.009	100	44	0	3	0	0	0	6	0	0	0	0	0	100	0	0	0
13	33.998	2.005	100	65	11	0	0	0	5	0	0	1	0	0	1	0	100	0	0
14	36.004	1.997	100	54	0	0	9	0	0	0	2	0	0	2	0	0	0	100	0
15	37.998	2.007	100	52	0	0	0	4	0	0	0	0	6	0	0	0	0	0	100

C/C_c = 2% in all modes. 20% noise. (See Figure 4 for mode shapes)

MODE NO.	FREQUENCY, HZ	C/C_c, %	OAMCF	NST	MSCC WITH INPUT MODE NO. -														
					1	2	3	4	5	6	7	8	9	10	11	12	13	14	15
1	9.983	4.373	95	65	100	0	0	0	6	0	0	0	0	0	8	0	11	0	0
2	11.973	4.475	88	53	0	99	0	0	0	3	0	0	0	0	0	4	0	0	0
3	14.008	2.927	98	61	0	0	100	0	0	0	4	0	0	1	0	0	0	9	0
4	15.982	3.159	91	50	0	0	0	100	0	0	0	0	5	0	0	0	0	0	4
5	17.987	2.396	93	65	6	0	0	0	100	0	0	0	0	0	0	0	5	0	0
6	20.002	2.752	89	50	0	3	0	0	0	100	0	0	0	0	0	5	0	0	0
7	21.983	2.432	86	61	0	0	4	0	0	0	100	0	0	1	0	0	0	2	0
8	24.004	2.334	89	64	0	0	0	0	0	0	0	100	0	0	1	0	1	0	0
9	26.016	2.598	94	55	0	0	0	5	0	0	0	0	99	0	0	0	0	0	6
10	28.026	2.785	93	61	0	0	1	0	0	0	1	0	0	99	0	0	0	2	0
11	30.031	2.492	81	58	8	0	0	0	0	0	0	1	0	0	100	0	1	0	0
12	31.973	2.608	72	55	0	3	0	0	0	6	0	0	0	0	1	99	0	0	0
13	34.014	2.393	89	64	10	0	0	0	5	0	0	1	0	0	1	0	99	1	0
14	36.053	2.541	75	58	0	0	9	0	0	0	2	0	0	2	0	0	0	99	0
15	37.954	2.429	86	53	0	0	0	4	0	0	0	0	6	0	0	0	0	0	100

C/C_c = 5% in all modes. 10% noise. (See Figure 5 for mode shapes)

MODE NO.	FREQUENCY, HZ	C/C_c, %	OAMCF	NST	MSCC WITH INPUT MODE NO. -														
					1	2	3	4	5	6	7	8	9	10	11	12	13	14	15
1	10.016	5.740	100	65	100	0	0	0	6	0	0	0	0	0	8	0	11	0	0
2	12.030	6.031	92	52	0	100	0	0	0	3	0	0	0	0	0	3	0	0	0
3	14.000	5.654	96	61	0	0	100	0	0	0	4	0	0	1	0	0	0	9	0
4	16.006	6.419	83	55	0	0	0	99	0	0	0	0	4	0	0	0	0	0	4
5	18.026	5.497	89	65	6	0	0	0	99	1	0	0	0	0	0	0	5	0	0
6	19.932	6.447	75	56	0	3	0	0	0	98	1	0	0	0	0	5	0	0	0
7	22.071	6.092	68	60	0	0	3	0	0	1	96	2	0	1	0	0	0	2	0
8	24.065	5.874	64	64	0	0	0	0	0	0	1	97	2	1	1	0	1	0	0
9	26.121	6.620	46	62	0	0	0	5	0	0	0	2	88	9	0	0	0	0	5
10	28.231	8.047	32	65	1	0	1	1	0	0	1	1	2	86	7	2	0	2	0
11	30.184	6.578	37	61	8	0	0	0	0	1	0	0	0	5	84	10	1	0	0
12	32.432	8.862	15	64	2	3	1	0	0	6	0	0	1	1	7	74	10	4	0
13	34.061	7.484	30	62	5	1	2	0	3	2	0	1	1	0	0	14	63	19	0
14	35.688	8.131	17	64	1	0	7	0	1	1	2	0	1	2	0	3	12	81	1
15	37.860	5.351	70	61	0	0	0	4	0	0	0	0	6	0	0	0	0	4	95

TABLE II.- IDENTIFICATION RESULTS FOR THE 2%-DAMPING, 20%-NOISE BASELINE MODEL AT HIGH ALLOWED DEGREES-OF-FREEDOM.

MODE NO.	NDOF = 65 (NCOL = 993)				NDOF = 200 (NCOL = 969)				NDOF = 250 (NCOL = 969)				NDOF = 300 (NCOL = 961)			
	F	C/C_c	OAMCF	MSCC	F	C/C_c	OAMCF	MSCC	F	C/C_c	OAMCF	MSCC	F	C/C_c	OAMCF	MSCC
1	9.99	8.11	90	99	10.01	2.70	96	100	10.01	2.44	98	100	10.01	2.31	98	100
2	11.99	7.69	80	99	11.99	2.72	94	100	11.99	2.48	92	100	11.99	2.42	94	100
3	13.99	4.28	95	99	14.00	2.44	100	100	14.01	2.27	98	100	14.01	2.18	96	100
4	15.99	5.39	76	99	16.00	2.53	98	100	16.01	2.38	96	100	16.01	2.34	93	100
5	17.99	3.44	87	98	18.01	2.29	95	100	18.01	2.21	96	100	18.00	2.11	96	100
6	20.05	4.36	76	98	19.99	2.49	89	100	19.99	2.32	90	100	20.00	2.24	95	100
7	22.02	3.59	77	98	22.01	2.28	89	100	22.01	2.15	93	100	22.00	2.08	93	100
8	24.04	2.84	85	99	24.01	2.16	95	100	24.00	2.13	92	100	24.01	2.07	93	100
9	26.09	3.87	59	96	26.02	2.34	96	99	26.02	2.22	94	100	26.01	2.13	92	100
10	28.00	4.64	35	95	28.00	2.57	89	99	27.99	2.48	88	100	27.99	2.27	93	100
11	30.04	3.51	70	95	30.00	2.31	94	100	30.00	2.25	91	100	30.02	2.14	87	100
12	32.05	4.41	39	91	32.03	2.39	85	99	32.03	2.21	81	100	32.03	2.09	87	100
13	34.25	4.22	33	86	34.00	2.18	89	99	33.99	2.15	89	100	34.00	2.07	90	100
14	36.30	5.24	17	51	36.02	2.29	85	100	36.02	2.21	83	100	35.99	2.08	85	100
15	37.43	6.12	19	87	37.98	2.22	94	100	37.98	2.14	96	100	37.97	2.06	88	100

(All "Noise Modes" had OAMCF < 2%)

TABLE III.- IDENTIFICATION RESULTS WITH FREQUENCIES OF MODES 7 AND 8 SET NEARLY EQUAL IN 2%-DAMPING, 2%-NOISE BASELINE MODEL.

(NDOF = 65; NCOL = 390 in each identification.)

Δf = 0.10 Hz					Δf = 0.05 Hz				Δf = 0.01 Hz			
INPUT PARAMETERS												
CASE	f_7(Hz)	f_8(Hz)	$(C/C_c)_7$	$(C/C_c)_8$	f_7(Hz)	f_8(Hz)	$(C/C_c)_7$	$(C/C_c)_8$	f_7(Hz)	f_8(Hz)	$(C/C_c)_7$	$(C/C_c)_8$
1	22.000	22.100	2.00	2.00	22.000	22.050	2.00	2.00	22.000	22.010	2.00	2.00
2				3.00				3.00				3.00
3				10.00				10.00				10.00

IDENTIFIED PARAMETERS												
CASE	MODE NO.	f	C/C_c	OAMCF	MSCC	f	C/C_c	OAMCF	MSCC	f	C/C_c	OAMCF	MSCC
1	7	21.998	2.51	87	78	21.941	4.28	57	66	21.184	36.69	1	33
	8	22.074	2.07	100	77	22.034	2.01	100	66	22.007	2.01	100	66
2	7	22.000	2.11	96	99	22.001	2.12	96	99	22.001	2.12	98	99
	8	22.101	3.08	98	99	22.053	3.09	100	99	22.015	3.09	100	99
3	7	22.001	2.01	100	100	22.001	2.01	100	100	22.001	2.01	100	100
	8	22.101	10.02	100	100	22.051	10.02	100	100	22.011	10.02	100	100

(Identification accuracy of other 13 modes comparable to values shown in Table I for 2%-damping, 2%-noise model.)

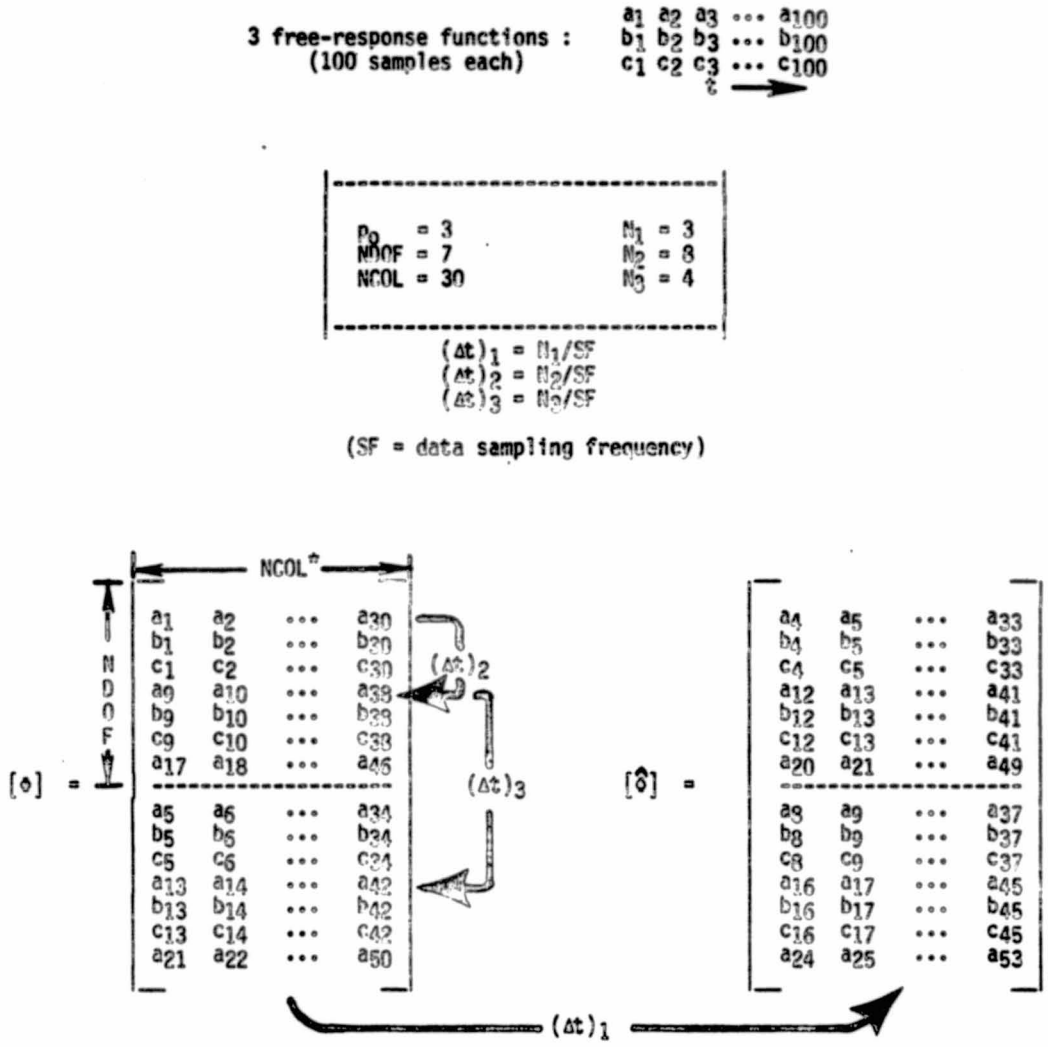

Figure 1.- Example Placement of Free-Response Data into the Two Response Matrices.

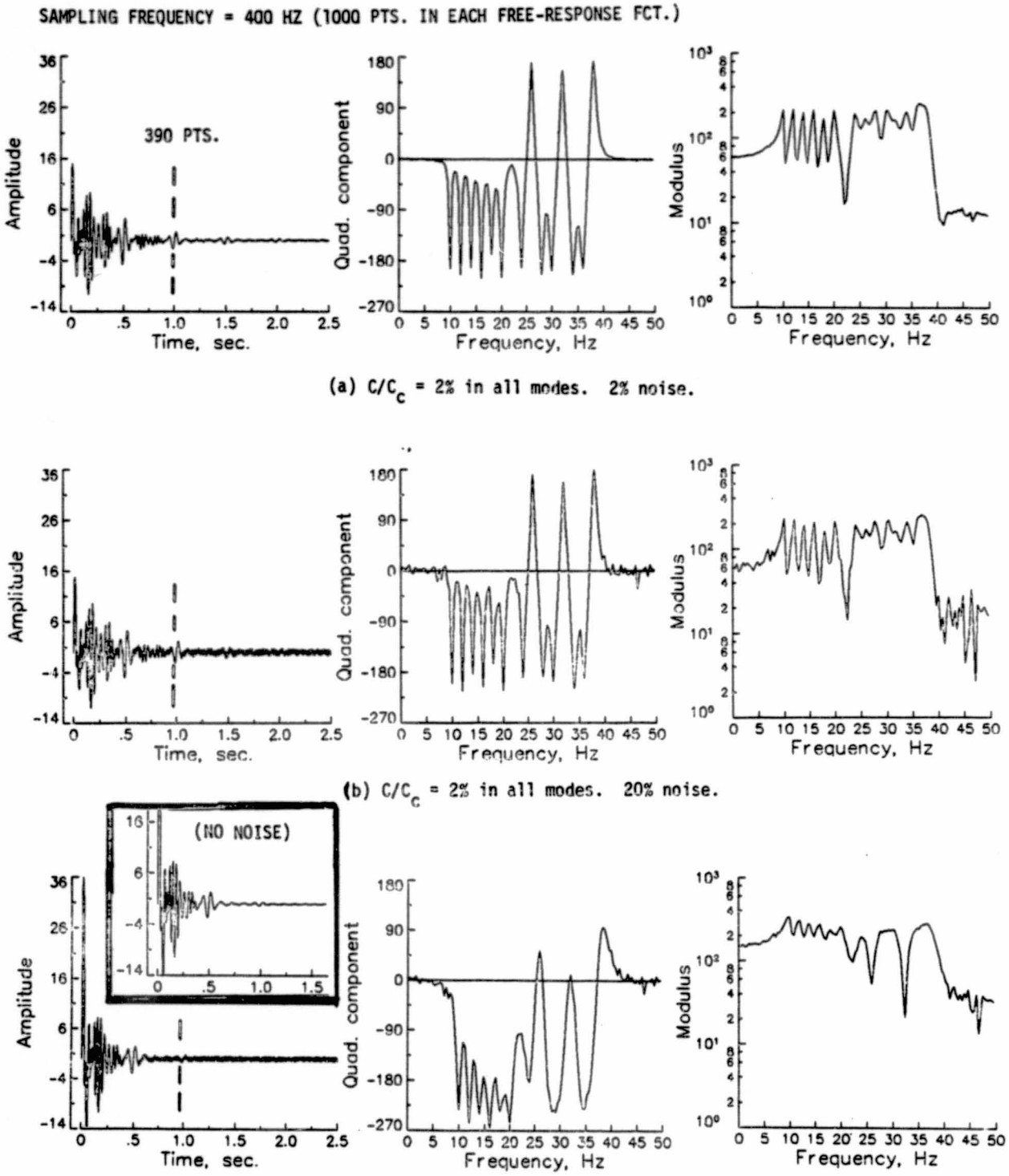

Figure 2.- Typical free-responses and frequency spectra for three baseline models, with modal frequencies spaced every 2 Hz from 10 to 38 Hz.

NDOF = 65; NCOL = 390.

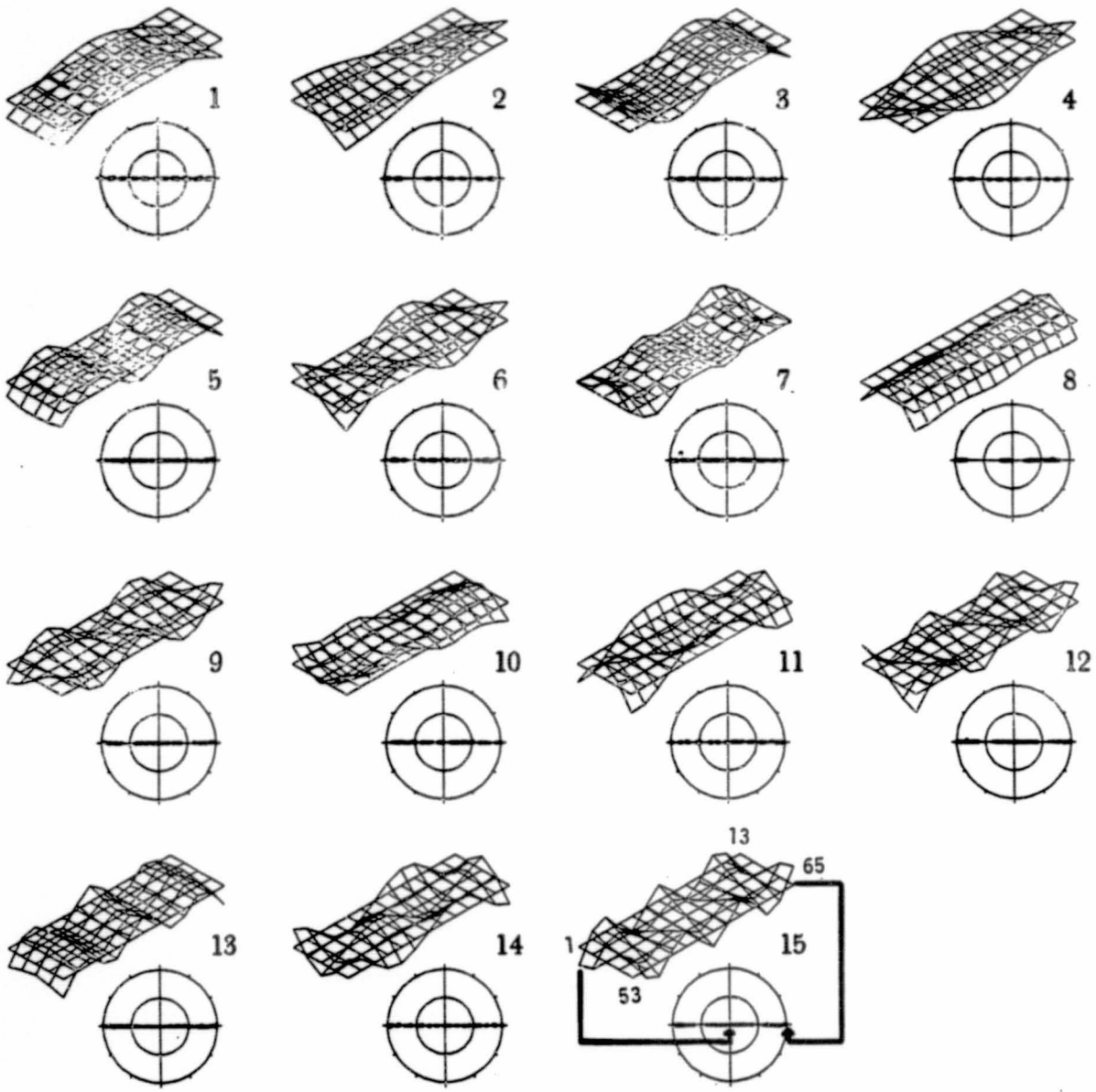

(Mode shape phase angles
indicated in polar plots)

Figure 3.- Identified (complex) mode shapes for baseline model with 2% damping in all modes and 2% noise.

NDOF = 65; NCOL = 390.

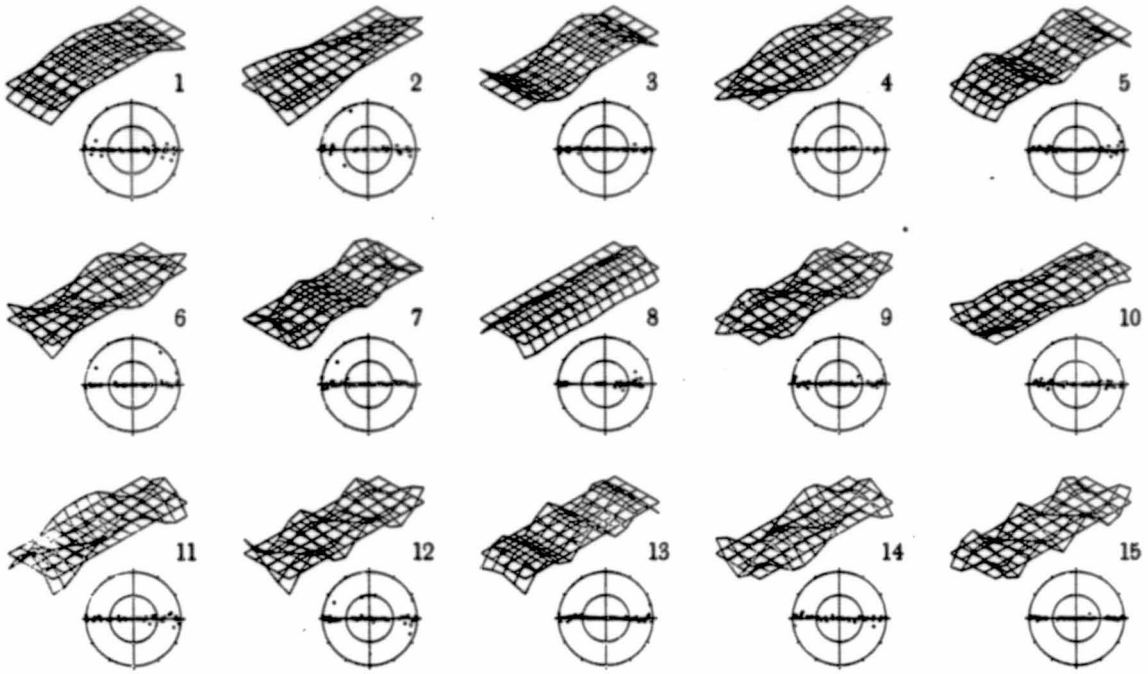

Figure 4.- Identified (complex) mode shapes for baseline model with 2% damping in all modes and 20% noise.

NDOF = 65; NCOL = 390.

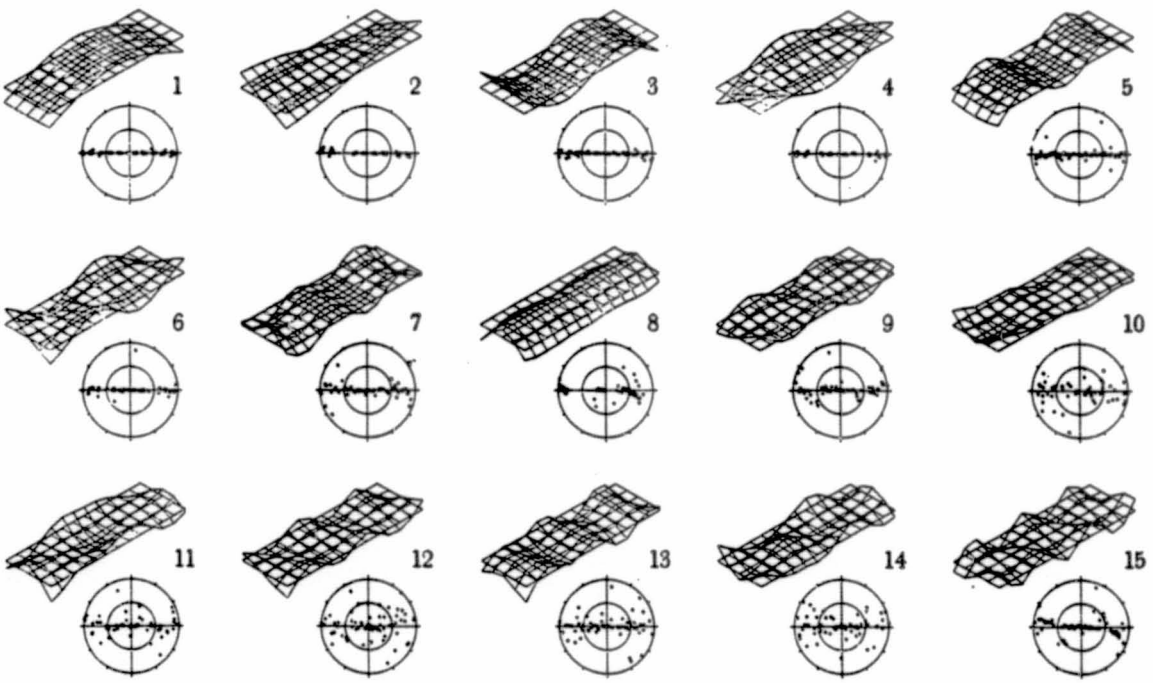

Figure 5.- Identified (complex) mode shapes for baseline model with 5% damping in all modes and 10% noise.

NCOL = 300 in each identification.

(Heights of vertical line segments proportional to OAMCF values)

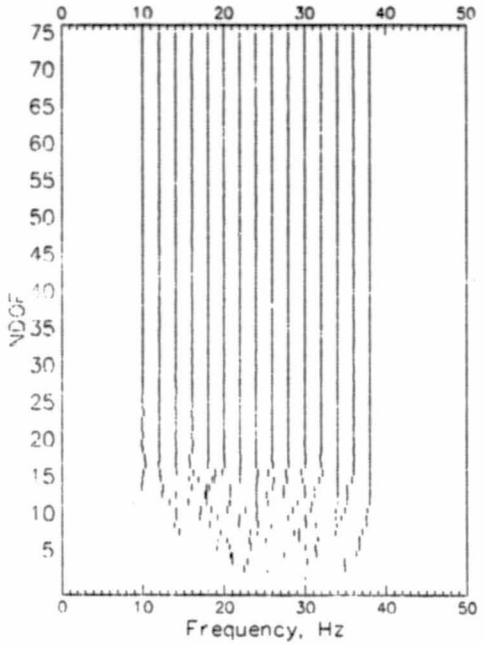

(a) 0.001% Noise

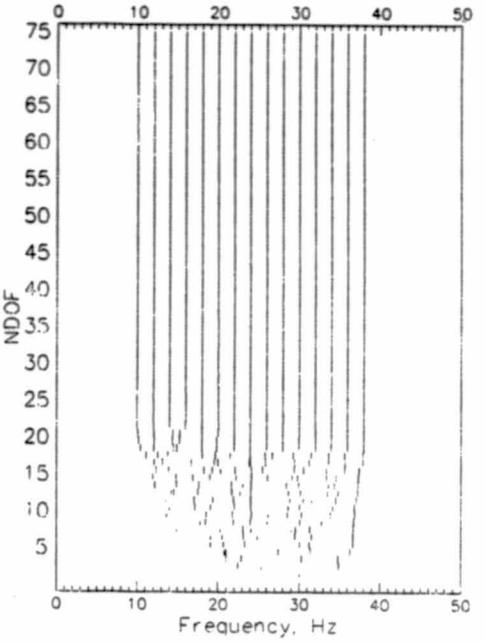

(b) 0.1% Noise

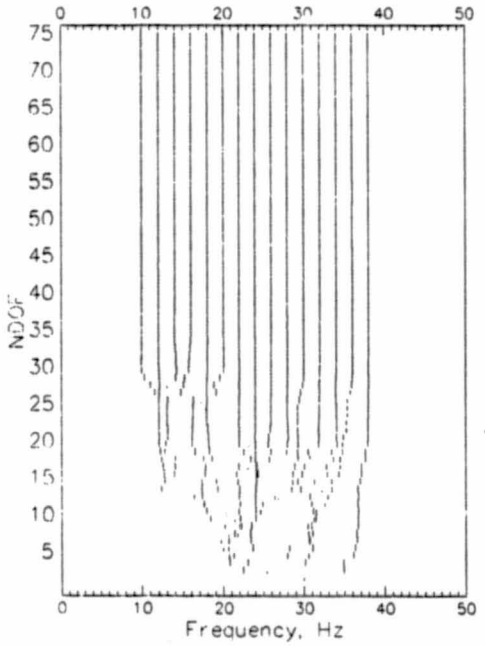

(c) 2% Noise

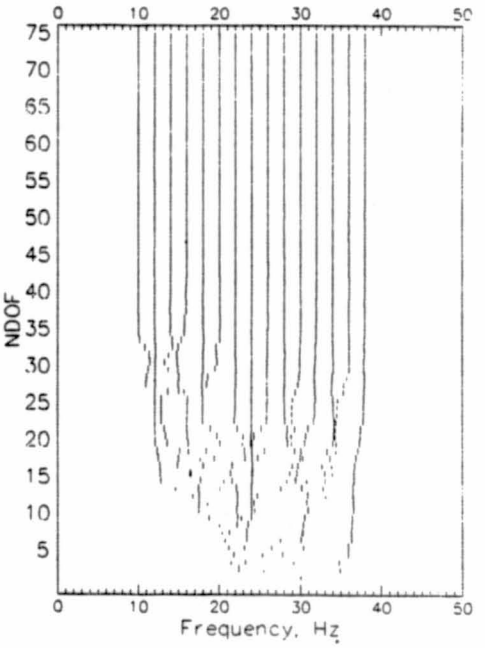

(d) 5% Noise

Figure 6.- "NDOF-Frequency Maps" for 2%-damping baseline model at several low noise/signal ratios.

NCOL = 300 in each identification.

(Heights of vertical line segments proportional to OAMCF values)

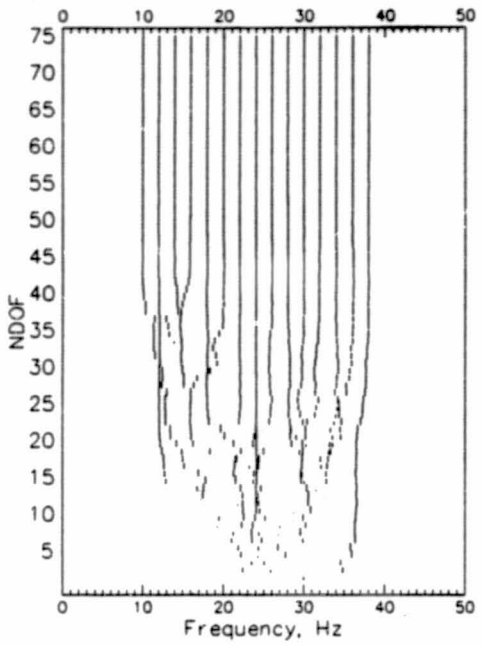

(a) 10% Noise

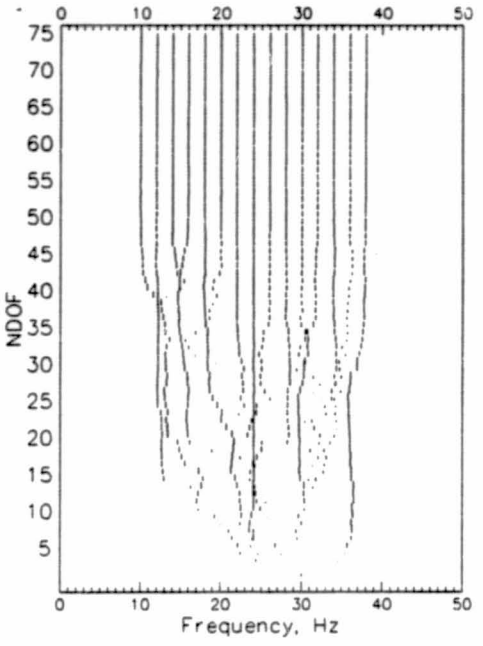

(b) 20% Noise

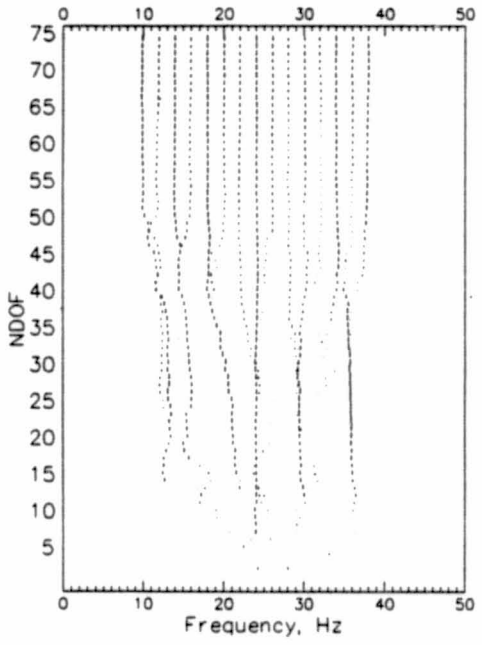

(c) 50% Noise

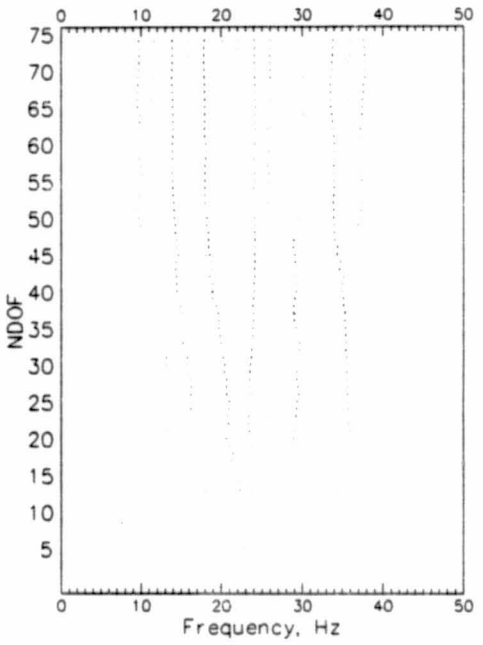

(d) 100% Noise

Figure 7.- "NDOF-Frequency Maps" for 2%-damping baseline model at several high noise/signal ratios.

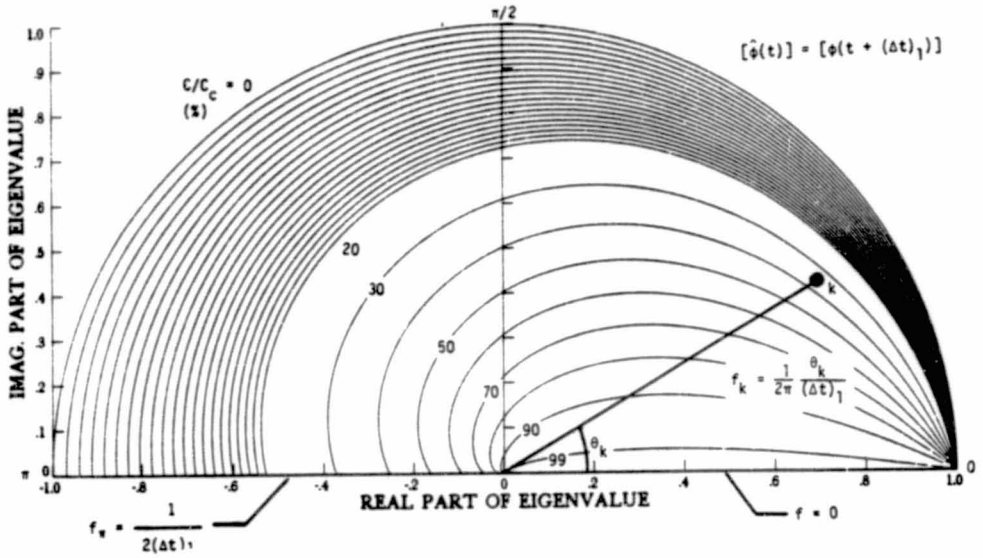

Figure 8.- Contours of equal damping factor in the plane of the eigenvalues of [A].

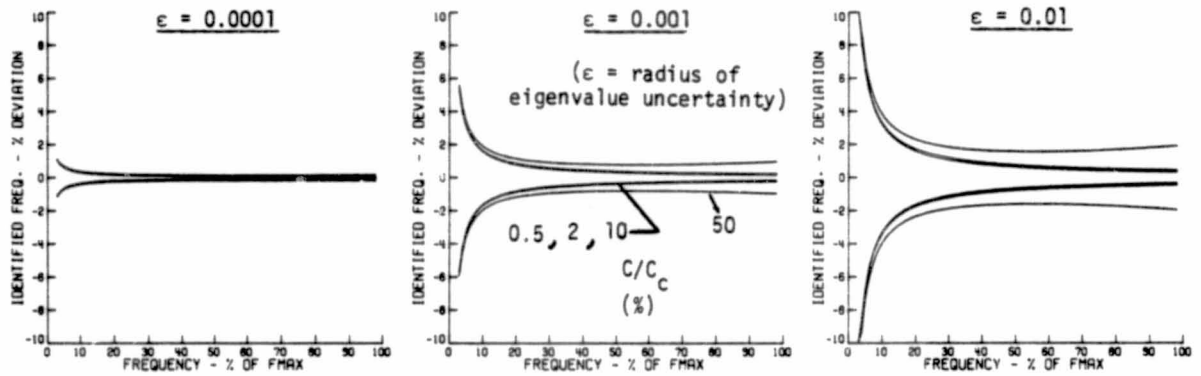

(a) Envelopes of % freq. deviation

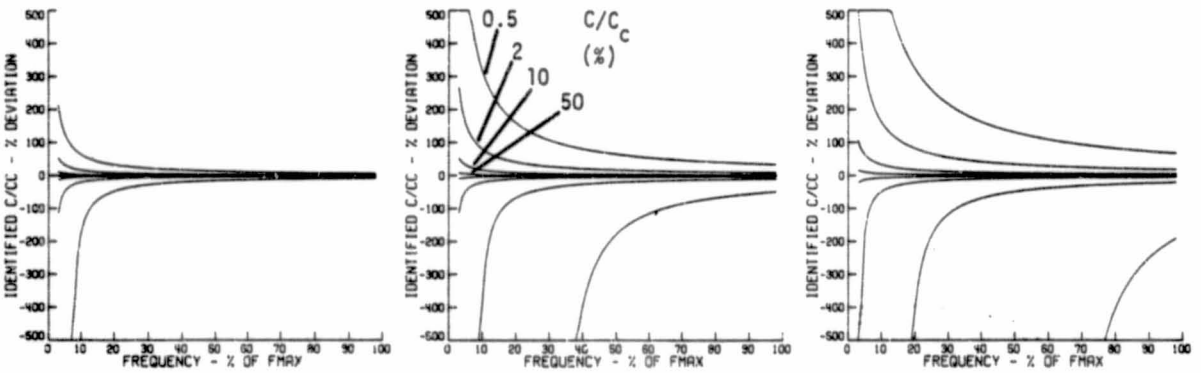

(b) Envelopes of % C/C_c deviation

Figure 9.- Sensitivity of identified frequency and damping factors at three uncertainty levels in computation of the eigenvalues of [A].

2%-damping, 20%-noise baseline model.

NDOF = 65; NCOL = 390.

Identification Results

Mode k	F, Hz	C/C_c, %	OAMCF	MSCC
1	9.97	10.26	95	99
2	12.02	8.98	80	98
3	14.00	4.22	93	99
4	16.03	6.20	84	99
5	17.98	3.24	89	99
6	19.94	4.10	85	98
7	22.02	3.51	84	98
8	24.02	3.06	85	99
9	25.98	3.72	68	96
10	27.99	4.10	51	96
11	30.07	3.12	78	97
12	32.07	3.99	37	96
13	34.02	3.28	68	93
14	36.03	3.70	59	94
15	37.92	3.30	79	98

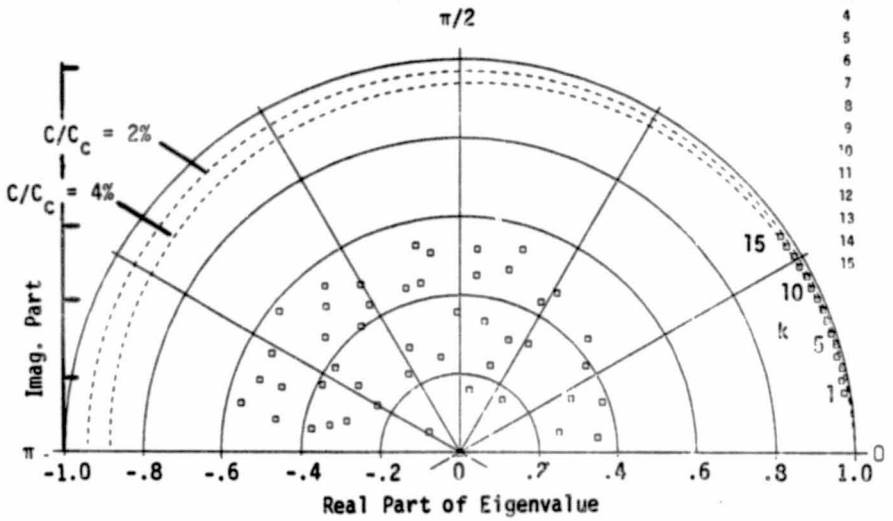

(a) $N_1 = 1$ [$(\Delta t)_1 = 1/SF$; $F_\pi = 200$ Hz]

Identification Results

Mode k	F, Hz	C/C_c, %	OAMCF	MSCC
1	9.98	4.37	95	100
2	11.97	4.48	88	99
3	14.01	2.93	98	100
4	15.98	3.16	91	100
5	17.99	2.40	93	100
6	20.00	2.75	89	100
7	21.98	2.43	86	100
8	24.00	2.33	89	100
9	26.02	2.60	94	99
10	28.03	2.79	93	99
11	30.03	2.50	81	100
12	31.97	2.61	72	99
13	34.01	2.40	87	99
14	36.05	2.54	75	99
15	37.95	2.43	86	100

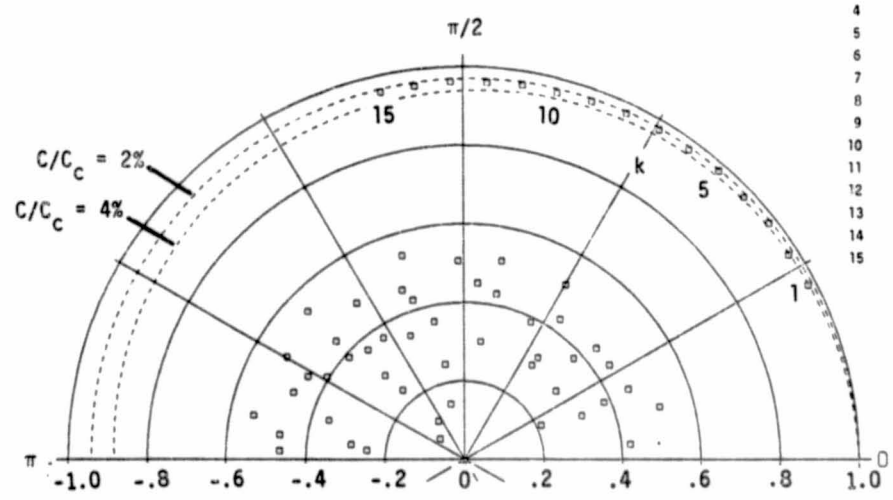

(b) $N_1 = 3$ [$(\Delta t)_1 = 3/SF$; $F_\pi = 66.67$ Hz]

Figure 10.- Typical effect of changing $(\Delta t)_1$ on identification accuracy. Polar plots show eigenvalues of [A].

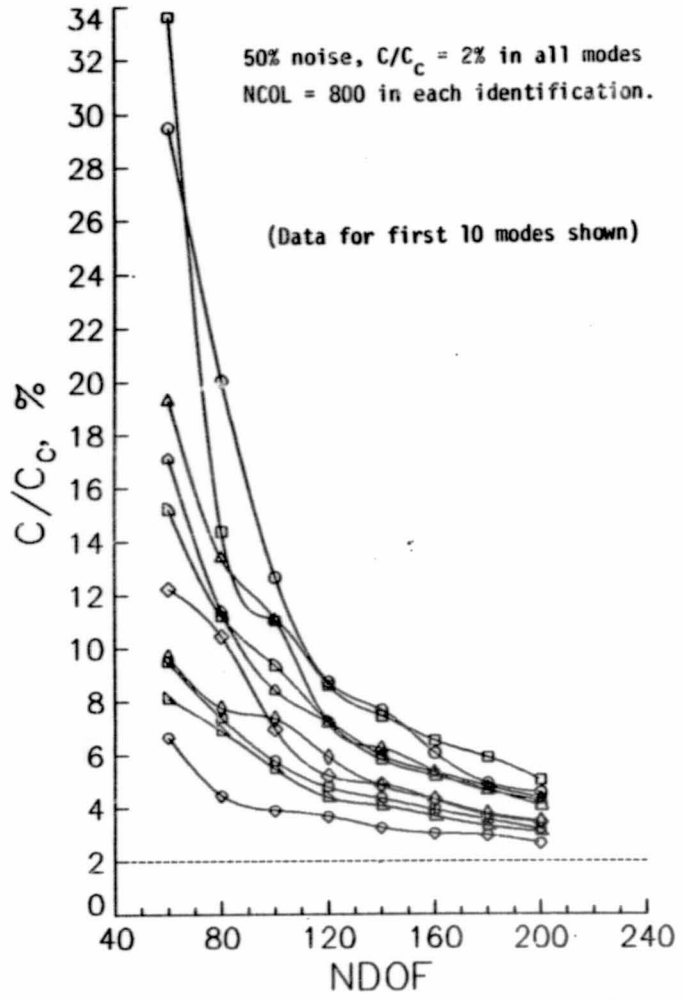

(a) Damping factors from eigenvalues of [A] (Std. method)

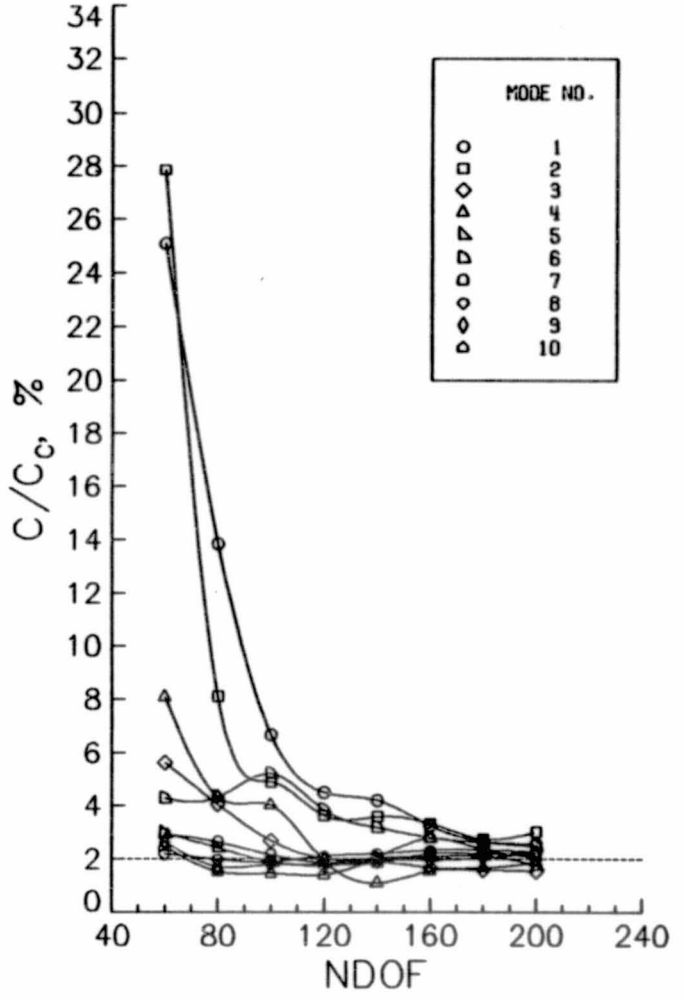

(b) Damping factors from eigenvector data using frequencies from eigenvalues of [A] (Alternate method)

Figure 11.- Comparison of modal damping computed by standard and alternate methods, for 2%-damping, 50%-noise baseline model.

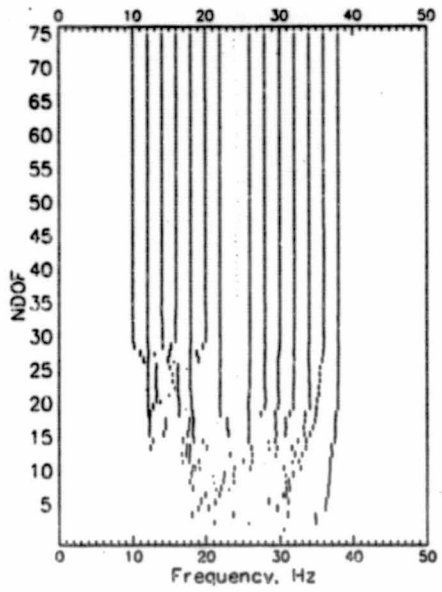

(a) NDOF-frequency map with mode 8 response level 1% that of other modes.

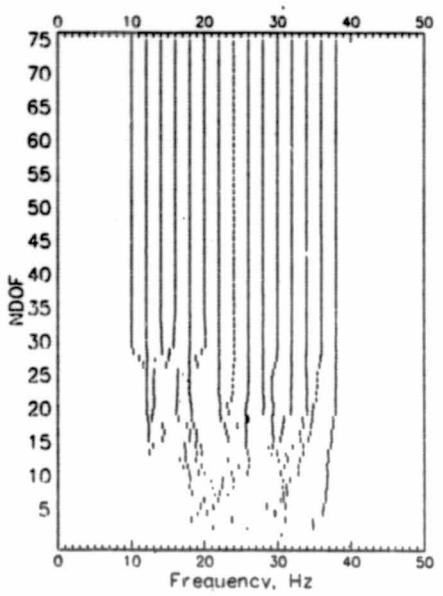

(b) NDOF-frequency map with mode 8 response level 5% that of other modes.

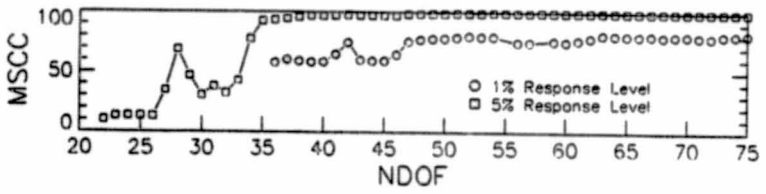

(c) Mode 8 MSCC values.

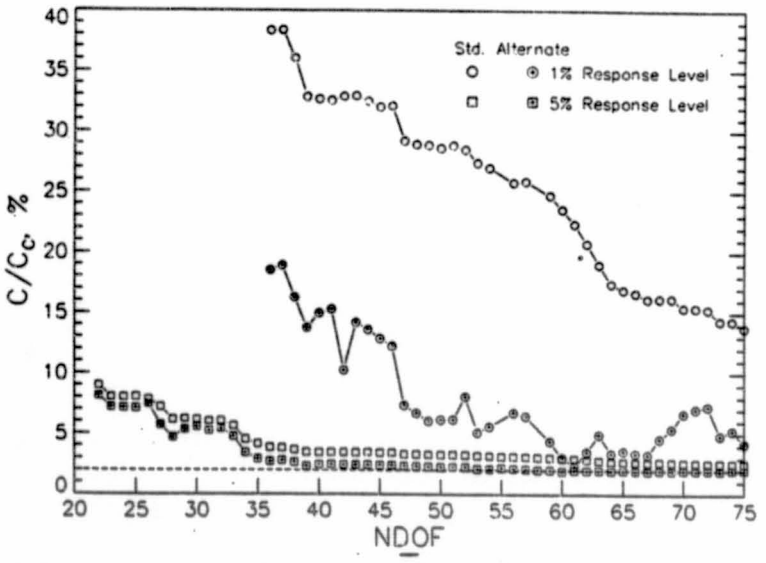

(d) Mode 8 damping factors calculated by standard and alternate methods.

Figure 12.- Identification results for 2%-damping, 2%-noise baseline model with response level of mode 8 equal to 1% and 5% that of other modes.

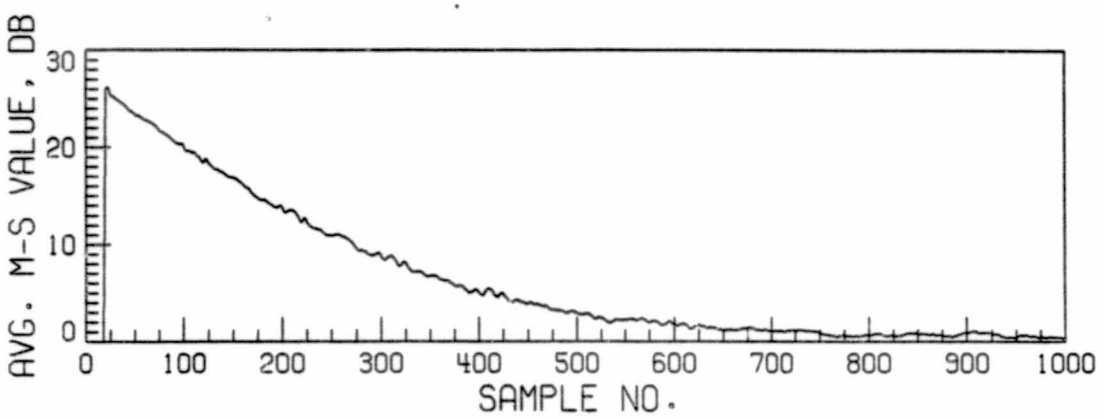

(a) Running average mean-square value of all 65 free-response functions for 2%-damping, 20%-noise baseline model.

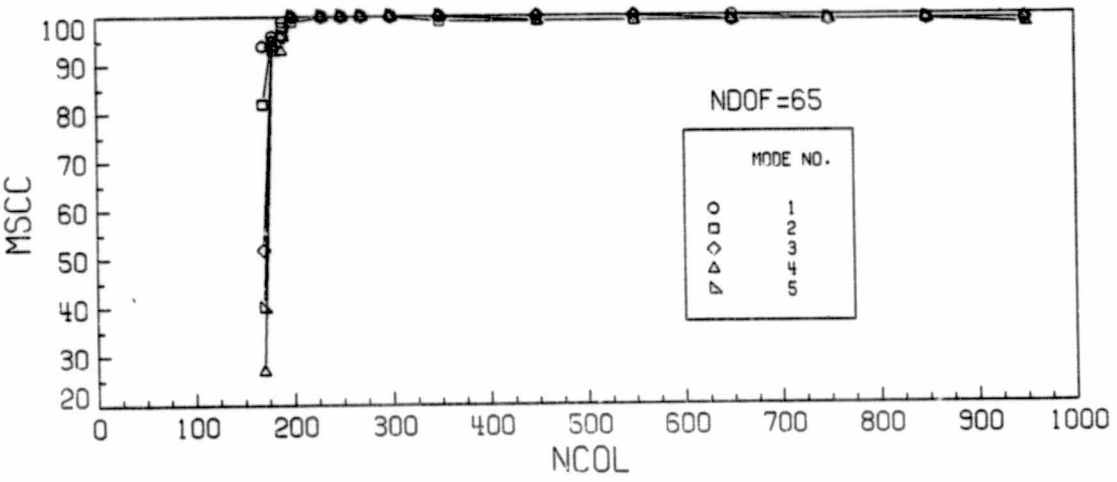

(b) Calculated MSCC values as a function of NCOL.

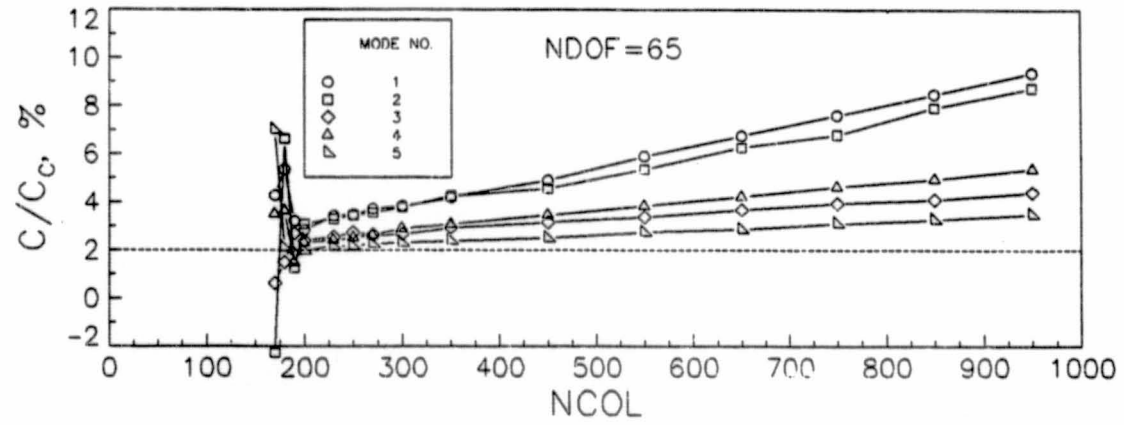

(c) Identified modal damping factors as a function of NCOL.

Figure 13.- Effect of NCOL on identification results for 2%-damping, 20%-noise baseline model.

NDOF = 65; NCOL = 390 in each identification.

C/C_c = 2% in modes 1-5 & 11-15.

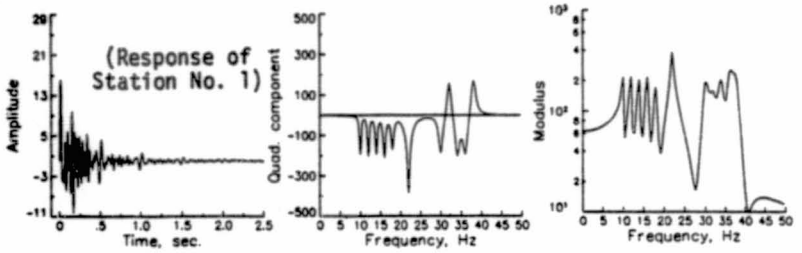

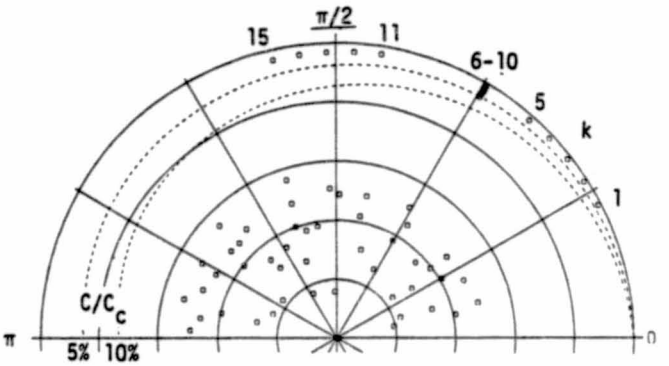

Mode k	F, Hz	C/C_c, %	OAMCF	MSCC
1	10.000	2.000	100	100
2	12.000	2.000	100	100
3	14.000	2.000	100	100
4	16.000	2.000	100	100
5	18.000	2.000	100	100
6	21.999	.996	100	100
7	21.995	2.068	95	100
8	21.994	3.061	98	99
9	22.008	3.995	96	98
10	21.998	5.022	100	100
11	30.000	2.000	100	100
12	32.000	2.000	100	100
13	34.000	2.000	100	100
14	36.000	2.000	100	100
15	38.000	2.000	100	100

(a) 5 modes at 22.000 Hz. C/C_c = 1, 2, 3, 4 & 5%. 0.01% noise.

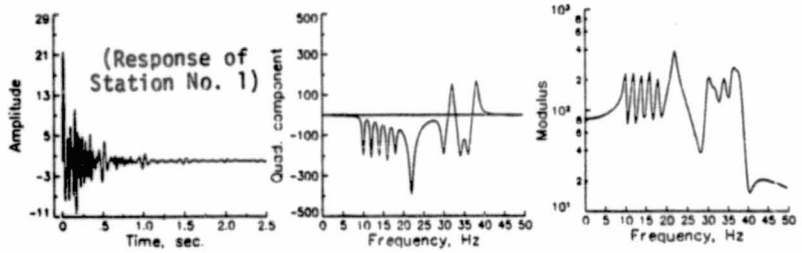

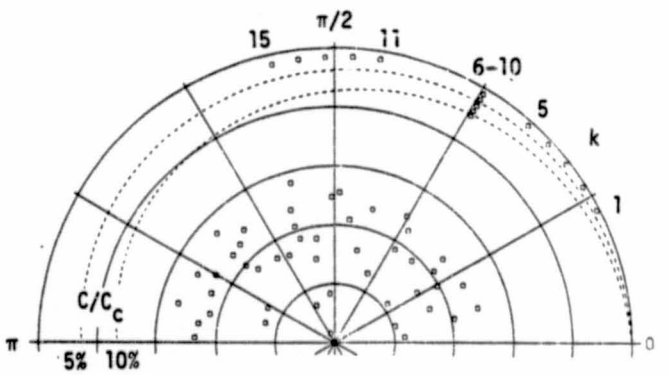

Mode k	F, Hz	C/C_c, %	OAMCF	MSCC
1	10.001	2.001	100	100
2	12.000	2.002	100	100
3	14.000	2.000	100	100
4	16.000	2.000	100	100
5	18.000	2.000	100	100
6	21.999	1.988	100	100
7	22.001	4.068	91	98
8	21.991	6.371	91	96
9	21.991	8.595	77	72
10	21.993	10.469	78	96
11	30.000	2.001	100	100
12	32.000	2.000	100	100
13	34.000	2.000	100	100
14	36.000	2.000	100	100
15	38.000	2.000	100	100

(b) 5 modes at 22.000 Hz. C/C_c = 2, 4, 6, 8 & 10%. 0.1% noise.

Figure 14.- Identification results for 15-mode model with FIVE modes at 22.000 Hz, for C/C_c separations of 1% and 2%. Polar plots show eigenvalues of [A].

DISCUSSION

Mr. Ewins (Imperial College,London): Are you convinced that the theoretical data you have used which was polluted with noise, realistically represents the kind of data you get from experiments on real structures?

Mr. Ibrahim: From my previous experience, I would rather work with experimental data than simulated data.

Mr. Ewins: I asked because we've been through a similar kind of process and we find that experimental data contains a quite different type of error to that which you put in with random errors superimposed on the theoretical ideal. The structures have systematic errors. You have non-linearities and I wonder whether the method is equally effective on real data as you have shown on the synthesized.

Mr. Ibrahim: Yes, we have lots of previous applications and we will put the paper in the AIAASDM Conference in April and we are dealing with large modal surveys of real experimental full scale structures. And to answer your question, I personally feel as comfortable with experimental noise as with simulated noise because the experimental noise is nice and random. What you generate in the computer usually has some distribution. The other question is non-linearity. We did not include a non-linearity here, but non-linearity of the structures is another completely different ball game and it has to be dealt with separately. But we get as good results with experimental data, yes.

AIAA 81-0528R

Large Modal Survey Testing Using the Ibrahim Time Domain Identification Technique

S. R. Ibrahim and R.S. Pappa

Reprinted from

Journal of Spacecraft and Rockets

Volume 19, Number 5, Sept-Oct. 1982, Page 459.

MERICAN INSTITUTE OF AERONAUTICS AND ASTRONAUTICS • 1290 AVENUE OF THE AMERICAS • NEW YORK, NEW YORK, N.Y. 10104

AIAA 81-0528R

Large Modal Survey Testing Using the Ibrahim Time Domain Identification Technique

Samir R. Ibrahim*
Old Dominion University, Norfolk, Va.
and
Richard S. Pappa†
NASA Langley Research Center, Hampton, Va.

The ability of the Ibrahim time domain identification algorithm to identify a complete set of structural modal parameters, using a large number of free-response time histories simultaneously in one analysis and assuming an identification model with a high number of degrees of freedom, has been studied. Identification results using simulated free responses of a uniform rectangular plate, with 225 measurement stations, and experimental responses from a ground vibration test of the long duration exposure facility (LDEF) Space Shuttle payload, with 142 measurement stations, are presented. As many as 300 degrees of freedom were allowed in analyzing these data. In general, the use of a significantly oversized identification model in the identification process was found to maintain or increase identification accuracy and to identify modes of low response level that are not identified with smaller identification model sizes. The concept of a mode shape correlation constant is introduced for use when more than one identification analysis of the same structure are conducted. This constant quantifies the degree of correlation between any two sets of complex mode shapes identified, using different excitation conditions, different user-selectable algorithm constants, or overlapping sets of measurements.

Nomenclature

$[A]$	= square system matrix (of order $2m$).
ITD	= Ibrahim time domain (technique)
m	= number of computational degrees of freedom (NDOF)
MCF	= modal confidence factor
MSCC	= mode shape correlation constant
NDOF	= number of computational degrees of freedom
N/S	= noise-to-signal ratio
$\{n(t)\}$	= vector of measurement noise time histories
OAMCF	= overall modal confidence factor
p	= number of structural modes
rms	= root mean square
s	= number of rows in $[\Phi]$ and $[\hat{\Phi}]$
t_j	= time instant j
$\{x(t)\}$	= vector of free-response time histories
α_k	= kth eigenvalue of $[A]$
$\{\gamma\}_k$	= portion of $\{\psi\}_k$
$(\Delta t)_l$	= time shift between $[\Phi]$ and $[\hat{\Phi}]$
ζ	= modal damping factor $= C/C_c$
λ_k	= kth characteristic root of structure
$[\Phi], [\hat{\Phi}]$	= response matrices $(2m \times s)$
$\{\psi\}_k$	= kth eigenvector (complex mode shape) of $[A]$
$\{\ \}^T$	= transpose of vector $\{\ \}$
$\{\ \}^*$	= complex conjugate of vector $\{\ \}$
$\|\ \|$	= magnitude

Introduction

USING a time-domain approach, it has been shown that the identification of structural modal parameters from experimental data can be placed in the form of a complex eigenvalue problem.[1] The resulting method, referred to as the Ibrahim time domain (ITD) technique, uses free-response time histories $\{x(t)\}$ measured at various points on a test structure to compute a square system matrix $[A]$, or order $2m$, in a least-squares sense from the equation

$$[A][\Phi\Phi^T] = [\hat{\Phi}\Phi^T] \tag{1}$$

In this equation, $[\Phi]$ and $[\hat{\Phi}]$ are rectangular matrices of size $2m \times s$, with $s \geq 2m$, whose elements are

$$\Phi_{ij} = x_i(t_j) \qquad \hat{\Phi}_{ij} = x_i[t_j + (\Delta t)_l] \tag{2}$$

The ith row of $[\Phi]$ corresponds to the ith measurement or a measurement delayed some arbitrary time, $\Delta\tau$. The use of delayed or "transformed" stations[1] allows the computation of a modal confidence factor[2] (MCF) at each station for each identified mode. The MCF parameter is used to differentiate the desired structural modes from "noise modes," computed whenever the number of structural modes contributing to the responses is smaller than m. A (complex valued) MCF is calculated for each station, and indicates the consistency of the modal deflection identified at each station with the deflection at the same station identified using data measured a small time later. Its value is near 100% in amplitude and 0 deg in phase for accurately identified structural modes.

Possible time-domain functions which can be used include actual free decays obtained following random excitation of the structure, unit-impulse response functions calculated by the inverse Fourier transform of frequency response functions, or "random-decrement" functions[3] calculated from random operating time histories.

After computing $[A]$ from Eq. (1), an eigenvalue problem of the form

$$[A]\{\psi\}_k = \alpha_k\{\psi\}_k \tag{3}$$

is solved. The kth eigenvector of $[A]$ is the kth complex mode shape of the structure and the kth eigenvalue of $[A]$ is related to the structure's characteristic root λ_k through the equation

$$\alpha_k = e^{\lambda_k(\Delta t)_l} \tag{4}$$

Details of the identification technique are contained in Refs. 1-4.

Presented as Paper 81-0528 at the AIAA/ASME/ASCE/AHS 22nd Structures, Structural Dynamics and Materials Conference, Atlanta, Ga., April 6-8, 1981; submitted April 15, 1981; revision received April 5, 1982. This paper is declared a work of the U.S. Government and therefore is in the public domain.

*Associated Professor, Department of Mechanical Engineering and Mechanics. Member AIAA.

†Aerospace Engineer, Structural Dynamics Branch. Member AIAA.

In previous applications of the technique using simulated and experimental data,[4-6] the primary purpose was to establish credibility of the method. The studies were limited, for research purposes, to problems with small numbers of measurement stations and structural modes. For large modal survey tests, however, it is not unusual to obtain responses at 200 or more measurement stations on a test structure.

If the response functions used in the identification technique are entirely noise-free, the size of the identification model, m (or "number of allowed computational degrees of freedom") must exactly equal the number of excited structural modes in the responses. When experimental data are processed, however, there is always some level of noise, and the number of structural modes contributing to the responses is not exactly known. Since the maximum number of modes identified in a single computer analysis is equal to the number of allowed degrees of freedom, an obvious question is whether all parameters can be accurately obtained by simply allowing the number of degrees of freedom to be unquestionably larger than the number of excited structural modes. Since the number of measurements analyzed in each identification run can be as high as the number of allowed degrees of freedom, the use of a large enough identification model would also allow the response functions for all stations selected for the modal survey to be processed simultaneously.

When the number of available measurements is less than the number of degrees of freedom desired in the identification process, extra "transformed stations" can be formed by delaying the original response functions by small arbitrary time increments. Using this approach, a large identification model can be used even when a relatively small number of responses are available.

If computer storage limitations restrict the processing of a large number of response measurements simultaneously, a technique is presented for correlating sets of identified mode shapes from different runs using data corresponding to a common set of measurements used in each analysis. With this approach, modes obtained for two or more portions of the available test measurements can be matched more accurately than on the basis of identified frequencies and damping values alone. A mode shape correlation constant (MSCC), whose value is zero for no correlation and 1.0 for complete correlation, is introduced for this purpose. The MSCC is a general procedure for measuring the degree of correlation between any two complex modal vectors. It has also been found useful in correlating mode shapes identified with responses from different excitation conditions or identified using different values of the few user-selectable algorithm constants, to provide additional confidence in the identification results by studying the consistency of independent analyses.

This paper presents typical results that have been obtained in processing simulated and experimental data with the ITD identification algorithm using a large number of measurement stations and/or large identification model sizes. The results indicate that the use of large identification models in the analysis procedure can result in the accurate identification of a large number of structural modes in a single analysis, often allowing all measured response data from a large model survey test to be used simultaneously in computing the modal parameters of a test structure.

Theory of Oversized Identification Model

A set of free-response functions containing modal information from p structural modes of vibration can be expressed as

$$\{x(t)\} = \sum_{k=1}^{2p} \{\psi\}_k e^{\lambda_k t} \tag{5}$$

If noise-free responses are used in the identification algorithm, the identification model must have exactly p degrees of freedom for unique identification. If more than p degrees of freedom are allowed, the $[\Phi]$ matrix is singular.

In experimental work, however, measured responses always contain a certain amount of noise. These responses can be expressed as

$$\{x(t)\} = \sum_{k=1}^{2p} \{\psi\}_k e^{\lambda_k t} + \{n(t)\} \tag{6}$$

In previous applications[1-6] it was found that using noisy responses in the identification process with the number of degrees of freedom larger than p yielded good results without encountering singularity. The results even improved as the identification model size was increased. The qualitative explanation for this situation is that the extra degrees of freedom act as outlets for the noise. In this case, the noisy responses can be expressed as

$$\{x(t)\} = \sum_{k=1}^{2p} \{\psi\}_k e^{\lambda_k t} + \sum_{k=2p+1}^{2m} \{N\}_k e^{r_k t} \tag{7}$$

in which the noise is modeled as a combination of $(2m-2p)$ complex exponential functions. Since the value of p, the number of excited modes, is a characteristic of the structural response and not the data analysis process, additional exponential functions are allowed to represent the noise in the math model as m is increased. This results in a higher-order fit for the noise portion of the responses, reducing residuals that would otherwise be included in the signal portion of the responses.

Mode Shape Correlation Constant

When two or more sets of measurements are used in identifying the modal parameters of a test structure, corresponding modes obtained from different identification

Table 1 Model and identification parameters for the four simulated plate tests

Test	No. of measurements	No. of modes	Natural frequency, Hz	Damping ζ, %	rms N/S ratio, %	Allowed NDOF
1	225	2	20.000	1.000	0.0001	300
			30.000	1.000		
2	225	2	30.000	1.000	0.0001	300
			30.000	1.000		
3	225	2	20.000	1.000	200	300
			30.000	1.000		
4	225	30	10.000	1.000	20	300
			11.000	1.000		
			12.000	1.000		
			...	...		
			39.000	1.000		

runs can often be matched by comparing modal frequencies and damping factors. This procedure can lead to mismatching of some modes, however, particularly in regions of high modal density, owing to variance in the identified frequency and damping data. To reduce the possibility of mismatching, mode shape matching can be used in addition to frequency and damping matching.

Let $\{\psi_1\}$ and $\{\psi_2\}$ be two identified (complex) modal vectors from identification runs 1 and 2 that use an overlapping set of measurements. If the modal vectors at the common measurements are denoted by $\{\gamma_1\}$ and $\{\gamma_2\}$, the correlation of the mode shapes can be estimated by the degree of correlation between $\{\gamma_1\}$ and $\{\gamma_2\}$ using a mode shape correlation constant (MSCC) defined as

$$\text{MSCC} = \frac{|\{\gamma_1\}^T\{\gamma_2\}^*|^2}{\{\psi_1\}^T\{\gamma_1\}^*\{\gamma_2\}^T\{\gamma_2\}^*} \tag{8}$$

where T denotes the transpose and $*$ the complex conjugate.

The MSCC between two (complex) modal vectors ranges from 0 for no resemblance to 100% for perfect resemblance. Values between 0 and 100% can be interpreted as the amount of coherent information in the two compared mode shapes. Of course, care should be exercised in using the MSCC information since it can indicate false correlation between overall mode shapes if the number of elements in $\{\gamma_1\}$ and $\{\gamma_2\}$ is small and only portions of the two shapes have some resemblance. Using frequencies and damping factors, together with MSCC, can significantly reduce the possibility of mismatching.

Results and Discussion

In this section, results from several data analyses of responses from two test structures are reported and discussed. The first structure is a NASTRAN-simulated rectangular plate. The other is the long duration exposure facility (LDEF) Space Shuttle payload. The simulated plate results are included to demonstrate typical accuracies which are obtained using simulated free responses from a system with known modal parameters and an overexpanded identification model. The results of the simulation study also help in interpreting and supporting the accuracy of the LDEF experimental results that follow.

Simulated Plate Results

An arbitrary number of NASTRAN mode shapes of a rectangular plate, with arbitrarily assigned natural frequencies, damping factors, and response levels, were used in constructing free-response functions analyzed with the identification algorithm. Four sets of response functions were formed for use in four different identification runs. The first three contained only two modes, with varying assigned modal frequencies and noise-to-signal (N/S) ratios. The number of measurement stations and structural modes in the fourth set were selected to simulate those of an actual large modal survey test. In each set, the response levels of all modes were set equal. Table 1 shows the parameters used in establishing and analyzing each of these simulation data sets. NDOF is the number of computational degrees of freedom allowed in the identification model.

Table 2 Identification results for the four simulated plate tests

Test	Mode No.	Natural frequency, Hz	Damping ζ, %	OAMCF,[a] %	MSCC, %
1	1	20.000	1.000	100	100
	2	30.000	1.000	100	100
2	1	30.000	1.000	100	100
	2	30.001	1.000	100	100
3	1	20.006	2.234	78	98
	2	29.989	1.981	72	98
4	1	9.998	2.100	91	99
	2	11.003	1.812	90	99
	3	11.990	1.746	95	99
	4	13.000	2.047	91	99
	5	14.006	1.492	98	99
	6	14.999	1.879	92	99
	7	16.005	1.505	93	99
	8	17.012	1.255	96	100
	9	17.999	1.615	88	99
	10	19.001	1.691	86	99
	11	20.003	1.435	94	99
	12	20.993	1.365	89	99
	13	22.007	1.260	93	99
	14	22.994	1.385	87	99
	15	23.985	1.334	88	99
	16	24.990	1.498	84	99
	17	26.000	1.194	95	99
	18	27.000	1.447	81	99
	19	28.009	1.314	87	99
	20	29.019	1.195	89	99
	21	30.006	1.373	83	99
	22	31.008	1.113	92	99
	23	32.010	1.394	81	99
	24	33.002	1.447	79	98
	25	34.007	1.299	78	99
	26	35.024	1.332	82	98
	27	36.026	1.387	75	98
	28	37.001	1.458	69	98
	29	37.982	1.459	76	96
	30	39.033	1.301	86	99

[a] All other modes ("noise modes") had an OAMCF of less than 2%.

The identified frequencies and damping factors for all four tests are listed in Table 2. Also included are the overall modal confidence factor[4] (OAMCF) for each identified mode and the MSCC value, showing the correlation between the identified and theoretical mode shapes. The OAMCF value is the percentage of measurement stations whose calculated MCF values for each mode were at least 95% in amplitude and no larger than 10 deg in phase. The OAMCFs for "noise modes" are very small, generally less than 2%.

The results for tests 1 and 2 are included to show that a significantly oversized identification model did not cause singularity or ill-conditioning even in cases of extremely low noise-to-signal ratio (tests 1 and 2) or with almost identical eigenvalues (test 2). Theoretically, for noise-free data, the rank of the $[\Phi]$ matrix is equal to the number of independent modal vectors (twice the number of structural modes) and its determinant is proportional to the differences between the system's eigenvalues.[1] Test 3 demonstrates the effect of using an oversized identification model when processing high noise-to-signal data in reducing errors in the identified parameters. Although the rms noise-to-signal ratio was 200%, negligible error was found in the identified frequencies and mode shapes, and the errors in the damping factor results were bounded. These characteristics also apply to the identification results of the 30-mode simulated data set, test 4.

All of the identified mode shapes are nearly indistinguishable from the theoretical shapes used in forming the simulated response functions. The largest identification error occurred in mode 29, with an MSCC value calculated between the theoretical and identified mode shapes of 96%.

For all four tests, even though the ratio of the number of allowed degrees of freedom in the identification model to the number of structural modes in the responses was very high (150 for tests 1-3 and ten for test 4), no false modes or numerical anomalies resulted in the identifications. All "noise modes" (298 in tests 1-3 and 270 in test 4) had an OAMCF less than 2%.

LDEF Results

The LDEF, shown in Fig. 1, is a 30-ft long, 12-sided cylindrical structure designed to hold 86 experiment trays around its periphery. It will be placed in Earth orbit for extended periods of time to study the effects of space on selected materials and scientific processes mounted in the experiment trays. A large modal survey program was conducted at the Langley Research Center with the structure suspended in a free-free configuration. For these tests the experiment trays were removed from the structure and 142 acceleration measurement stations were used. Data obtained with the structure excited with single-shaker, wide-band random noise in the y (lateral) and z (vertical) directions will be shown. Unit-impulse response functions, obtained by inverse Fourier transformation of acceleration/force frequency response functions, are used in the ITD identification runs. A photograph of the structure with the trays removed, mounted on a transport vehicle, is shown in Fig. 1b. Figure 1c illustrates the positions of the y and z exciters and the location and sensing direction of accelerometers placed on the structure for the vibration tests.

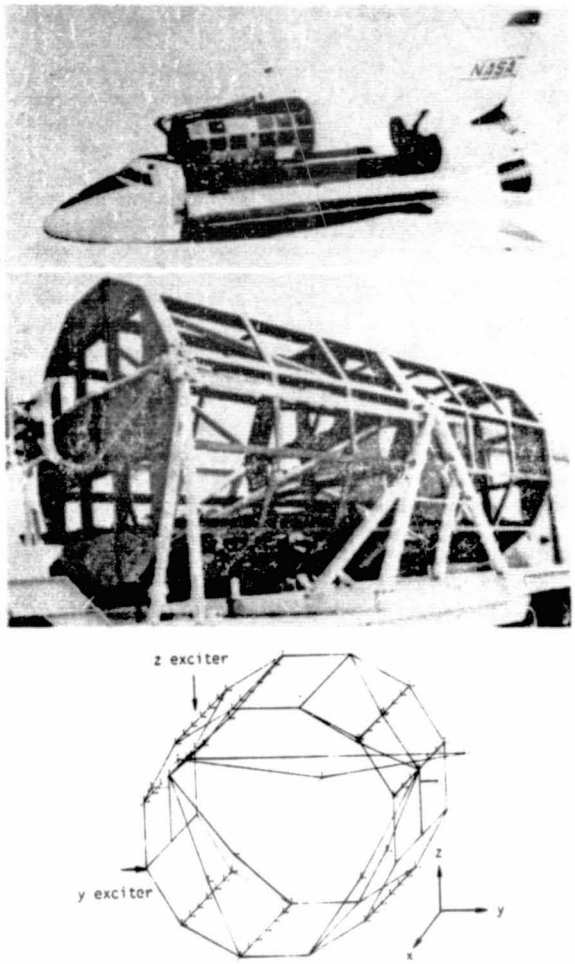

Fig. 1 Long duration exposure facility (LDEF). a) Typical deployment from the Space Shuttle. b) On transport vehicle with experiment trays removed. c) Measurement positions and two exciter locations used for vibration tests.

Table 3 Test and analysis information for the LDEF identification runs

Run	Force excitation direction	No. of measurement stations	Analysis frequency range, Hz	Allowed NDOF
1	z	142	5-55	1-75 Steps of 1 and 80-200 Steps of 10
2	z	142	5-55	150
3	z	142	5-55	300
4	z	142	19.75-32.25	150
5	y	142	5-55	300
6	z	81 (measurements 1-81)	5-55	81
7	z	81 (measurements 62-142) 142)	5-55	81

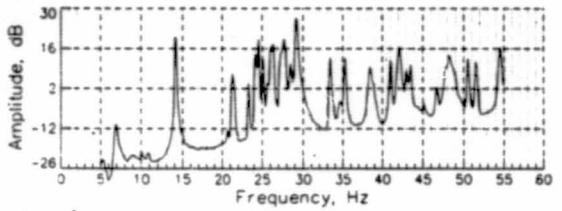

Fig. 2 Average quadrature component of 142 frequency response functions used to form impulse responses for LDEF identification runs 1-3.

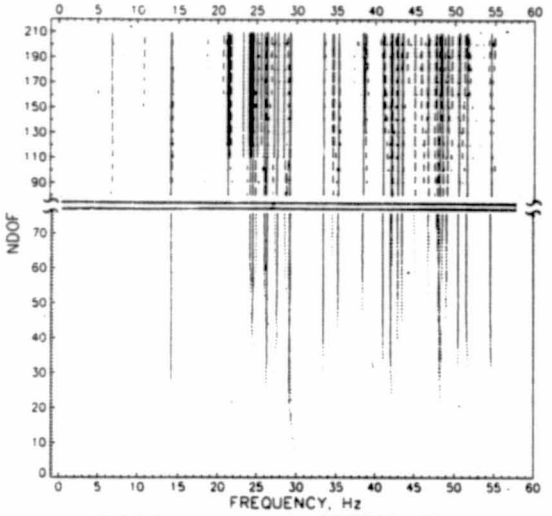

Fig. 3 NDOF-frequency map for LDEF identification run 1.

Results for seven identification runs, using a range of allowed degrees of freedom and two different excitation conditions, will be shown. Table 3 summarizes the test and analysis parameters for each run.

Figure 2 shows the average value of the quadrature components of all 142 frequency response functions for the z-excitation test, over the 5-55-Hz frequency range. The absolute value of each quadrature function was taken prior to averaging, and the result is presented on a logarithmic scale. This "composite" function provides a good indication of both the natural frequencies and relative response levels of the structural modes excited in the z-excitation test. For this plot, the reference decibel level has no special significance.

In run 1, the number of allowed degrees of freedom (NDOF) was incremented from 1 to 75 in steps of 1, and then from 80 to 200 in steps of 10. Figure 3 shows a "map" of the identified modal frequencies as a function of NDOF. The identified frequencies are denoted by vertical line segments at the corresponding frequencies whose heights are proportional to the OAMCF value calculated for each mode. An OAMCF of 100% is represented by a line height equal to the distance between adjacent NDOF values used in the analysis. A continuous vertical line indicates higher confidence in the identified mode, while a dashed line shows lower confidence.

It is of interest to note the order in which modes appear on the map as NDOF is increased. The first mode to appear, near 30 Hz, has the largest average response level, as seen in Fig. 2. The next two modes appear near 27 Hz, followed by ones near 14, 42, and 48 Hz. As NDOF is increased further, some lower level modes near 7 and 21 Hz are identified. As suggested by Eq. (7), the average strength of the "noise modes" decreases when the size of the identification model is expanded, allowing lower strength structural modes to be identified. This behavior is clearly indicated in Fig. 3. As NDOF increases from 80 to 200, more new vertical lines start to form, indicating new identified modes. Based on the results of many other simulated plate experiments,[4] no evidence exists to suggest that these new modes are adverse effects resulting from the expansion of the identification model size used in the identification. The straightness of the vertical lines in this map illustrates the insensitivity of the identified frequencies to higher numbers of degrees of freedom than necessary for initial identification, and the consistency and stability of the analysis process at high NDOF values.

In runs 2 and 3, unit-impulse responses for the 142 stations over the 5-55-Hz frequency range, with single-shaker z excitation of the structure, are used in identifications with 150 and 300 degrees of freedom (DOF), respectively. In run 4, "zoomed" transfer functions over the frequency interval of 19.75 to 32.25 Hz, transformed to the time domain, were analyzed with 150 DOF. For run 5, responses to single-shaker y excitation of the structure, over the 5-55-Hz range, were analyzed with NDOF of 300.

The curves in Figs. 4a-d show the average quadrature component of all 142 frequency response functions obtained for runs 2-5, respectively. The curves consist of 512 equally spaced values each. The diamond symbols placed above the curves denote the frequencies of all ITD-identified modes with an OAMCF of 60% or larger, for each of the four runs. The 60% OAMCF cutoff is arbitrarily selected to single out strongly identified modes. These figures are provided to illustrate three basic results of this study: The strong correlation between ITD-identified modal frequencies and peaks in measured frequency response functions; the identification of modes with low response level as the number of allowed degrees of freedom is increased; and the ability of the identification algorithm to identify modes which are spaced closer in frequency than the resolution of classical Fourier analysis. In these figures the diamond symbols are placed equidistant from the composite quadrature functions at each ITD-identified frequency, and indicate the identified modal frequencies only.

Many interesting comparisons of the results shown in Fig. 4 can be made, some of which are highlighted by circled letters a-d. Near 21.5 Hz, denoted region a, three modes are identified using 150 DOF in Fig. 4a, and four modes are identified using 300 DOF in Fig. 4b. On examining Fig. 4c, in which the resolution of the frequency response function is four times greater than in 4a or 4b, the existence of four distinct response peaks is apparent in region a. In both Figs. 4a and 4b, a mode was identified at 24.0 Hz, denoted by b, where no indication of a structure mode was apparent. Again on examining Fig. 4c, the existence of this mode is just discernible along the ramp of the more strongly excited mode at 24.2 Hz. Region c shows several highly coupled modes identified with the z-excitation response data in Figs. 4a and 4b, but are better separated in the y-excitation data, Fig. 4d. Region d shows two identified modes in Fig. 4d near 43 Hz, where a more-defined response is noted in Fig. 4b.

To study the consistency of the identifications and to demonstrate an application of the MSCC parameter, Figs. 5a and 5b provide "cross-plots" of the ITD-identified modal frequencies and damping factors, respectively, determined from two independent tests of the LDEF: run 3 for z excitation and run 5 for y excitation. Both identifications were run using 300 allowed degrees of freedom. The data shown in these plots represent results of correlating all 300 identified modes ("noise" and structural) from run 3 with all 300 from run 5, using the MSCC parameter. Results for all pairs of modes with a calculated MSCC of 80% or larger are shown. The excellent agreement of identified frequencies shown in Fig. 5a implies not only that consistent mode shapes were determined in two independent tests of the structure, but that the calculation of MSCC values using a large number of measurements (142 for these data) can potentially match identified modes independent of a comparison of identified

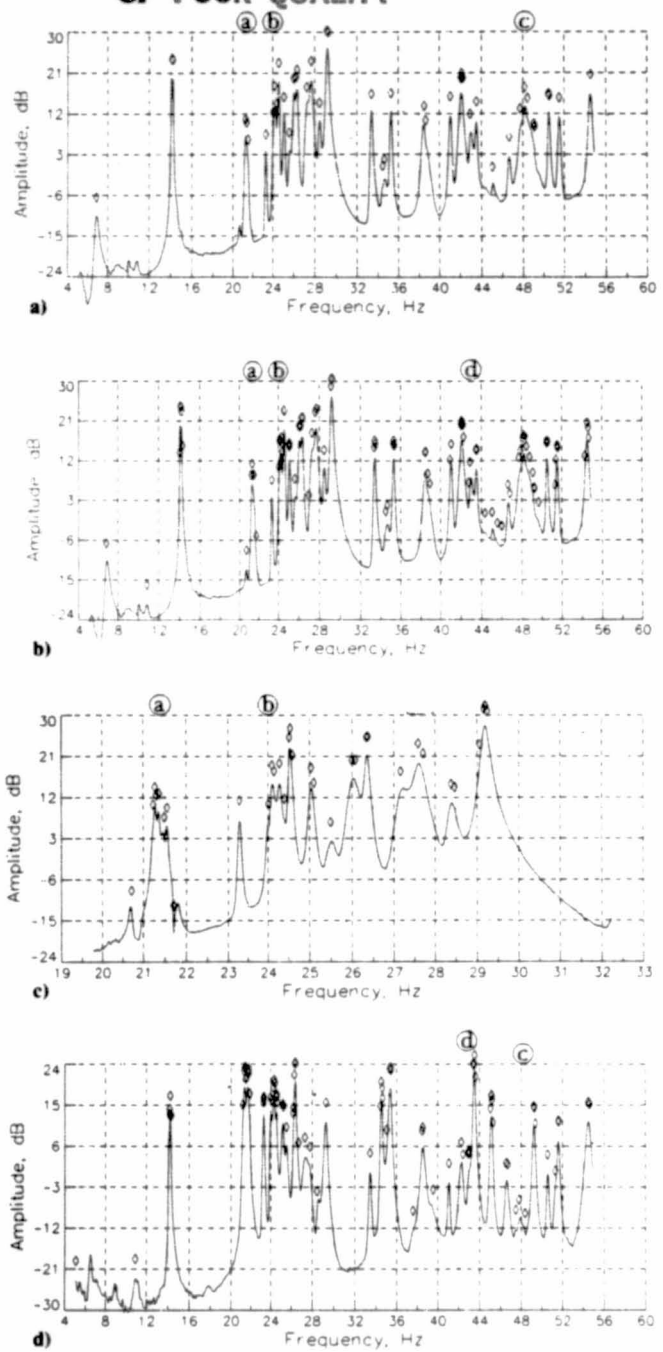

Fig. 4 Comparison of ITD-identified modal frequencies with average quadrature component of frequency response functions used to form impulse responses for LDEF runs 2-5. a) Run 2: NDOF = 150, z excitation, 5-55 Hz. b) Run 3: NDOF = 300, z excitation, 5-55 Hz. c) Run 4: NDOF = 150, z excitation, 19.75-32.25 Hz. d) Run 5: NDOF = 300, y excitation, 5-55 Hz.

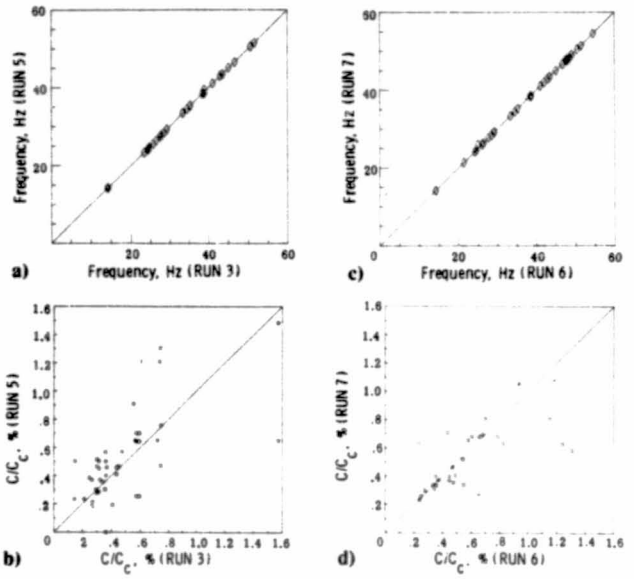

Fig. 5 Cross plots of identified frequencies and damping factors for mode pairs with high MSCC (>80%) using different exciter directions (runs 3 and 5) and overlapping measurements (runs 6 and 7). a) Frequencies: z excitation (run 3) vs y excitation (run 5). b) Damping factors: for modes shown in a. c) Frequencies: stations 62-81 from run 6 vs stations 62-81 from run 7. d) damping factors: for modes shown in c.

modal frequencies and damping factors. The damping factors identified for each pair of modes whose frequencies are shown in Fig. 5a are included in Fig. 5b.

Identification runs 6 and 7 illustrate a method for matching modes identified in two or more separate runs, using several common measurements in each. This process can be used in analyzing data from a test where limited computer memory restricts the processing for all available response measurements simultaneously. In run 6, stations 1-81 were used with 81 allowed degrees of freedom, and in run 7, stations 62-142, also with 81 DOF. Figures 5c and 5d show the results, in the same format used in Figs. 5a and 5b, of the correlation of two ITD identifications where 20 of the available free-response functions are common in each run. These plots show those mode pairs with MSCC > 80%, calculated using only the 20 common elements of the identified mode shapes, and with OAMCF > 15%. Several of the modes from run 6 correlated at 80% or higher with more than one mode in run 7 when only the 20 common mode shape elements were used in the calculation of MSCC. In these cases, only the pair of modes whose MSCC was highest is included in Figs. 5c and 5d. In nearly every case, this pairing is the same as that resulting from pairing those modes closest in identified frequency from each of the groups. As in Figs. 5a and 5b, the identified frequencies paired in this manner are almost identical, and the scatter in the corresponding damping factors is small for most modes.

Conclusions

The number of degrees of freedom to be allowed in the ITD identification algorithm can be several times larger than the number of structural modes of vibration excited in the time response functions used for the identification of modal parameters. No adverse effects, in either the accuracy or consistency of identification, resulted from the use of significantly oversized identification models. Such large models are useful in identifying a complete set of modal parameters for all available measurements in one computer analysis. This is valuable for large modal survey tests when a large number of response measurements are obtained. Furthermore, it was found that larger models improved the identification accuracy when noise was present and also allowed the identification of modes of low levels of response. Identifications with identification models of up to 300 DOF proved accurate for data with 200% noise-to-signal ratio and did not result in ill-conditioning for data with infinitesimal noise.

A mode shape correlation constant was used in matching mode shapes obtained from different identification runs, reducing the possibility of mismatching if only frequencies and damping factors are used. This concept was demonstrated in matching experimentally identified modal parameters from two sets of overlapping measurements due to the same excitation, and from different excitation conditions.

References

[1] Ibrahim, S.R. and Mikulcik, E.C., "A Method for the Direct Identification of Vibration Parameters from the Free Response," *Shock and Vibration Bulletin*, No. 47, Part 4, Sept. 1977, pp. 183-198.

[2] Ibrahim, S.R., "Modal Confidence Factor in Vibration Testing," *Journal of Spacecraft and Rockets*, Vol. 15, Sept. 1978, pp. 313-316.

[3] Ibrahim, S.R., "Random Decrement Technique for Modal Identification of Structures," *Journal of Spacecraft and Rockets*, Vol. 14, Nov. 1977, pp. 696-700.

[4] Pappa, R.S. and Ibrahim, S.R., "A Parametric Study of the Ibrahim Time Domain Modal Identification Algorithm," *Shock and Vibration Bulletin*, No. 51, Part 3, May 1981, pp. 43-72.

[5] Hanks, B.R., Miserentino, R., Ibrahim, S.R., Lee, S.H., and Wada, B.K., "Comparison of Modal Test Methods on the Voyager Payload," *Transactions of the SAE*, Vol.87, 1978.

[6] Ibrahim, S.R., "Application of Random Time Domain Analysis to Dynamic Flight Measurements," *Shock and Vibration Bulletin*, No. 49, Part 2, Sept. 1979, pp. 165-170.

Computation of Normal Modes from Identified Complex Modes

S. R. Ibrahim

Reprinted from

AIAA Journal Volume 21, Number 3, March 1983, Page 446

D3

N86-13590

Computation of Normal Modes from Identified Complex Modes

S. R. Ibrahim*
Old Dominion University, Norfolk, Virginia

A technique is presented to compute a set of normal modes from a set of measured (damped) complex modes. The number of elements in the modal vectors, which is equal to the number of measurements, can be larger than the number of modes under consideration. It is also shown in this paper that the practice of normal mode approximation to complex modes can lead to considerably large errors when the modes are too complex. A numerical example and a simulated experiment are presented to illustrate the concepts discussed and to support the theory presented.

Nomenclature

$[C]$ = damping matrix
$[c]$ = modal damping matrix (diagonal)
f = frequency, Hz
I_j = imaginary part of the jth element of a complex modal vector
$[K]$ = stiffness matrix
$[k]$ = modal stiffness matrix (diagonal)
$[M]$ = mass matrix
$[m]$ = modal mass matrix (diagonal)
$n(t)$ = measurements noise
$\{p_j\}$ = jth eigenvector of the state variable equation
$\{Q_j\}$ = jth assumed modal vector
R_j = real part of the jth element of a complex modal vector
s_j = jth assumed characteristic root
$\{x(t)\}$ = state vector, $= \begin{Bmatrix} y(t) \\ \dot{y}(t) \end{Bmatrix}$
$y(t)$ = free-response time function
α_1, α_2 = two angles defining sign ($\pm$) boundaries for the approximated normal mode elements
β_j = phase angle for the jth element of a normal modal vector (0.0 or 180.0 deg)
θ_j = phase angle of the jth element of a complex modal vector
ϕ_j = jth element of the normal modal vector
$\{\phi\}_j$ = jth normal modal vector
ψ_j = jth element of the complex modal vector
$\{\psi\}_j$ = jth complex modal vector
λ_j = jth characteristic root
ω = natural frequency, rad/s
ζ = damping factor
$[\ ]^T$ = transpose of a matrix
$[\ ]^{-1}$ = inverse of a matrix

Introduction and Background

MODAL vibration tests are carried out to experimentally determine a set of modal parameters for the structure under test. These modal parameters are usually used to verify, determine, or improve some analytical model of the structure.[1-8]

Most of the approaches that use experimentally determined modal parameters for dynamic modeling of structures use one or more of the following equations:

$$[M]^{-1}[K]\{\phi\} = \omega^2\{\phi\} \tag{1}$$

$$[\phi]^T[M][\phi] = [m] \tag{2}$$

$$[\phi]^T[K][\phi] = [k] \tag{3}$$

$$[\phi]^T[C][\phi] = [c] \tag{4}$$

In all these equations, the $\{\phi\}$ are the normal modes even though, in practice, the measured modes are the damped complex modes, which in some cases can be very different from normal modes. As a matter of fact, in vibration testing and analysis work it is frequently assumed that damping levels are very small and/or the damping matrix is proportional to either the mass or stiffness matrices, an assumption that is not valid for many of today's complex structures. Such assumptions and the lack of differentiation between normal and complex modes may be attributed to the lack of a tool to measure or compute the normal modes.

With the introduction of computer technology to modal identification in the early 1970s in both frequency domain[9,10] and time domain[11-18] techniques, the question of normal vs complex modes started to need answers. In frequency domain approaches, even with light damping and well-spaced modes, users frequently encountered a scatter of the phase angles associated with the measured modal vector.[14] Some researchers and users even went to the extent of questioning the test and data analysis procedures when the phase angles were not within ± 10 deg at 0-180 deg.

It is to be noted also that measurement of phase angles in the frequency domain can be subject to high levels of errors especially in cases of high modal densities. This is due to the limited frequency resolution and the rapid change in the phase angles around the resonant frequencies. In some cases, the scatter of the phase angles of the modal vectors was due to the fact that the damping is nonproportional, and hence the mode shapes are complex. Time domain approaches to modal identification, which contain no assumptions regarding the level or proportionality of damping, also indicated that structures, in many cases, possess complex modes.

Normal Mode Approximation to Complex Modes

Normal modes are defined as modal vectors whose phase angles are either 0.0 or 180.0 deg. Such modes exist for extremely simple structures, that do not need any testing anyway. They also exist for structures with no damping or structures tailored with proportional damping, none of which represents today's complex structures.

Unlike normal modes, complex modes may possess any phase angle distribution. Each element of the modal vector is

Received Dec. 1, 1981; revision received May 28, 1982.

*Associate Professor, Department of Mechanical Engineering and Mechanics. Member AIAA.

described by a real and imaginary part or an amplitude and phase angle relative to some arbitrary element. A scatter in the phase angles of as much as ±90.0 deg from 0.0 or 180.0 deg is not uncommon.

Recognizing the phase angle scatter for measured (complex) modes and the need for normal modes for use in equations such as (1-4), researchers and users have frequently used normal mode approximation to complex modes.

Figure 1a shows an element of a complex modal vector ψ_j, which is complex and can be expressed as.

$$\psi_j = R_j + iI_j \tag{5}$$

The approximate normal mode element ϕ_j corresponding to ψ_j is

$$\phi_j = \pm\sqrt{R_j^2 + I_j^2} \tag{6a}$$

where the assignment of a positive or negative sign, which is equivalent to 0.0 or 180.0 deg phase angle, depends on the angle θ_i ($\theta_i = \tan^{-1} I_j/R_j$) of the complex modal element and its relation to some arbitrary angles α_1 and α_2 as shown in Fig. 1b. In other words, the phase angle β_j for the approximated normal mode element ϕ_j is assigned according to the equations,

$$\beta_j = 0.0 \text{ deg} \qquad \alpha_2 < \theta_i < \alpha_1 \tag{6b}$$

$$\beta_j = 180.0 \text{ deg} \qquad \alpha_1 < \theta_i < \alpha_2 \tag{6c}$$

It is enough to state that, irrespective of the choice of α_1 and α_2, it is unacceptable to assign two different signs to two elements of the approximated normal modal vector because the phase angles of the corresponding elements of the complex modal vector differ by a fraction of a degree.

Such approximation can lead to erroneous and misleading results and conclusions. An example is the orthogonality check where the orthogonality of the measured modes with respect to the mass matrix is tested. Large off-diagonal terms may result not only because of errors in the mass matrix or inaccuracies in the identification process, but also because of the normal mode approximation to complex modes.

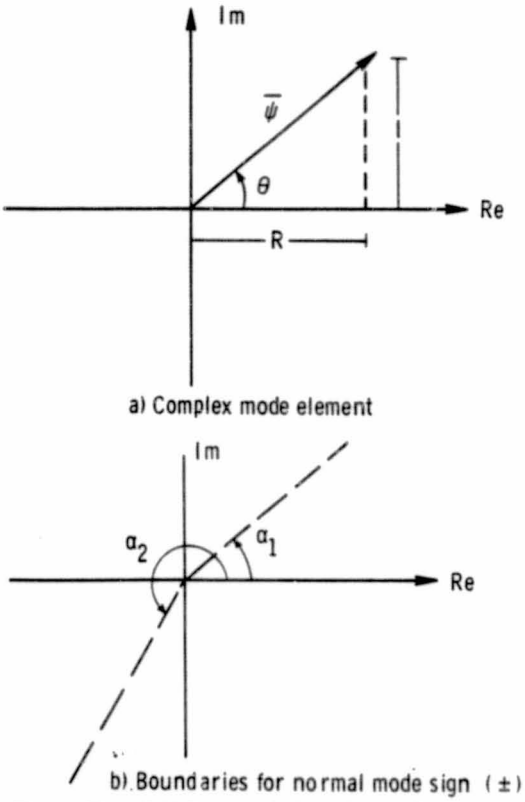

Fig. 1 Normal mode approximation to complex modes.

Numerical Example

The purpose of this example is to show that even though all the parameters used are exact:

1) Complex modes can be very different from normal modes, even for lightly damped modes and small non-proportionality in the damping matrix.

2) Large errors may result from assuming that normal modes approximated from complex modes are orthogonal with respect to the mass matrix.

The system used in this example is a 10 degree-of-freedom system. This system was constructed (simulated) by analytically generating 10 normal modes at 10 measurement stations of a simply supported beam, 10 undamped natural frequencies, and a stiffness matrix for the system. The natural frequencies were selected corresponding to 10.0, 12.0, 15.0, 20.0, 24.0, 30.0, 36.0, 43.0, 46.0, and 50.0 Hz. Then, a proportional damping matrix (equivalent to 1.0% modal damping factor for all 10 modes) and the mass matrix were computed from the assumed information.

To make the damping matrix nonproportional, the damping elements $C(3,3)$, $C(4,4)$, $C(3,4)$, and $C(4,3)$ were doubled. Complex modes, damping factors, and damped natural frequencies were computed for the system. Damping factors changed from 1.0% for all modes for proportional damping case to 2.6, 1.3, 1.2, 1.2, 1.1, 1.8, 2.9, 3.8, 1.7, and 1.0% for the nonproportional damping case. These damping factors are relatively small but nevertheless, some modes showed high levels of complexity. Table 1 shows the two most complex mode shapes, modes 9 and 10, listed with the corresponding normal modes. Phase angles of as much as 98.9 and 74.8 deg

Table 1 Comparison of complex and normal modes

9th mode			10th mode		
Normal f=46.00 Hz ± Amplitude	Complex ζ=1.75% f=45.83 Hz Amplitude	Phase	Normal f=50.00 Hz ± Amplitude	Complex ζ=1.04% f=49.99 Hz Amplitude	Phase
100.00	100.00	0.0	100.00	100.00	0.0
26.00	53.27	64.3	56.00	57.95	175.1
−136.00	144.46	−155.5	−0.00	9.94	−72.9
168.00	167.74	−0.3	56.00	54.85	7.3
−98.00	144.19	136.7	−100.00	102.48	176.0
−26.00	113.55	−98.9	114.00	119.61	−7.9
136.00	135.26	3.3	−98.00	102.24	172.3
−168.00	220.22	143.3	56.00	55.70	0.3
98.00	188.00	−54.8	−0.00	9.73	−74.8
26.00	36.38	48.7	−56.00	58.22	173.0

for modes 9 and 10 are noticed, respectively. Also, large differences in amplitudes exist between normal and complex modes.

To illustrate the large errors that may result from normal modes approximation to complex modes, approximated normal modes were used in checking their orthogonality with respect to the exact mass matrix. The orthogonality matrix results for different values of α_1 and α_2 are

$$\begin{bmatrix}
1.0000 & & & & & & & & & \\
0.0003 & 1.0000 & & & & & & & & \\
-0.0000 & -0.0002 & 1.0000 & & & & & & & \\
-0.0004 & -0.0009 & -0.0003 & 1.0000 & & & & & & \\
0.0010 & -0.0002 & 0.0027 & -0.0007 & 1.0000 & & & & & \\
0.0010 & 0.0033 & 0.0097 & -0.0174 & 0.0013 & 1.0000 & & & & \\
0.0003 & 0.0138 & 0.0054 & 0.0010 & 0.0029 & 0.0074 & 1.0000 & & & \\
0.0013 & 0.0003 & -0.0005 & -0.0026 & -0.0071 & -0.0136 & 0.0070 & 1.0000 & & \\
-0.0597 & 0.0178 & 0.2339 & -0.0639 & -0.0895 & 0.0826 & -0.268 & 0.0316 & 1.0000 & \\
0.0071 & -0.0005 & 0.0150 & -0.013 & -0.0091 & 0.0042 & -0.0209 & -0.0004 & -0.2281 & 1.0000
\end{bmatrix} \tag{7a}$$

$$\begin{bmatrix}
1.0000 & & & & & & & & & \\
0.0003 & 1.0000 & & & & & & & & \\
-0.000 & -0.0002 & 1.0000 & & & & & & & \\
-0.0004 & -0.0009 & -0.0003 & 1.0000 & & & & & & \\
0.0010 & -0.0002 & 0.0027 & -0.0007 & 1.0000 & & & & & \\
0.0010 & 0.0033 & 0.0097 & -0.0174 & 0.0013 & 1.0000 & & & & \\
0.0003 & 0.0138 & 0.0054 & 0.0010 & 0.0029 & 0.0074 & 1.0000 & & & \\
0.0013 & 0.0003 & -0.0005 & -0.0026 & -0.0071 & -0.0136 & 0.0070 & 1.0000 & & \\
-0.2035 & 0.3549 & -0.1791 & 0.0311 & 0.0073 & -0.3108 & 0.1137 & 0.2265 & 1.0000 & \\
-0.0124 & -0.0144 & -0.1338 & 0.0016 & 0.0053 & -0.0241 & -0.0214 & 0.0254 & 0.1672 & 1.0000
\end{bmatrix} \tag{7b}$$

In Eq. (7a) α_1 and α_2 were chosen as 90 and 270 deg, while in Eq. (7b) they are 135 and 315 deg. Errors in the off-diagonal terms are as high as 23.29% for the first case and 35.49% for the second case.

Theory: Computation of Normal Modes

In this section, two approaches are presented to compute normal modes from a measured set of complex modes. The required data are a set of modal parameters such as may be identified from a modal survey test. These modal parameters are namely a set of complex modes $\{\psi\}_i$, $i=1,\ldots m$ and a set of corresponding characteristic roots λ_i, $i=1,\ldots m$ (and their complex conjugates). The modal vectors have n elements where $n>m$, which is a typical test situation. To compute the normal modes from this given set of complex modes, one of the following two approaches may be used.

Approach 1: Using an Oversized Mathematical Model

From the given modal parameters, displacement, velocity, and acceleration responses are formed according to the equations,

$$\{y(t)\} = \sum_{i=1}^{2m} \{\psi\}_i e^{\lambda_i t} + \{n_1(t)\} \tag{8a}$$

$$\{\dot{y}(t)\} = \sum_{i=1}^{2m} \lambda_i \{\psi\}_i e^{\lambda_i t} + \{n_2(t)\} \tag{8b}$$

$$\{\ddot{y}(t)\} = \sum_{i=1}^{2m} \lambda_i^2 \{\psi\}_i e^{\lambda_i t} + \{n_3(t)\} \tag{8c}$$

where $n_1(t)$, $n_2(t)$, $n_3(t)$ are added random noise of uniform distribution. These responses are then used in the state vector equation,

$$\begin{Bmatrix} \dot{y}(t) \\ \ddot{y}(t) \end{Bmatrix} = \begin{bmatrix} 0 & I \\ -M^{-1}K & -M^{-1}C \end{bmatrix} \begin{Bmatrix} y(t) \\ \dot{y}(t) \end{Bmatrix}$$

or

$$\{\dot{x}\} = [A]\{x\} \tag{9}$$

where $\{x\}$ is now the system's state vector containing the displacements and velocities responses. By repeating Eq. (9) for $2n$ time instants, the following equation is satisfied:

$$[\dot{X}] = [A][X] \tag{10}$$

where $[X]$ and $[\dot{X}]$ contain responses measured at the $2n$ time instants. From Eq. (10) the $[A]$ matrix can be identified as,

$$[A] = [\dot{X}][X]^{-1} \tag{11}$$

By computing matrix [A], the $[M^{-1}K]$ matrix gives normal modes according to the eigenvalue equation,

$$[M^{-1}K]\{\phi\} = \omega^2\{\phi\} \tag{12}$$

Naturally, without any noise, the matrix [X] is singular since the number of degrees of freedom is larger than the number of modes present in the responses. A small amount of noise makes the inversion of [X] possible for the purpose of extracting modal information. For example, noise to signal ratios of as little as 0.000001 were used[17] to invert a 600×600 matrix of a rank of 4 without signs of ill-conditioning on a 60 bit word computer. Higher levels of noise may be needed for computers with less accuracy.

The mechanism on which the success of this approach is based can be explained as follows.

The state vector's $2n$ free-response functions containing modal information from m structural modes of vibration can be expressed as,

$$\{x(t)\} = \sum_{k=1}^{2m} \{p\}_k e^{\lambda_k t} \tag{13}$$

where $\{p\}$ represents the m complex pairs of the systems independent eigenvectors. If noise-free responses are used in the identification algorithm, the math model must have exactly m degrees of freedom for unique identification. If more than m degrees of freedom are allowed, the [X] matrix is singular.

In experimental work, however, measured responses always contain a certain amount of noise (or as in this case a small amount of noise is added on purpose). These noisy responses can be expressed as,

$$\{x(t)\} = \sum_{k=1}^{2m} \{p\}_k e^{\lambda_k t} + \{n(t)\} \tag{14}$$

In previous applications[11-17] it was found that using noisy responses in the identification process, with the number of degrees of freedom larger than m, yielded good results without encountering singularity. The results even improved as the math model size was increased. The qualitative explanation for this situation is that the extra degrees of freedom act as outlets for the noise. In this case, the noisy responses can be expressed as,

$$\{x(t)\} = \sum_{k=1}^{2m} \{p\}_k e^{\lambda_k t} + \sum_{k=2m+1}^{2n} \{N\}_k e^{r_k t} \tag{15}$$

in which the noise is modeled as a combination of $(2n-2m)$ complex exponential functions. Since the value of m, the number of excited modes, is a characteristic of the structural response and not the data analysis process, additional exponential functions are allowed to represent the noise in the math model as n is increased. This results in a higher-order fit for the noise portion of the responses, reducing residuals that would otherwise be included in the signal portion of the responses.

Approach 2: Using Assumed Modes

The given set of complex modal parameters satisfy the equation

$$[M^{-1}K \quad M^{-1}C] \begin{Bmatrix} \psi_i \\ \lambda_i\psi_i \end{Bmatrix} = \{-\lambda_i^2\psi_i\} \quad (i=1,\ldots m) \tag{16}$$

Since we have only m modes and the system has n degrees of freedom, Eq. (16) cannot be solved for $[M^{-1}K\,M^{-1}C]$. Let us assume that there exists a set of vectors $\{Q\}_j$ and a set of characteristic roots s_j, $j=m+1,\ m+2,\ldots n$. This set of assumed parameters are selected such that

$$\lambda_i \neq s_j \tag{17a}$$

$$\{Q\}_j \neq [\psi_1\ \psi_2 \ldots \psi_m]\{a\} \tag{17b}$$

where $\{a\}$ is any vector of coefficients. Equation (17b) implies that $\{Q\}_j$ and $\{\psi\}_i$ for all i and j form a linearly independent set of vectors. In such a case, it can be written that

$$[M^{-1}K \quad M^{-1}C] \begin{Bmatrix} Q_j \\ s_jQ_j \end{Bmatrix} = \{-s_j^2Q_j\}$$

$$(j=m+1,\ m+2,\ldots n) \tag{18}$$

and Eqs. (16) and (18) can be solved for $[M^{-1}K\,M^{-1}C]$ from which normal modes are computed according to Eq. (12).

To illustrate the soundness of this second approach, let it be assumed that there exists a hypothetical system whose n free response time functions are linear combinations of the two independent sets of modes $\{\psi\}$ and $\{Q\}$. These responses can then be expressed as

$$\{y(t)\} = \sum_{k=1}^{2m} \{\psi\}_k e^{\lambda_k t} + \sum_{j=1}^{2n-2m} \{Q\}_j e^{s_j t}$$

$$= [\psi_1\psi_2\ldots\psi_{2m}] \begin{Bmatrix} e^{\lambda_1 t} \\ e^{\lambda_2 t} \\ \cdots \\ e^{\lambda_{2m} t} \end{Bmatrix} + [Q_1Q_2\cdots Q_{2n-2m}] \begin{Bmatrix} e^{s_1 t} \\ e^{s_2 t} \\ \cdots \\ e^{\lambda_{2n-2m} t} \end{Bmatrix}$$

$$= [\psi_1\psi_2\ldots\psi_{2m}Q_1Q_2\cdots Q_{2n-2m}] \begin{Bmatrix} e^{\lambda_1 t} \\ e^{\lambda_2 t} \\ \cdots \\ e^{\lambda_{2m} t} \\ e^{s_1 t} \\ e^{s_2 t} \\ \cdots \\ e^{s_{2n-2m} t} \end{Bmatrix} \tag{19}$$

The responses of Eq. (19) are typical of a second order dynamic system whose state vector equation is

$$\begin{Bmatrix} \dot{y} \\ \ddot{y} \end{Bmatrix} = \begin{bmatrix} 0 & I \\ A & B \end{bmatrix} \begin{Bmatrix} y \\ \dot{y} \end{Bmatrix}$$

where the [A] matrix represents the inertia-stiffness information and the [B] matrix represents the inertia-damping characteristics.

If these responses, as expressed in Eq. (19), are to be used in any identification algorithm, the vectors $\{\psi\}$ and $\{Q\}$ and the characteristic roots λ and s will be uniquely identified. The identified properties of the initial set of modes $\{\psi\}$ should be unique and independent of the assumed Q and s as long as the conditions of Eq. (17) are satisfied.

An appropriate selection for the set of assumed modal parameters would be from the structure's finite element model. Higher analytical modes, other than the measured ones, are highly recommended for such a use.

It is extremely important to point out that $[M^{-1}K]$ and $[M^{-1}C]$ obtained from either approach are not unique since

Table 2 Identified complex mode and normal mode

Mode 9						Mode 10					
Theoretical			Identified			Theoretical			Identified		
Normal $f=46.00$ Hz ± Amplitude	Complex $\zeta=1.75\%$ $f=45.83$ Hz Amplitude	Phase	Normal $f=46.00$ Hz ± Amplitude	Complex $\zeta=2.60\%$ $f=45.93$ Hz Amplitude	Phase	Normal $f=50.00$ Hz ± Amplitude	Complex $\zeta=1.04\%$ $f=50.00$ Hz Amplitude	Phase	Normal $f=50.00$ Hz ± Amplitude	Complex $\zeta=1.74\%$ $f=50.00$ Hz Amplitude	Phase
100.00	100.00	0.0	100.00	100.00	0.0	100.00	100.00	0.00	100.00	100.00	0.0
26.00	53.27	64.3	25.18	64.93	59.0	−56.00	57.95	175.1	−55.07	57.27	170.7
−136.00	144.46	−155.5	−136.76	152.63	−154.0	0.00	9.94	−72.9	0.39	13.54	−74.4
168.00	167.74	−0.3	170.00	164.89	−2.2	56.00	54.85	7.3	54.08	53.19	8.8
−98.00	144.19	136.7	−97.65	135.86	132.6	−100.00	102.48	176.0	−94.95	97.74	175.6
−26.00	113.55	−98.9	−36.95	107.75	−109.2	114.00	119.61	−7.9	109.92	116.18	−9.6
136.00	135.26	3.3	145.63	140.38	−0.3	−98.00	102.24	172.3	−90.82	94.78	171.5
−168.00	220.22	143.3	−167.51	202.69	143.7	56.00	55.70	0.3	59.42	58.61	−1.1
98.00	188.00	−54.8	94.81	164.94	−54.7	−0.00	9.73	−74.8	−0.44	4.01	−48.1
26.00	36.38	48.7	28.32	36.51	41.5	−56.00	58.22	173.0	−55.36	57.71	170.9

they are functions of the introduced noise or the assumed modes. However the set of normal modes, corresponding to the set of given complex modes, was found to be independent of the introduced small levels of noise or the assumed modes.

Simulated Experiment

To test the validity of the theories presented in this paper, the 10 degrees-of-freedom system previously discussed in the section on numerical example is used here as a simulated test structure. Response time histories containing contribution from the last four modes measured at the 10 stations were generated. The last four modes were selected because the last two modes show a high level of complexity. Simulated measurements noise was added to these responses, with a noise/signal rms ratio of 20%, to represent conditions in a real vibration test. From these responses, the complex modes and characteristic roots were identified, using the time domain approach.[11] Normal modes were then computed using the two approaches presented here. A noise to signal ratio of 0.00001 was used for Eqs. (8). The assumed modes approach produced results identical to those of the oversized math model approach.

Table 2 lists the identified complex modes and the computed normal modes for the last two modes. A close examination of the computed normal modes, in comparison with the theoretical ones, indicate the validity of the approaches presented.

Using the identified complex modes and the computed normal modes, the orthogonality check matrices are

$$\begin{bmatrix} 1.0000 & & & \\ -0.0438 & 1.0000 & & \\ -0.0018 & -0.0300 & 1.0000 & \\ -0.0205 & 0.0365 & -0.2091 & 1.0000 \end{bmatrix} \quad (20a)$$

$$\begin{bmatrix} 1.0000 & & & \\ -0.0438 & 1.0000 & & \\ 0.0899 & 0.0999 & 1.0000 & \\ -0.0282 & 0.0626 & -0.4802 & 1.0000 \end{bmatrix} \quad (20b)$$

$$\begin{bmatrix} 1.0000 & & & \\ -0.0464 & 1.0000 & & \\ 0.0228 & -0.0353 & 1.0000 & \\ -0.0082 & 0.0531 & -0.0546 & 1.0000 \end{bmatrix} \quad (20c)$$

In Eqs. (20a) and (20b) approximated normal modes were used with (90, 270 deg) and (135, 315 deg) for (α_1, α_2), respectively. In Eq. (20c) the computed normal modes were used. Errors of 21 and 48% are noticed in the off-diagonal terms for cases a and b, respectively, while the maximum error for case c was only 5%.

Conclusions

It is shown in this paper that even for low levels of damping for structures with nonproportional damping, complex modes can be very different from normal modes. In such cases, normal mode approximation to complex modes may lead to large errors in mass-weighted orthogonality checks or in any other use of these complex modes approximated as normal modes.

A technique is presented to compute normal modes from measured complex modes. Computed normal modes eliminate possible errors that may result from using normal mode approximation to complex modes produced by non-proportional damping.

Acknowledgment

This work was partially supported by a grant from NASA Langley Research Center.

References

[1] Young, J. P. and On, F. J., "Mathematical Modeling Via Direct Use of Vibration Data," Paper presented at SAE National Aeronautic and Space Engineering and Manufacturing Meeting, Los Angeles, Calif., Oct. 1969.

[2] Thoren, A. R., "Derivation of Mass and Stiffness Matrices from Dynamic Test Data," *Proceedings of the AIAA/ASME/SAE 13th Structures, Structural Dynamics and Materials Conference*, San Antonio, Texas, April 1972.

[3] Berman, A., "System Identification of a Complex Structure," *Proceedings of the AIAA/ASME/SAE 16th Structures, Structural Dynamics and Materials Conference*, Denver, Colo., May 1975.

[4] Potter, R. and Richardson, M., "Mass Stiffness and Damping Matrices from Measured Modal Parameters," Paper presented at International Instrumentation-Automation Conference, New York, Oct. 1974.

[5] Berman, A., "Mass Matrix Correction Using an Incomplete Set of Measured Modes," *AIAA Journal*, Vol. 17, Oct. 1979.

[6] Chen, J. C. and Garba, J. A., "Matrix Perturbation for Analytical Model Improvement," *Proceedings of the AIAA/ASME/ASCE/AHS 20th Structures, Structural Dynamics and Materials Conference*, St. Louis, Mo., April 1979.

[7] Baruch, M., "Optimization Procedure to Correct Stiffness and Flexibility Matrices Using Vibration Tests," *AIAA Journal*, Vol. 16, April 1978.

[8] Berman, A., Wei, F. S., and Rao, K. W., "Improvement of Analytical Models Using Modal Test Data," *Proceedings of the AIAA/ASME/ASCE/AHS 21st Structures, Structural Dynamics and Materials Conference*, Seattle, Wash., May 1980.

[9] Klosterman, A. and Zimmerman, R., "Modal Survey Activity Via Frequency Response Functions," SAE Paper 751068, 1975.

[10] Brown, D. L., Allemang, R. J., Zimmerman, R., and Mergeay, M., "Parameter Estimation Techniques for Modal Analysis," SAE Paper 790221, Feb. 1979.

[11] Ibrahim, S. R. and Mikulcik, E. C., "A Method for the Direct Identification of Vibration Parameters from the Free Response," *Shock and Vibration Bulletin*, No. 47, Pt. 4, Sept. 1977, pp. 183-198.

[12] Ibrahim, S. R., "Random Decrement Technique for Modal Identification of Structures," *Journal of Spacecraft and Rockets*, Vol. 14, Nov. 1977, pp. 696-700.

[13] Ibrahim, S. R., "Modal Confidence Factor in Vibration Testing," *Journal of Spacecraft and Rockets*, Vol. 15, Sept. 1978, pp. 313-316.

[14] Hanks, B. R., Miserentino, R., Ibrahim, S. R., Lee, S. H., and Wada, B. K., "Comparison of Modal Test Methods on the Voyager Payload," *Transactions of Society of Automotive Engineers*, Vol. 87, 1978.

[15] Ibrahim, S. R., "Application of Random Time Domain Analysis to Dynamic Flight Measurements," *Shock and Vibration Bulletin*, No. 49, Pt. 2, Sept. 1979, pp. 165-170.

[16] Pappa, R. S. and Ibrahim, S. R., "A Parametric Study of the Ibrahim Time Domain Modal Identification Algorithm," *Shock and Vibration Bulletin*, No. 51, Pt. 3, May 1981, pp. 43-72.

[17] Ibrahim, S. R. and Pappa, R. S., "Large Modal Survey Testing Using the Ibrahim Time Domain (ITD) Identification Technique," *Journal of Spacecraft and Rockets*, Vol. 19, Sept.-Oct. 1982, pp. 459-465.

[18] Andrew, L. V., "An Automated Application of Ibrahim's Time Domain Method to Responses of the Space Shuttle," *Proceedings of the AIAA/ASME/ASCE/AHS 22nd Structures, Structural Dynamics and Material Conference*, Atlanta, Georgia, April 1981.

Dynamic Modeling of Structures from Measured Complex Modes

S. R. Ibrahim

Reprinted from

AIAA Journal Volume 21, Number 6, June 1983, Page 898

AMERICAN INSTITUTE OF AERONAUTICS AND ASTRONAUTICS • 1290 AVENUE OF THE AMERICAS • NEW YORK, NEW YORK, N.Y. 10104

Dynamic Modeling of Structures from Measured Complex Modes

Samir R. Ibrahim*
Old Dominion University, Norfolk, Virginia

A technique is presented to use a set of identified complex modes together with an analytical mathematical model of a structure under test to compute improved mass, stiffness, and damping matrices. A set of identified normal modes, computed from the measured complex modes, is used in the mass orthogonality equation to compute an improved mass matrix. This eliminates possible errors that may result from using approximated complex modes as normal modes. The improved mass matrix, the measured complex modes, and the higher analytical modes are then used to compute the improved stiffness and damping matrices. The number of degrees-of-freedom of the improved model is limited to equal the number of elements in the measured modal vectors. A simulated experiment shows considerable improvements, in the system's analytical dynamic model, over the frequency range of the given measured modal information.

Nomenclature

$[C_A]$ = $(n \times n)$ analytical damping matrix
$[C_E]$ = $(n \times n)$ exact damping matrix
$[C]$ = $(n \times n)$ improved damping matrix
j = $\sqrt{-1}$
$[K_A]$ = $(n \times n)$ analytical stiffness matrix
$[K_E]$ = $(n \times n)$ exact stiffness matrix
$[K]$ = $(n \times n)$ improved stiffness matrix
m = number of measured modes
$[m_A]$ = $(n \times n)$ analytical modal mass matrix (diagonal)
$[M_A]$ = $(n \times n)$ analytical mass matrix
$[M_E]$ = $(n \times n)$ exact mass matrix
$[M]$ = $(n \times n)$ improved mass matrix
n = number of degrees-of-freedom of math models
$\{\phi_i\}$ = ith normal modal vector (n elements)
$\{\psi_i\}$ = ith complex modal vector (n elements)
ζ_i = ith damping factor
λ_i = ith characteristic root
ω_d = damped natural frequency
ω_n = natural frequency

Introduction

DUE to the increasing complexity of modern aerospace, and some nonaerospace structures, and due to the nature, sensitivity, and sophistication of the missions of such structures, an accurate mathematical model has become a necessity for successful performance. Such models are needed for responses and loads prediction, stability analysis, and control system design.

Past, and sometimes current, common practice, in spite of the advanced state-of-the-art in both finite element and structural dynamic identification, in arriving at a dependable mathematical model was done primarily by trial and error approach. An analyst, using some modal test data, adjusts his or her model, using personal judgment and experience, to make it fit the available modal test data. During the last three decades there have been continuous efforts by researchers and practitioners in the area of dynamic modeling of structures using identified modal parameters. The survey paper,[1] covering work done in the 1960's, pointed out a need to improve the state-of-the-art of dynamic modeling.

Subsequent work in dynamic modeling from test data can be divided into two categories. The first category uses only experimental data to derive the mass, stiffness, and damping matrices.[2-4] The other category deals with using identified modal data to improve an existing, sometimes larger, analytical model.[5-8]

One of the important and basic relations often used in dynamic modeling is that the measured modes satisfy the theoretical requirement of weighted orthogonality with respect to the mass and stiffness matrices. Such a requirement can only be satisfied assuming no or proportional damping and a symmetrical stiffness matrix,[9] in which a case damped and normal modes are the same. For simpler structures the measured modes (complex modes) are very close to the normal modes. For more complex structures, the complex modes can be very much different from the normal modes. Attempts to use these complex modes, as normal modes, for satisfying the orthogonality requirement may lead to adverse effects on the process of dynamic modeling.

Complexity of modes, indicated by a scatter in the phase angles associated with the modal vector, is becoming more noticeable to today's dynamicist due to the complexity and damping characteristics of modern structures. Naturally, such a scatter in the phase angles could be due to measurement errors, erroneous identification, nonlinearities, as well as just the mere fact of having a case of complex modes as a result of the presence of nonproportional damping.

For structures with nonproportional damping, it is extremely difficult to measure normal modes even by using techniques such as multiple-sine-dwell, since this very technique is based on the assumption of proportional damping.[10] Using measured modes directly in the equation of orthogonality requirement can result in large errors in the off-diagonal terms.[11,12] Such errors can be due to the fact that the structure has complex modes (nonproportional damping) among other reasons.

The approach proposed herein is designed to circumvent using complex modes as normal modes, when correcting the analytical mass matrix. Instead, the procedure allows for the computation of normal modes from the given set of measured complex modes.

Theory and Procedure

In this procedure, it is assumed that the structure under consideration has an analytical mathematical model that needs improvements. Such a model can, as in most cases, be a finite element model. Furthermore, it is assumed that the structure has been tested in a modal survey test for the identification of its modal parameters. The following in-

Presented as Paper 82-0770 at the AIAA/ASME/ASCE/AHS 23rd Structures, Structural Dynamics and Materials Conference, New Orleans, La., May 10-12, 1982; submitted May 12, 1982; revision received Sept. 17, 1982.

*Associate Professor, Department of Mechanical Engineering and Mechanics. Member AIAA.

formation is required for the procedure of improving the analytical model.

1) Modal Test Data. It is assumed that a complete modal survey test has been conducted and that the following test data are available: a) the complex modal vectors $\{\psi_i\}$, $i=1,...m$, measured at n measurement stations where $n>m$; b) the damped natural frequencies $(\omega_d)_i$, $i=1,...m$; and c) the damping factors ζ_i, $i=1,...m$.

2) Analytical Model Data. From the analytical model, the following information is required: a) an $n\times n$ mass matrix $[M_A]$ or the n elements of the modal mass matrix $[m_A]$; b) the normal modes $\{\phi_i\}$, $i=1,...n$, at the n measurement stations of the modal survey test; and c) the natural frequencies $(\omega_n)_i$, $i=1,...n$. The preceding information will be used to compute improved mass and stiffness matrices $[M]$ and $[K]$ and a damping matrix $[C]$.

Computation of $[M^{-1}K]$ and $[M^{-1}C]$

Assuming that the structure under consideration is linear, the measured modal parameters satisfy the following equation:

$$[M^{-1}K\ M^{-1}C]\begin{Bmatrix}\psi_i\\ \lambda_i\psi_i\end{Bmatrix}=\{-\lambda_i^2\psi_i\}... \quad (i=1,2,...m) \tag{1}$$

where λ_i is the ith characteristic root of the system which is related to the ith damping factor and the ith damped natural frequency through the equation

$$\lambda_i=(\omega_d)_i\left\{\frac{\zeta_i}{\sqrt{1-\zeta_i^2}}+j\right\}... \tag{2}$$

Equation (1) represents $n\times m$ complex equations or $2n\times m$ real equations. These equations are not sufficient to solve for system's $[M^{-1}K\,M^{-1}C]$.

Since no information is available to correct the analytical model beyond the frequency range over which the modal test was conducted, the analytical higher modes will be assumed to also satisfy Eq. (1). This will give the following set of equations:

$$[M^{-1}K\ M^{-1}C]\begin{Bmatrix}\phi_i\\ \lambda_i\phi_i\end{Bmatrix}=\{-\lambda_i^2\phi_i\}... \quad (i=m+1,...n) \tag{3}$$

where λ_i in this case is:

$$\lambda_i=(\omega_n)_i\{-\zeta+j\sqrt{1-\zeta^2}\}... \tag{4}$$

It is to be noted here that most analytical models do not have damping information. It is reasonable to assume that these higher analytical modes have a damping factor equal to the average damping factor of the m measured modes

$$\zeta=\frac{1}{m}\sum_{i=1}^{m}\zeta_i \tag{5}$$

Equation (3) represents $2n\times(n-m)$ equations. Combining Eqs. (1) and (3), the $2n^2$ linear equations can be solved for $[M^{-1}KM^{-1}C]$.

Computation of Experimental Normal Modes

The purpose of this section is to compute the set of normal modes, corresponding to the set of measured complex modes, for use in correcting the mass matrix. This step is essential in case the measured modes indicate the presence of non-proportional damping in the structure under test. This can be indicated clearly by large scatter in the phase angles associated with the measured modal vectors, a phenomenon found in several of today's modern complex structures. Such a complexity of measured modes is especially noticed in the higher modes that are needed badly to increase the frequency range of the dynamic model correction. It is the author's opinion that any effort to use complex modes, approximated as normal modes, to correct an analytical mass matrix may worsen rather than improve the analytical mass matrix.

Two approaches[13] were presented to compute normal modes from measured complex modes, one of which is similar to the method presented in the preceding section to compute $[M^{-1}K\,M^{-1}C]$. The $[M^{-1}K]$ matrix can yield a set of normal modes, corresponding to the set of measured complex modes, through the relation

$$[M^{-1}K]\{\phi\}=\omega^2\{\phi\}... \tag{6}$$

This eigenvalue equation will give n eigenvalues and n eigenvectors. The first m of these eigenvectors are the m computed normal modes corresponding to m measured complex modes. The remainder eigenvectors will be the higher analytical modes used in Eq. (3).

Correction of the Mass Matrix

Several approaches can be used to correct the mass or stiffness matrices. The approach based on minimum changes,[8] gives the corrected mass matrix as

$$[m_A]=[\phi]^T[M_A][\phi]$$

$$[M]=[M_A]+[M_A][\phi][m_A]^{-1}[I-m_A][m_A]^{-1}[\phi]^T[M_A]$$

where $[\phi]$ is $(n\times m)$ "measured" normal modes, and $[m_A]$ is $m\times m$.

The approach used herein is simply based on computing a mass matrix that satisfies the orthogonality condition for the measured normal modes and the higher analytical normal modes, i.e.,

$$[\phi]^T[M][\phi]=[m_A] \tag{7}$$

where the columns of $[\phi]$ in this case are the eigenvectors computed from Eq. (6).

Computation of Corrected Stiffness and Damping Matrices

After computing $[M^{-1}K\,M^{-1}C]$ from Eqs. (1) and (3) and $[M]$ from Eq. (7), the stiffness and damping matrices can be given by

$$[K]=[M][M^{-1}K] \tag{8}$$

$$[C]=[M][M^{-1}C] \tag{9}$$

and this completes the computation of corrected or improved mass, stiffness, and damping matrices.

Criteria for Evaluating Dynamic Model Improvements

The question of judging the success of any dynamic model improvements technique is quite a difficult one. Should the changes to the analytical model be minimum? Should the improved model represent a physical system rather than just a set of numbers? What about ending with negative masses or negative stiffness in the improved mass matrix? The answer to the question of success should be very much dependent on the intended use of the improved model.

In the work reported here, the goal of improving the analytical mathematical model is to make the improved model respond to any input as close as possible to the response of the exact model (real structure) over the correction frequency range. This makes the improved model suitable for responses and loads prediction and control system design but not for structural modifications. If the improved model is to be used for structural modifications, the number of degrees-of-

Table 1 Exact, analytical, and improved frequencies and damping factors

Mode	Frequency, Hz Exact	Analytical	Improved	Damping factor ζ, % Exact	Analytical	Improved	Notes
1	9.999	10.082	9.998	2.00	1.00	2.00	Frequency
1	11.998	12.142	11.998	2.00	1.00	2.00	range of
3	14.997	15.204	14.997	2.00	1.00	2.00	modal test
4	19.996	19.254	19.996	2.00	1.00	2.00	data
5	23.995	23.911	23.911	2.00	1.00	1.00	
6	29.994	31.683	31.683	2.00	1.00	1.00	
7	35.993	33.740	33.740	2.00	1.00	1.00	
8	42.991	41.020	41.020	2.00	1.00	1.00	
9	45.991	44.293	44.293	2.00	1.00	1.00	
10	49.990	46.104	46.104	2.00	1.00	1.00	

Table 2 Exact, analytical, and improved mode shapes

Mode	Exact Amplitude	Phase, deg	Analytical Amplitude	Phase, deg	Improved Amplitude	Phase, deg
	100.00	0.0	100.00	0.0	100.00	0.0
	157.00	−0.4	148.49	0.0	157.00	−6.4
	155.56	−19.7	141.85	0.0	155.56	−19.7
	116.55	−45.5	93.71	0.0	116.55	−45.5
	81.11	−93.2	29.97	0.0	81.11	−93.2
2	81.11	−156.7	29.06	180.0	81.11	−156.7
	116.55	155.6	95.00	180.0	116.55	155.6
	155.56	129.8	134.79	180.0	155.56	129.8
	157.00	116.5	141.71	180.0	157.00	116.5
	100.00	110.1	101.35	180.0	100.00	110.1
	100.00	0.0	100.00	0.0	100.00	0.0
	74.24	−18.0	70.32	0.0	74.24	−18.0
	51.66	−150.3	43.19	180.0	51.66	−150.3
	99.08	166.7	91.65	180.0	99.08	166.7
	63.70	116.5	44.89	180.0	63.70	116.5
4	63.70	6.4	43.48	0.0	63.70	6.4
	99.08	−43.8	89.33	0.0	99.08	−43.8
	51.66	−86.8	42.40	0.0	51.66	−86.8
	74.24	−140.9	72.75	180.0	74.24	140.9
	100.00	122.9	106.09	180.0	100.00	122.9

freedom of the analytical model should be larger than the number of elements in the measured modal vectors. This will require the computation of the unmeasured modal vectors' elements. That is a point to be considered for future investigations.

Illustrative Simulated Experiment

The purpose of selecting a simulated experiment, rather than a real experiment, is to test the effectiveness of the proposed technique under controlled conditions. In this simulated study an exact mathematical model is available as a reference for comparison. This exact mathematical model is corrupted with random errors to produce an analytical model which is to be corrected to produce the improved mathematical model. A comparison is later conducted between the improved, analytical, and exact mathematical models.

Exact Model

The exact model possesses ten degrees-of-freedom. It is derived through assuming ten complex modes of the form

$$\psi_{ik} = \sin\frac{ik\pi}{11} + j0.5\sin\frac{i(k+1)\pi}{11} \qquad (i=1,2,\ldots 10 \text{ and } k=1,2,\ldots 10) \qquad (10)$$

The ten modes were assumed to have undamped natural frequencies of 10, 12, 15, 20, 24, 30, 36, 43, 46, and 50 and a damping factor of 2.0% for all ten modes.

Using the preceding modal information, $[M_E^{-1}K_E]$ and $[M_E^{-1}C_E]$ were computed. From $[M_E^{-1}K_E]$ the normal modes were computed and then used in the equation

$$[\phi]^T[M_E][\phi] = [M_A] \qquad (11)$$

with all elements of $[m_A]$ assumed equal 1.0×10^{-5}; $[M_E]$ and, subsequently, $[K_E]$ and $[C_E]$ were calculated.

Analytical Model

Random errors ranging between ±1.0% for first mode to ±10.0% for the tenth mode were introduced in the ten undamped natural frequencies. Random errors of ±5.0% were introduced to exact normal modes. These corrupted modal parameters were then used to calculate $[M_A^{-1}K_A\ M_A^{-1}C_A]$ for the analytical mathematical model with proportional damping equivalent to 1.0%. The modal mass matrix $[m_A]$ from the exact model was used with ±5.0% random errors to calculate $[M_A]$, $[K_A]$, and $[C_A]$.

Improved Model

Exact modal parameters (complex mode shapes, damped natural frequencies, and damping factors) of the first four modes here are considered as the measured modal parameters. These four modes together with the six higher analytical modes were used to correct the analytical model as previously described.

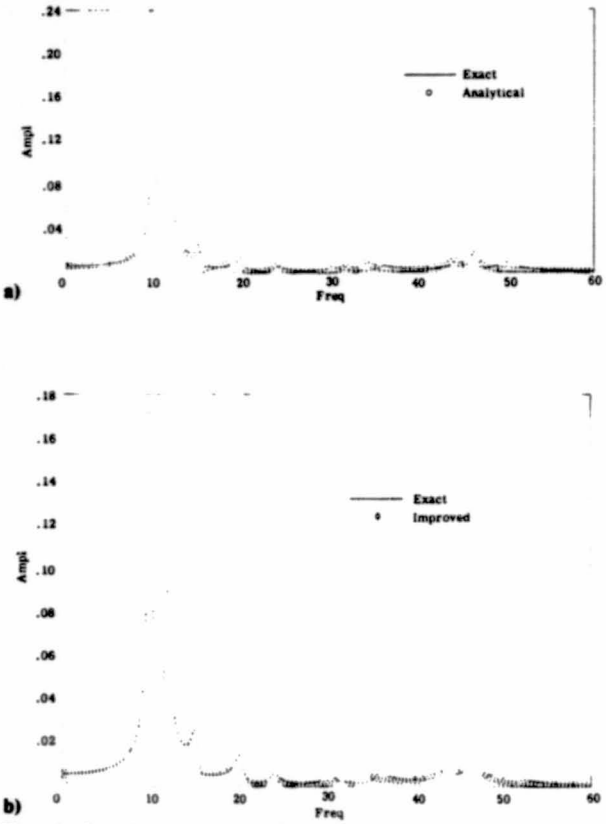

Fig. 1 Impulse responses of station four: a) analytical model b) improved model.

Results and Discussion

Table 1 shows the exact, analytical, and improved natural frequencies and damping factors. The second and fourth mode shapes for the exact, analytical, and improved mathematical models are listed in Table 2 for comparison. Figures 1a and 1b show the fourth station response of the analytical model and improved model, respectively, plotted on the exact response due to an impulse at the first station. These figures show responses over the whole frequency range (0-60.0 Hz). While noticeable improvements are produced over the correction frequency range (0-20.0 Hz), no adverse effects resulted from the improvement process over the remainder of the frequency range.

Conclusions

A direct technique to use experimental and analytical modal parameters to improve an existing analytical model is presented. The corrected model's response resembles the exact model's response more accurately than the analytical model over the frequency range of the measured modal test data. No adverse effects on the improved system's responses resulted beyond the correction frequency range. Built into the algorithm procedure is the computation of the normal modes, corresponding to the set of measured complex modes, that are used for mass matrix correction. This feature promises to eliminate the errors that may result from using approximated complex modes as normal modes for mass matrix correction, which makes this technique advantageous when dealing with complex structures possessing, not necessarily high levels of damping, but a high degree of nonproportionality in damping.

Acknowledgment

This work was supported by a grant from NASA Langley Research Center.

References

[1] Young, J. P. and On, F. J., "Mathematical Modeling Via Direct Use of Vibration Data," SAE National Aeronautic and Space Engineering and Manufacturing Meeting, Los Angeles, Calif., Oct. 1969.

[2] Thoren, A. R., "Derivation of Mass and Stiffness Matrices from Dynamic Test Data," *Proceedings of the AIAA/ASME/SAE 13th SDM Conference*, San Antonio, Tex., April 1972.

[3] Berman, A., "System Identification of a Complex Structure," *Proceedings of the AIAA/ASME/SAE 16th SDM Conference*, Denver, Colo., May 1975.

[4] Potter, R. and Richardson, M., "Mass Stiffness and Damping Matrices from Measured Modal Parameters," International Instrumentation-Automation Conference, New York, Oct. 1974.

[5] Berman, A., "Mass Matric Correction Using and Incomplete Set of Measured Modes," *AIAA Journal*, Vol. 17, Oct. 1979.

[6] Chen, J. C. and Garba, J. A., "Matrix Perturbation for Analytical Model Improvement," *Proceedings of the AIAA/ASME/ASCE/AHS 20th SDM Conference*, St. Louis, Mo., April 1979.

[7] Baruch, M., "Optimization Procedure to Correct Stiffness and Flexibility Matrices Using Vibration Tests," *AIAA Journal*, Vol. 16, April 1978.

[8] Berman, A., Wei, F. S., and Rao, K. W., "Improvement of Analytical Models Using Modal Test Data," *Proceedings of the AIAA/ASME/ASCE/AHS 21st SDM Conference*, Seattle, Wash., May 1980.

[9] Meirovitch, L., *Analytical Methods in Vibrations*, McMillan Publishing Co., 1967.

[10] Lewis, R. C. and Wrisley, D. L., "A System for the Excitation of Pure Natural Modes of Complex Structures," *Journal of the Aerospace Sciences*, Vol. 17, 1950, pp. 705-722.

[11] Leppert, E. L., Lee, S. H., Day, F. D., Chapman, P. C., and Wada, B. K., "Comparison of Modal Test Results: Multipoints Sine Versus Single Point Random," ASE Paper 760879, Nov. 1976.

[12] Chu, F. H., Voorhees, C., Metzger, W. W., and Wilding, R., "Spacecraft Modal Testing Using Systematic Multi-Shaker Sine-Dwell Testing Techniques," *Shock and Vibration Bulletin 51*, Pt. 2, May 1981, pp. 41-58.

[13] Ibrahim, S. R., "Computation of Normal Modes from Identified Complex Modes," *AIAA Journal*, Vol. 21, No. 3, March 1983, pp. 446-451.

Reprinted from CP832, A Bound Collection of Technical Papers

AIAA-83-0811-CP
Time-Domain Quasi-Linear Identification of Nonlinear Dynamic Systems

S.R. Ibrahim

AIAA/ASME/ASCE/AHS
24th STRUCTURES, STRUCTURAL DYNAMICS AND MATERIALS CONFERENCE

Lake Tahoe, Nevada
May 2-4, 1983

TIME-DOMAIN QUASI-LINEAR IDENTIFICATION OF NONLINEAR DYNAMIC SYSTEMS

83-0811

Samir R. Ibrahim*
Department of Mechanical Engineering
and Mechanics
Old Dominion University
Norfolk, Virginia

Abstract

A time-domain linear modal identification technique is applied to identify some highly nonlinear dynamic systems. The modal concept is used to identify such nonlinear systems with the understanding that the resulting modes are only a mathematical representation of the series solution of the nonlinear system under consideration. Naturally these identified modal parameters are not unique, for nonlinear systems, since they are functions of the systems' amplitudes and hence referred to as quasi-linear. The approach presented in this paper can be useful in predicting signs of nonlinearities when linearity is assumed. It can also be used to analyze and understand types of nonlinearities of nonlinear systems through successive identifications at different levels of responses.

Nomenclature

f	frequency in Hz
F_i	force in restoring force element i
M	mass
m	number of degrees of freedom of the identification math model
n	number of harmonics
$\{n(t)\}$	measurements noise vector
$\{N_i\}$	modal vector for noise representation
p	number of degrees of freedom of system under identification
q	number of degrees of freedom allowed for measurements noise
r_i	the ith characteristic root for noise representation
$\{x(t)\}$	linear system response vector
$\{y(t)\}$	nonlinear system response vector
$\{z(t)\}$	displacement in restoring force element
α_i	the ith characteristic root for harmonics
Γ	the ith modal vector of harmonics
ζ_i	the ith damping factor (%)
θ	angular displacement
$\{\phi_i\}$	the ith vector in the systems response matrix $[\Phi]$
$\{\psi_i\}$	the ith linear (or equivalent linear) modal vector
ITD	Ibrahim Time Domain modal identification technique
NMO	number of modes allowed in the identification math model
SDOF	single degree-of-freedom system
TDOF	two degrees-of-freedom system

Introduction

With the increasing complexity of modern aerospace and non-aerospace structures, accurate dynamic identification has become a necessity. Dynamic identification is usually carried out through identifying the structure's modal parameters. These modal parameters are required for modeling, responses and loads prediction, stability analysis and control system design.

The demand for more sophisticated dynamic identification techniques, to match the stringent accuracy requirements, for dynamic design and performance analysis, has resulted in numerous research efforts in this area during the last two decades.

Presently, for dynamic identification, a structural dynamicist has a choice between frequency domain-techniques[1,2] and time-domain techniques.[3-11] Although quite different and their merits are still and will be debatable for a while, the two approaches so far have been dealing with only linear systems.

There have been few efforts for the dynamic identification of nonlinear dynamic systems.[12-19] Unfortunately these efforts are limited to lumped parameter systems and are still academic and far away from being applicable to real structures that possess some unknown forms of nonlinearity as well as unknown number of degrees of freedom.

The assumption of linearity in dynamic identification has been found to be a reasonable assumption for many applications. This is true where amplitudes of vibration are small or when in general the levels of nonlinearities are small and can be ignored. On the other hand, some applications require serious considerations for their high levels of nonlinearities where assuming linearity can be highly erroneous. An example of such applications is the case of large amplitude responses of panels subjected to acoustic and mechanical excitation.[20-26]

The efforts presented in this paper are first to study the applicability of a linear modal identification technique to nonlinear systems. The term quasi-linear used in this paper is meant to perform the identification at one certain level of excitation or response. Although the modal approach may be nonexistent for a nonlinear system as a whole, the modal concept will be used here and it is understood that the identified modal parameters will be function of the level of response of the system.

The second purpose of this paper is to identify the type of nonlinearities in the system. This can be attained by identifying the quasi-linear modal parameters of the system at different levels of responses and study the changes in these modal parameters.

*Associate Professor, Member AIAA

The linear modal identification method selected here for the quasi-linear identification of nonlinear systems is a time-domain technique referred to as the Ibrahim Time Domain (ITD) technique,[3-11] Appendix A.

It is to be noted here that although the examples used in this paper are lumped parameter systems, the method is applicable as well to distributed parameter systems. The identification technique is not dependent on the number of degrees of freedom of the system under consideration. The identification model allows any larger number of degrees of freedom such that all modal information in the responses can be identified.

Theory: Linearized Identification Model

For linear systems, the ITD technique is based on that the free-decay responses of a structure $\{x(t)\}$ are linear combinations of the excited modes:

$$\{x(t)\} = \sum_{i=1}^{2p} \{\psi_i\} e^{\lambda_i t} + \{n(t)\} \qquad (1)$$

where $\{\psi_i\}$ is the ith modal vector, λ_i is the ith characteristic root, p is the number of modes excited in the responses ($2p$ complex conjugate modes), and $n(t)$ is measurements noise.

The linear ITD technique also uses the concept of an oversized identification model[11] to reduce effects of measurement noise on the identified parameters. It was shown that allowing more degrees of freedom in the identification model improves accuracy of identification since the extra degrees of freedom act as outlets for the noise and equation (1) becomes

$$\{x(t)\} = \sum_{i=1}^{2p} \{\psi_i\} e^{\lambda_i t} + \sum_{k=2p+1}^{2m} \{N_k\} e^{r_k t} \qquad (2)$$

where m is greater than p.

This same concept can be used to develop a linearized identification model for nonlinear responses. The free-decay responses of a p degrees-of-freedom nonlinear system can be expressed as:

$$\{y(t)\} = \sum_{i=1}^{2p} \{\psi_i\} e^{\lambda_i t} + \sum_{k=1}^{\infty} \{\Gamma_k\} e^{\alpha_k t} + \{n(t)\} \qquad (3)$$

where in this case the first set of modes represents the fundamental solutions and the second set represents the harmonics.

If only a finite number of m degrees-of-freedom ($m > p$) are allowed in the identification model then equation (3) becomes

$$\{y(t)\} = \sum_{i=1}^{2p} \{\psi_i\} e^{\lambda_i t} + \sum_{k=1}^{2n} \{\Gamma_k\} e^{\alpha_k t} + \sum_{\ell=1}^{2q} \{N_\ell\} e^{r_\ell t} \qquad (4)$$

where

$$p + n + q = m$$

With the understanding that usually the amplitudes of higher harmonics get smaller for higher orders, the number of high harmonics to be identified will be dependent on identification accuracy and levels of noises in the responses.

Applications

To test the validity and applicability of the preceding theory, the proposed approach is applied to three different nonlinear systems. These systems were selected to represent single-degree-of-freedom systems with and without damping and a damped two-degrees-of-freedom system. The nonlinear terms are restricted to the stiffness terms while the damping terms were kept linear. For nonlinear stiffness, soft and hard springs are represented. High nonlinearities were achieved through having the nonlinear term coefficient larger than that of the linear term and or having large amplitudes of responses.

The simulated responses of these systems were obtained by numerically integrating the nonlinear differential equations with some specified initial displacements and zero initial velocities. A fourth order Runge-Kutta with variable step method was used for the numerical integration.

Simulated Systems

Three systems are simulated and identified using the preceding theory. These systems are:

1. A Simple Pendulum:

The nonlinear differential equation of motion of the simple pendulum, Fig. 1, is:

$$\ddot{\theta} + 4\pi^2 \sin\theta = 0 \qquad (5a)$$

$$\ddot{\theta} + 0.04\pi\dot{\theta} + 4\pi^2 \sin\theta = 0 \qquad (5b)$$

where equation (5a) represents the undamped case with a linear natural frequency of 1.0 Hz and equation (5b) has a 1.0% equivalent damping factor.

Responses were simulated for initial amplitudes θ_o of $\pi/6$, $\pi/3$, $\pi/2$, and $2\pi/3$.

2. A Mass-Spring System:

A single-degree-of-freedom system, Fig. 2, was designed to have hardening spring with an equivalent linear frequency of 1.0 Hz and equivalent linear damping of 1.0%. The governing equations of motion of such a system for undamped and damped cases are:

$$\ddot{y} + 4\pi^2(y + 2.0y^3) = 0 \qquad (6a)$$

$$\ddot{y} + 0.04\pi\dot{y} + 4\pi^2(y + 2.0y^3) = 0 \qquad (6b)$$

Responses were simulated for initial amplitudes of 0.5, 1.0, 1.5 and 2.0 units.

3. Two-Degrees-of-Freedom System:

To simulate a multi-degree-of-freedom nonlinear system with damping, a nonlinear system with two masses, three linear viscous dampers and three nonlinear springs, Fig. 3, is analyzed. The two springs were selected with cubic nonlinearity representing hardening springs with the coefficients of the nonlinear term being 50 and 100% of that of the linear term. The equations of motion of such system are:

$$\begin{Bmatrix} \ddot{y}_1 \\ \ddot{y}_2 \end{Bmatrix} + \begin{bmatrix} 0.06\pi & -0.02\pi \\ -0.02\pi & 0.06\pi \end{bmatrix} \begin{Bmatrix} \dot{y}_1 \\ \dot{y}_2 \end{Bmatrix} + \begin{bmatrix} 10\pi^2 & -6\pi^2 \\ -6\pi^2 & 10\pi^2 \end{bmatrix} \begin{Bmatrix} y_1 \\ y_2 \end{Bmatrix}$$

$$+ \begin{bmatrix} 7\pi^2 & -3\pi^2 \\ -3\pi^2 & 7\pi^2 \end{bmatrix} \begin{Bmatrix} y_1^3 \\ y_2^3 \end{Bmatrix} = \{0\} \qquad (7)$$

Free responses due to initial displacements were obtained by numerically integrating equation (7). Two sets of initial conditions were used. The first was to represent small amplitudes {0.3, 0.1} and the second set was to simulate larger amplitudes {3.0, 1.0}.

Identification

The numerically integrated responses were sampled at the rate of 50 Hz for the simple pendulum and the spring mass system and 100 Hz for the two-degrees-of-freedom system. Four seconds (200 samples) were used for the identification of both the SDOF and the TDOF systems. The number of modes allowed in the identification program was changed from 1 to 6 for the SDOF systems and from 1 to 12 for the TDOF system. Two samples were used to create the pseudo stations for the SDOF systems and six samples for the TDOF system. The parameter for delaying $[\hat{\phi}]$ from $[\phi]$ was taken as two samples for the SDOF system and four for the TDOF. This means an aliasing frequency of 12.5 Hz for all cases. Unaccounting for the errors arising from the numerical integration, cases with 0.0% and 1.0% noise/signal ratios were considered.

Discussions

1. The Undamped Case (SDOF)

For the simple pendulum and single mass-spring system, the ITD was able to identify very accurately the fundamental frequency and also harmonics up to the ninth harmonic. Tables 1 and 2 list the identified harmonics for the two cases and Figs. 4 and 5 show these identified frequencies. Table 3 lists identified damping factors for the undamped simple pendulum.

Tables 4 and 5 list the level of contribution of each harmonic showing the extremely small levels of contribution of higher harmonics.

Figures 6 and 7 show the identified fundamental frequencies, as functions of the initial amplitude, and their relation to the theoretical frequency of the nonlinear system. The same results are also shown in Tables 6 and 7.

As expected more harmonics are identifiable for higher levels of nonlinearities. This also is evident from determinant plots shown in Figs. 8 and 9. For smaller initial amplitudes, smaller nonlinearities, the determinants decreased at a faster rate indicating a lesser number of harmonics.

2. The Damped Case (SDOF)

The identification technique identified a strong fundamental frequency and very weak signs of a third harmonic. Without noise added to the responses, early signs of singularities were noticed when the number of degrees of freedom was increased beyond two, an indication of extremely small nonidentifiable higher harmonics.

For noise-free data larger number of degrees-of-freedom in the identification model revealed the changing frequency due to the decreasing amplitude of response due to damping. The accuracy of the identification program detected the change in frequency between the measurement response and the pseudo measurements. This phenomenon was not found when a small amount of noise, 1.0%, was added to the response. This can also be avoided by using shorter time records for identification.

3. The Two-Degrees-of-Freedom System

Equations (7) were integrated with two sets of initial conditions (0.3, 0.1) and (3.0, 1.0). These are only the initial conditions; responses in the second set had maximum displacements of 3.0 for both measurements.

Identification results showed no more than two modes for the small displacement case. For the larger displacement case (high nonlinearities), the two fundamental frequencies are much higher than the linear case - a result that is expected from a system with hard springs. Also, four other harmonics appeared in the identification output. Tables 10 and 11 summarize the identified quasi-linear modal parameters for the system. Table 11 shows that for the large amplitude case, the first two modes have the largest contributions to the responses, also indicating that these two modes are the fundamental modes.

For better understanding of the results in Table 11, the linear modes of the system would have resulted in modal contribution vectors of {0.2 0.2} and {0.1 -0.1} for the small amplitude case and {2.0 2.0} and {1.0 -1.0} for the larger amplitude case. For the nonlinear identified modal vectors, the amplitudes of the fundamental modes did not change much from the linear amplitudes, but large changes in the phase angles occurred.

Concluding Remarks

The time-domain, linear modal identification technique is found to be useful for the quasi-linear modal identification of nonlinear dynamic system. Such approach can be used to detect non-linearities, and their types, in structures by performing the identification at different levels of response and study the changes in the identified modal parameters.

References

1. Klosterman, A. and Zimmerman, R., "Modal Survey Activity Via Frequency Response Functions." SAE Paper 751068, 1975.

2. Brown, D. L., Allemang, R. J., Zimmerman, R. and Mergeay, M., "Parameter Estimation Techniques for Modal Analysis." SAE Paper 790221, 1979.

3. Ibrahim, S. R. and Mikulcik, E. C., "The Experimental Determination of Vibration Parameters from Time Responses." Shock and Vibrations Bulletin, no. 46, part 5, August 1976, pp. 187-196.

4. Ibrahim, S. R. and Mikulcik, E. C., "A Method for the Direct Identification of Vibration Parameters from the Free Response." Shock and Vibration Bulletin, no. 47, part 4, September 1977, pp. 183-198.

5. Ibrahim, S. R., "Random Decrement Technique for Modal Identification of Structures." J. Spacecraft and Rockets, vol. 14, no. 11, November 1977, pp. 696-700.

6. Ibrahim, S. R., "Modal Confidence Factor in Vibration Testing." J. Spacecraft and Rockets, vol. 15, no. 5, September 1978, pp. 313-316.

7. Ibrahim, S. R., "Application of Random Time Domain Analysis to Dynamic Flight Measurements." Shock and Vibration Bulletin, no. 49, part 2, September 1979, pp. 165-170.

8. Hanks, B. R., Miserentino, R., Ibrahim, S. R., Lee, S. H., and Wada, B. K., "Comparison of Modal Test Methods on the Voyager Payload." SAE Paper 781044, November 1978.

9. Ibrahim, S. R. and Mikulcik, E. C., "Time Domain Identification of Standing Wave Parameters in Gas Piping Systems." J. Sound and Vibration, vol. 60, part 1, 1978, pp. 21-31.

10. Pappa, R. S. and Ibrahim, S. R., "A Parametric Study of the Ibrahim Time Domain Modal Identification Algorithm." Shock and Vibration Bulletin, no. 51, June 1981.

11. Ibrahim, S. R. and Pappa, R. S., "Large Modal Survey Testing Using the Ibrahim Time Domain (ITD) Identification Technique." AIAA Paper 81-0528-CP, April 1981.

12. Beliveau, J. G., "Identification of Viscous Damping in Structures from Model Information." J. Appl. Mech., ASME 43, pp. 335-339 (1976).

13. Berman, A., "System Identification of a Complex Structure." AIAA/ASME/SAE 16th Structures, Structural Dynamics, and Materials Conference, Denver, Colorado, May 27-29, 1975.

14. Collins, J. D., et al., "Statistical Identification of Structures." AIAA Journal, vol. 12, pp. 185-190, 1970.

15. Distefano, N. and Todeschini, R., "Modeling, Identification and Prediction of a Class of Nonlinear Viscoelastic Materials." International Journal of Solid and Structures (part 1), vol. 9, pp. 805-818, 1973.

16. Udwadia, F. E. and Shah, P. C., "Identification of Structures Through Records Obtained During Strong Earthquake Ground Motion." ASME, Journal of Engineering for Industry, vol. 98, no. 4, pp. 1347-1362, 1976.

17. Masri, S. F. and Caughey, T. K., "A Non-parametric Identification Technique for Non-Linear Dynamic Problems." J. Appl. Mech., ASME 46, pp. 433-447, 1979.

18. Udwadia, F. E. and Kuo, C. P., "Non-Parametric Identification of a Class of Non-Linear Close-Coupled Dynamic Systems." Earthquake Engn. and Structural Dynamics, vol. 9, pp. 385-409, 1981.

19. Yang, Y. and Ibrahim, S. R., "A Nonparametric Identification Technique for a Variety of Discrete Nonlinear Systems." To be presented at the 1982 ASME Winter Annual Meeting, Phoenix, Arizona, November 1982. Also under publication in ASME Transaction.

20. Holehouse, I., "Sonic Fatigue Design Techniques for Advanced Composite Aircraft Structures." AFWAL-TR-80-3019, Flight Dynamics Laboratory, Wright Aeronautical Laboratories, WPAFB, Ohio, April 1980.

21. Mei, C., "Large Amplitude Response of Complex Structures Due to High Intensity Noise." AFFDL-TR-79-3028, Flight Dynamics Laboratory, Wright Aeronautical Laboratories, WPAFB, Ohio, April 1979.

22. Mei, C., "Response of Nonlinear Structural Panels Subjected to High Intensity Noise." AFWAL-TR-80-3018, WPAFB, Ohio, March 1980.

23. Mei, C. and Wentz, K. R., "Large Amplitude Random Response Angle-Ply Laminated Composite Plates." Proceedings AIAA Dynamics Specialists Conference, Atlanta, Georgia, April 1981.

24. Chu, H. N. and Herrmann, G., "Influence of Large Amplitudes on Free Flexural Vibrations of Rectangular Elastic Plates." J. Applied Mechanics, vol. 23, December 1956, pp. 532-540.

25. Mei, C. and Wentz, K. R., "Analytical and Experimental Nonlinear Response of Rectangular Panels to Acoustic Excitation." Proceedings of AIAA SDM Conference, New Orleans, May 1982, pp. 514-520.

26. White, R. G., "Comparison of the Statistical Properties of the Responses of Aluminum and CFRP Plates to Acoustic Excitation." J. Composites, October 1978, pp. 251-258.

APPENDIX A

Background - ITD Modal Identification Technique

The ITD modal identification technique is based on the fact that a vector of free-decay responses of $2m$ measurements, and or pseudo measurements, and containing contributions from p modes can be expressed as:

$$\{\phi(t)\} = \sum_{i=1}^{2p} \{\psi_i\} e^{\lambda_i t} \tag{A1}$$

To allow using an identification mathematical model with an m degrees of freedom, where $m >> p$, the vector $\{\phi(t)\}$ is arbitrarily selected as:

$$\{\phi(t)\} = \begin{Bmatrix} \{x(t)\} \\ \{x(t + \Delta t_2)\} \\ \{x(t + 2\Delta t_2)\} \\ \vdots \\ \{x(t + \Delta t_3)\} \\ \{x(t + \Delta t_2 + \Delta t_3)\} \\ \{x(t + 2\Delta t_2 + \Delta t_3)\} \\ \vdots \end{Bmatrix} \tag{A2}$$

where $\{x(t)\}$ is the measured response vector. Equation (1) can be written for the same responses delayed Δt_1 in time as:

$$\{\hat{\phi}(t)\} = \{\phi(t + \Delta t_1)\} = \sum_{i=1}^{2p} \{\psi_i\} e^{\lambda_i \Delta t_1} \cdot e^{\lambda_i t} \tag{A3}$$

By repeating these measurements vectors $\{\phi\}$ and $\{\hat{\phi}\}$ for $2r$ times where $r > m$, to form the two $2m \times 2r$ response matrices $[\Phi]$ and $[\hat{\Phi}]$, and computing a matrix $[A]$ where:

$$[A]\,[\phi][\phi]^T = [\hat{\phi}][\phi]^T \tag{A4}$$

the modal parameters of the system under consideration can be determined from the eigenvalue problem.

$$[A]\{\psi_i\} = e^{\lambda_i \Delta t_1} \{\psi_i\} \tag{A5}$$

For complete details on ITD please refer to references 3-11.

Table 1 Ratios to fundamental of identified frequencies for undamped simple pendulum

Mode no. (N)	$\theta_o = 30^o$		$\theta_o = 60^o$		$\theta_o = 90^o$		$\theta_o = 120^o$	
	f_N	f_N/f_1	f_N	f_N/f_1	f_N	f_N/f_1	f_N	f_N/f_1
1	0.9829	1.000	0.9318	1.000	0.8472	1.000	0.7284	1.000
2	2.9846	3.037	2.7949	2.999	2.5417	3.000	2.1854	2.999
3	4.9162	5.002	4.6747	5.017	4.2360	5.000	3.6415	4.999
4	-	-	6.5269	7.005	5.9334	7.004	5.0987	7.000
5	-	-	-	-	-	-	6.5681	9.017
6	-	-	-	-	-	-	-	-

Table 2 Ratios to fundamental of identified frequencies for undamped spring-mass system

Mode no. (N)	$y_o = 0.5$		$y_o = 1.0$		$y_o = 1.5$		$y_o = 2.0$	
	f_N	f_N/f_1	f_N	f_N/f_1	f_N	f_N/f_1	f_N	f_N/f_1
1	1.1708	1.000	1.5691	1.000	2.0651	1.000	2.6032	1.000
2	3.5124	3.000	4.7073	3.000	6.1953	3.000	7.8116	3.001
3	5.8529	4.999	7.8456	5.000	10.3256	5.000	13.0204	5.002
4	-	-	10.9841	7.000	14.4605	7.002	18.2261	7.001
5	-	-	-	-	-	-	23.4437	9.006
6	-	-	-	-	-	-	-	-

Table 3 Identified damping factors for undamped simple pendulum

θ_o	Damping factors* ζ_i				
	1	2	3	4	5
30	0.00000	0.00065	0.00002	-	-
60	0.00001	0.00000	0.00050	-0.00096	-
90	0.00006	0.00001	0.00000	0.00122	-
120	0.00000	0.00002	0.00030	0.00866	0.00593

*All theoretical damping factors were equal to zero.

*The listed values were obtained from different identification runs for optimum damping identification.

Table 4 Amplitudes of identified harmonics for undamped simple pendulum

Initial amplitude θ_o (rad.)		Identified $\theta_o = \theta_1 + \theta_3 + \theta_5 + \theta_7 + \theta_9$				
Theory	Identified	θ_1	θ_3	θ_5	θ_7	θ_9
0.5236	0.5236	0.5244×10^{0}	-0.7474×10^{-3}	-0.1080×10^{-4}	-	-
1.0472	1.0274	0.1054×10^{1}	-0.6429×10^{-2}	0.6942×10^{-4}	-0.2919×10^{-6}	-
1.5708	1.5708	0.1594×10^{1}	-0.2396×10^{-1}	0.6300×10^{-3}	-0.1930×10^{-4}	-
2.0944	2.0944	0.2158×10^{1}	-0.6697×10^{-1}	0.3449×10^{-2}	-0.2058×10^{-3}	0.1156×10^{-4}

Table 5 Amplitudes of identified harmonics for undamped spring-mass system

Initial amplitude y_o		Identified $y_o = y_1 + y_3 + y_5 + y_9$				
Theory	Identified	y_1	y_3	y_5	y_7	y_9
0.5000	0.5000	0.4942×10^{0}	0.5697×10^{-2}	0.6270×10^{-4}	-	-
1.0000	1.0000	0.9741×10^{0}	0.2529×10^{-1}	0.6399×10^{-3}	0.1577×10^{-4}	-
1.5000	1.5000	0.1449×10^{1}	0.4913×10^{-1}	0.1617×10^{-2}	0.6205×10^{-4}	-
2.0000	2.0005	0.1924×10^{1}	0.7323×10^{-1}	0.29871×10^{-2}	-0.3066×10^{-3}	0.7986×10^{-3}

Table 6 Theoretical and identified fundamental frequency for undamped simple pendulum

$\theta_o{}^o$	f_1 (Hz)	
	Theory	Identified
30	0.9829	0.9829
60	0.9318	0.9318
90	0.8472	0.8472
120	0.7284	0.7284

Table 7 Theoretical and identified fundamental frequency for undamped spring-mass system

y_o	f_1 (Hz)	
	Theory	Identified
0.5	1.1708	1.1711
1.0	1.5691	1.5693
1.5	2.0651	2.0650
2.0	2.6032	2.6042

Table 8 Identified frequencies and damping factors for simple pendulum

θ_o^o	f (Hz)	ζ (%)
30	0.9906	0.93
	2.9186	3.50
60	0.9398	1.15
	2.7712	2.89
90	0.8678	1.30
	2.5698	2.60
120	0.7714	1.89
	2.2955	4.67

Table 9 Identified frequencies and damping factors for spring-mass system

y_o	f (Hz)	ζ (%)
0.5	1.1542	0.76
	3.4240	2.11
1.0	1.5242	0.49
	4.5873	1.98
1.5	1.9935	0.36
	6.0214	1.89
2.0	2.5064	0.33
	7.5700	1.58

Table 10 Identified frequencies and damping factors for the two-degree-of-freedom system*

y_{01}, y_{02}	Mode no.	f (Hz)	ζ (%)
0.3, 0.1	1	1.0185	0.95
	2	2.0359	0.99
3.0, 1.0	1	2.2783	1.40
	2	4.0214	1.34
	3	5.7955	1.07
	4	8.5792	0.65
	5	10.4157	1.47
	6	12.1253	1.60

*Theoretical linear frequencies are 1.0 and 2.0 Hz and damping factors are 1.0% for the two modes.

Table 11 Identified quasi-linear mode shapes for the two-degree-of-freedom system

Case (y_{01}, y_{02})	Station	Mode no. 1	2	3	4	5	6
0.3, 0.1	1 - Ampl.	0.1992	0.10156				
	Pha.^{o}	0.21	0.23				
	2 - Ampl.	0.1995	0.1014				
	Pha.^{o}	0.25	178.84				
3.0, 1.0	1 - Ampl.	2.0408	1.7412	0.0643	0.1191	0.0455	0.0578
	Pha.^{o}	-8.10	-29.30	-106.00	-71.94	-94.91	-126.47
	2 - Ampl.	1.9648	1.8263	0.0828	0.1121	0.0333	0.0547
	Pha.^{o}	-11.45	99.10	-154.79	-96.12	-35.31	78.94

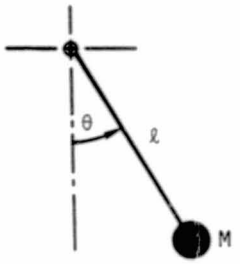

Fig. 1 Simple pendulum.

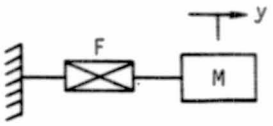

$m = 1$

$F = 4\pi^2(y + 2y^3) + 0.04\pi\dot{y}$

Fig. 2 Single-mass-spring system.

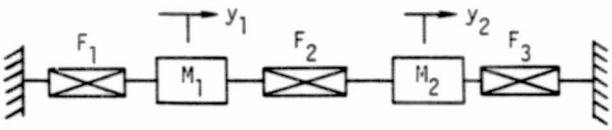

$M_1 = M_2 = 1$

$F_1 = F_3 = 4\pi^2(z + z^3) + 0.04\pi\dot{z}$

$F_2 = 6\pi^2(z + 0.5\ z^3) + 0.06\pi\dot{z}$

(z is displacement of restoring force element)

Fig. 3 Two-degree-of-freedom system.

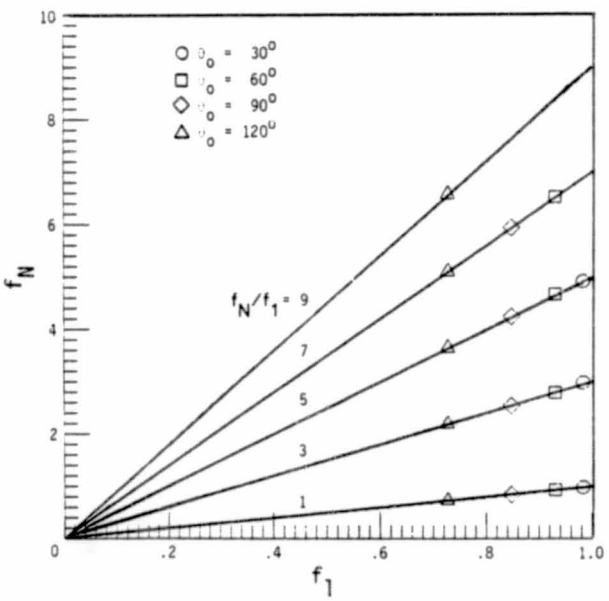

Fig. 4 Identified harmonics versus fundamental frequencies of simple pendulum.

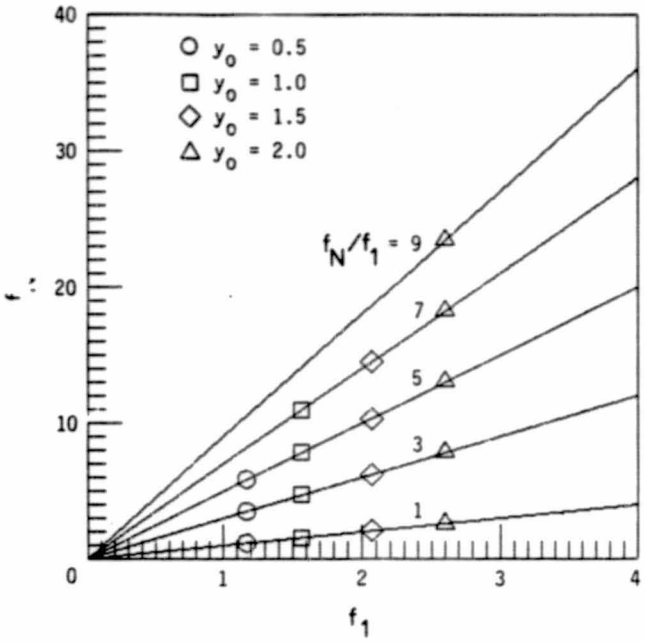

Fig. 5 Identified harmonics versus fundamental frequency for spring-mass system.

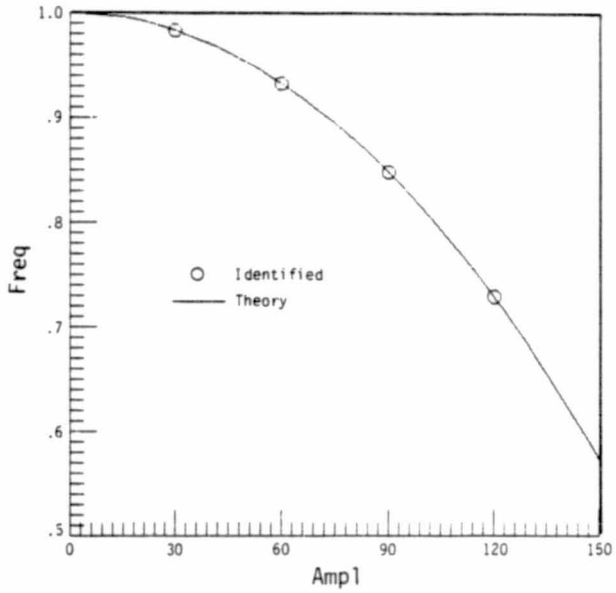

Fig. 6 Theoretical and identified fundamental frequency of simple pendulum.

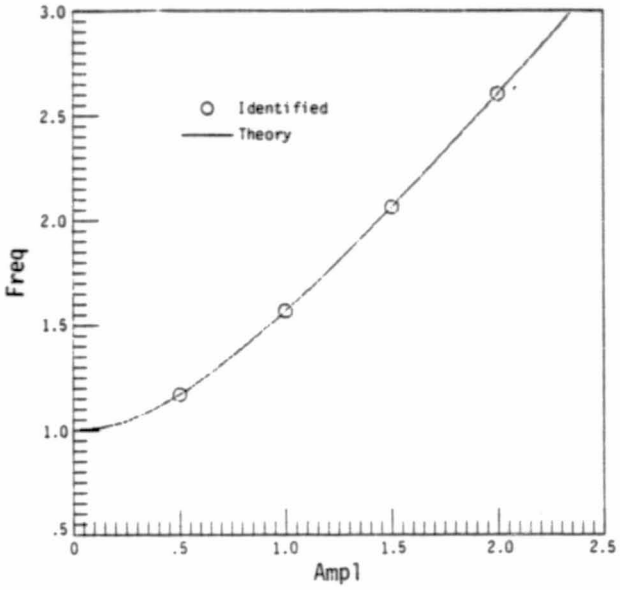

Fig. 7 Theoretical and identified fundamental frequency of spring-mass system.

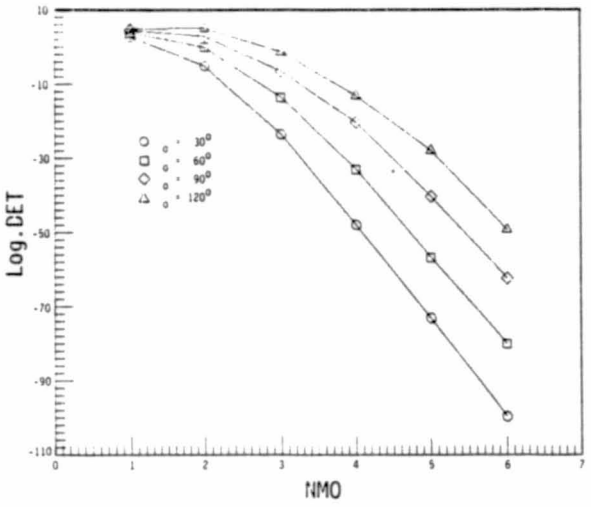

Fig. 8 Determinant versus DOF of identification model for simple pendulum.

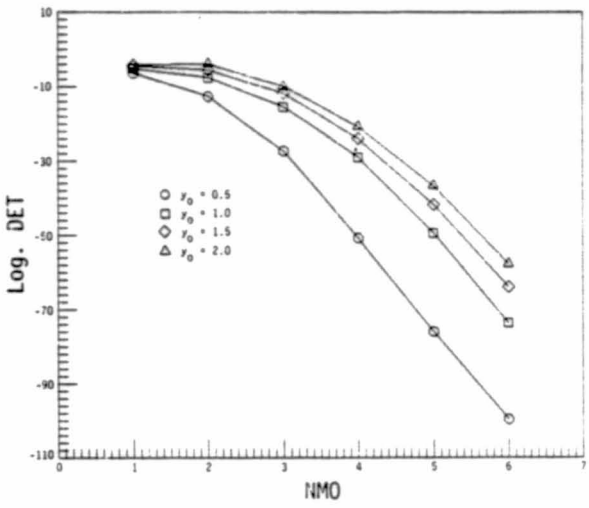

Fig. 9 Determinants versus DOF of identification model for spring-mass system.